NATIONAL TECHNICAL UNIVERSITY OF ATHENS
SCHOOL OF NAVAL ARCHITECTURE AND MARINE ENGINEERING
DEPARTMENT OF MARINE ENGINEERING

Development of a Method for Simulation and Optimization of Integrated Thermal Energy Systems of Ships

George N. Sakalis

Thesis submitted in partial fulfillment
of the requirements for the Ph.D. Degree

Thesis Supervisor
Prof. Em. Christos A. Frangopoulos

Athens, November 2018

Abstract

The research subject of the present work is the development of a method for the simulation and optimization of the synthesis, design and operation of integrated thermal energy systems of ships.

The term *integrated* implies energy systems which are proposed for covering the various types of energy loads encountered on ships in forms of propulsion, electric and thermal power with a minimum of energy resources. From a technical point of view, such systems may serve their purpose through the application of heat recovery concepts, leading to the construction of energy systems that operate on a combined thermodynamic cycle and can also be cogeneration plants.

The method developed may be used as an aid to engineering decisions regarding the utilization of alternative layouts of the energy systems, the determination of the characteristics of the main components of such systems and the appropriate states of operation of the subsystems and the system as a whole. The technical solutions proposed are justified taking into account certain techno−economic criteria.

An important effort has been made towards the direction of developing a unified approach to the simulation of the energy system as a whole and the application of optimization algorithms. More specifically, all the three levels of the problem on which optimal solutions are sought, that is, the synthesis, design and operation levels, are simultaneously taken into account in search of the overall optimum. The simulation and design procedures of the individual components are also developed by keeping the needs of comprehensive modeling of the subsystems in mind, which are to be used in several operating conditions.

The applicability and versatility of the method is demonstrated with the solution of a number of numerical examples and the parametric study, which reveals the effects of important technical and economic parameters on the optimal solution.

Acknowledgments

A lot of people have made important contributions during the carrying out and to the completion of the present dissertation. I would like to thank Professors N. Kyrtatos and K. Giannakoglou, members of my Ph.D. studies advisory committee, for their constructive comments and guidance through the years past, based every time on their deep technical and scientific knowledge related to the subject matters of my studies, as also for their approval on the track followed and on the final outcome of my thesis.

This work has been possible due to the economic support granted by the Lloyd's Register Foundation (formerly Lloyd's Register Educational Trust), which is gratefully acknowledged. Lloyd's Register Foundation is a charitable foundation, helping to protect life and property by supporting engineering−related education, public engagement and the application of research.

I wish to express my gratitude towards my family, my father Nikos, my mother Anthoula and my sister Maria, who have supported my decision of taking up the really difficult work of a Ph.D. candidate and have continued to support me in every possible way, till the present day. I know how important their role has always been, and I also know that they would have been this supportive towards my professional aims in any case.

A big *"thank you for all"* goes to my friend and colleague, also Ph.D. candidate, George Tzortzis, with whom we have been together throughout our studies, nearly for about half of our lives. No need to say more…

Last, but most importantly, I wish to express my sincere gratitude towards Professor Ch. Frangopoulos for everything he has done for me. Professor Frangopoulos has placed unconditioned trust on my capabilities from the beginning of our collaboration. He has given me a unique opportunity for acquiring deep and substantial knowledge on thermal energy systems engineering, as also on the application of optimization, which I have always been regarding as the utmost duty of any engineer. The occupation with both of these subjects, on a professional level, has been a personal aspiration of mine and I cannot think of any other possible situation that all these would have been combined in a harmonic, meaningful and effective manner. I would also like to thank Professor Frangopoulos for all the times that he stood beside me being more than a dissertation supervisor and for tolerating the peculiarities of my character. I am sure he knows what I mean, and addressing towards him, I want to sincerely say *"I wish the best for you!"*.

The present thesis is the outcome of the work that the author undertook several years ago. The author likes to think of this work as the chariot of his later youth, that by riding on which, he has gained a deep understanding of what means to be dedicated, persistent and really committed towards the completion of a task, so complex and sophisticated as the

carrying out of a Ph.D. dissertation. Through the years, the journey had some unexpected turns and some unwanted implications. But there are several kinds of commitment. One kind begins with misplaced desire and degenerates into a burden of a dull obligation. Then, there is a kind of commitment to which one can resort to whenever asked, and always performs beautifully... leaving behind all obstacles, all difficulties, all the externally posed hindrances and dire straits. A kind of commitment that makes you feel young, when you go for a ride… Now that the journey comes to its end, and I realize that the time has come to bid farewell to my sweet chariot of youth, I understand that, apart from the knowledge and experience gained, one more important thing to be grateful for is the joy I had by letting myself on this nice, long ride, always feeling as young as the first day…

Contents

List of abbreviations

AB	Auxiliary boiler
CCHP	Combined cooling, heating and power
CHP	Combined heat and power
D	Diesel engine
DG	Diesel-generator
EGB	Exhaust gas boiler
FWT	Feed water tank
GT	Gas turbine
HFO	Heavy fuel oil
HRSG	Heat recovery steam generator
LHV	Lower heating value
LNG	Liquefied natural gas
MCR	Maximum continuous rating
MDO	Marine diesel oil
ME	Main engine
MILP	Mixed integer linear programing
MINLP	Mixed integer non linear programing
NPV	Net present value
NTU	Number of transfer units
O&M	Operation and maintenance
PWC	Present worth cost
PWF	Present worth factor
SCR	Selective catalytic reaction
SDO	Synthesis, design and operation
SFOC	Specific fuel oil consumption
ST	Steam turbine

Chapter 1

Introduction

1.1 Scope of the Thesis

The research subject of the present work is the analysis, simulation and synthesis, design and operation optimization of integrated energy systems of ships taking into consideration certain technical and economic criteria. The goal is the development of a method that can be used for jointly addressing the needs for simulating the overall system as well as facilitating the application of optimization algorithms.

The term ‘integrated energy system’ implies a system being built with the aim of covering the various energy demands, which come in the forms of propulsion, electric and thermal loads. Towards this aim, the intention for such systems is also to serve these loads by the least of supplies of energy resources, to the extent possible. From a technical point of view, such systems may be designed with the employment of waste heat recovery techniques. In the present work, the application of water−steam bottoming cycles for serving all of the aforementioned types of loads is investigated.

The energy demands of ships are inherently not constant and may present large variations over time, which will typically be the case during different operating modes of the ship. This is an important fact that has to be taken into account during the design stages of such energy systems, so that their design and operating characteristics are the most appropriate for effectively serving their purposes through the whole life span of the ship operation.

Apart from the time varying nature of the energy loads, the large variety of technically feasible configurations, design specifications and operating states of the system make the application of optimization methods necessary in order to identify the configuration, the design specifications and the operating states that give the best performance. The optimization of energy systems can be distinguished at three levels:

Synthesis: The term “synthesis” implies the components that appear in a system and their interconnections. After the synthesis of a system has been composed, the flow diagram of the system can be drawn.

Design: The word “design” is used to imply the technical characteristics (specifications) of the components and the properties of the substances entering and exiting each component at the “design” point (nominal load) of the system. One may argue that design includes synthesis too. However, in order to distinguish the various levels of optimization and due to the lack of a better term, the word “design” will be used with the particular meaning given here.

Operation: For a given system (i.e. one in which the synthesis and design are known) under specified conditions, the optimal operating point is requested, as it is defined by the operating properties of components and substances in the system (speed of revolution, power output, mass flow rates, pressures, temperatures, composition of fluids, etc.).

The three levels of the synthesis, design and operation (SDO) optimization problem are tightly interconnected to each other, and the decisions taken on one of the three levels largely affect the decisions to be taken on the two other levels. Thus, the complete SDO optimization problem cannot be thoroughly investigated without a formulation that permits for the concurrent assessment that the decisions on all the three levels have on the final outcome. In the present work, an effort has been made for the development of a method in which the three levels of the problem are tackled in a unified approach.

In the present work, the optimization objective functions are based on economic criteria. From a technical point of view, the integrated energy system must be able to cover all of the energy demands presented, but the decisions to be taken must also be economically justified. Two alternative economic criteria are used: the present work cost and the net present value of the investment of acquiring and operating the marine energy system.

1.2 Literature Review

The subject of the SDO optimization of thermal energy systems has emerged as one of the academic community interests several years ago. One of the earliest works addressing formally the specific research subject has appeared in the publication [1][1], with a more complete formulation of the theory given in [2] and application in [3]. A more formal approach for the application in largely time varying systems appears in [4].

The SDO optimization problem in these publications is tackled with a decomposition approach that is, optimization algorithms are applied on a certain level (or alternatively two levels) of the complete SDO problem and with given the results of this application, optimization algorithms are applied on the subsequent levels. This decomposition approach seems to be predominant in the related literature even in later years. In the works [1−4], the synthesis and design optimization problems are solved on Level A, while the operation optimization problem is solved on Level B for given synthesis of the system and design specifications of components (bi−level optimization). This approach of decomposition of the complete problem or similar techniques seem also to be quite predominant in the related literature, even in cases where not all of the three levels of the SDO problem are tackled.

The synthesis optimization of energy systems has been approached with various methods, which can generally be classified as methods a) based on heuristics and evolutionary search, b) attempting to reach predetermined targets, which have been identified by the application of physical rules, and c) starting with a superconfiguration (called also superstructure), which is reduced to the optimal configuration [5].

---

[1] References are included at the end of each chapter.

A decomposition approach has been used for the synthesis and design optimization of aircraft energy systems in [6]. A similar approach is used in [7] for fuel cell cogeneration systems, in which, after the solution of the synthesis and design problem, investigations are carried out for evaluating the influence of off−design operating conditions on the optimality of the system designed. The operating states of the system are not explicitly accounted for in the optimization procedure.

In [8], the synthesis and design of a hybrid fuel cell−gas turbine system are optimized with a formulation of the problem that permits the synthesis and design optimization of the system only, with no other considerations regarding the system operation. A similar approach is followed in [9] for the synthesis and design of combined cycle power plants, where also alternative optimization criteria of economic and/or environmental nature are used. The operation optimization is also addressed in a decomposed manner, as above mentioned.

In [10], the optimal synthesis and design of a combined electric power and desalination plant are formulated as a mixed integer non linear programing (MINLP) problem and solved with deterministic optimization algorithms. The integer variables are binary and their values determine the potential existence of certain components. The problem is formulated in a way that the demand for only one of the products (electric power or water) is specified at the nominal operating point, while the magnitude of the other is determined by the application of optimization. In [11], tri−generation facilities are optimized with respect to synthesis and design, taking additionally into account that these systems have to operate efficiently when alternative operating strategies may be employed, but no explicit specification of the operating demands regarding the magnitude of the energy loads is made.

While many works deal with the synthesis and design optimization, other works tackle the problem of design and operation optimization (with fixed synthesis). An application of the aforementioned decomposition approach for the design and operation of combined heat and power Organic Rankine Cycles appears in [12, 13], where bi−level optimization is applied with only optimal design specifications of the components being sought on Level A. Other characteristic examples of systems in which this bi-level decomposition approach include applications related to building energy systems [14], small size trigeneration plants for civil users [15], oxyfuel natural gas plants [16], polygenerative energy grids [17], integrated gas and electricity network systems [18].

The work presented in [19] is concerned with the design and operation of combined heat and power (CHP) systems for residential applications, and the optimization problem is solved using a temporal Lagrangean decomposition method, which permits for the simultaneous optimization of the design specifications and the operational strategy. A single−level solution approach is also employed in [20] for the design and operation of residential CHP systems, in which the design characteristics of the components are practically defined by the capacities needed for covering the loads during operation. This single−level approach for combined cooling, heating and power (CCHP) systems is applied also in [21], in which the nominal power capacities of the components are determined in a more formal way by the application of the optimization algorithms. In [22], a CCHP system

with compressed air energy storage is studied on three levels. The design optimization consists of two levels: the first level addresses the effect of the design variables on the thermodynamic performance, while the second level addresses the effect of the design variables on the economic performance of the system. The operation optimization is performed on a third level. The bi−level optimization of design and operation of a CHP system is studied in [23], where furthermore the effects of the probabilistic nature of the energy demands are tackled with a risk analysis approach based on the Monte Carlo method. A different approach appears in [24], where the operation optimization is tackled as an optimal control problem.

The complete SDO optimization problem has been addressed with a single−level solution approach in few works. In [25], the superconfiguration−based SDO optimization of decentralized energy systems producing electricity, heating and cooling is performed with economic criteria. An important aspect of the approach presented is that the problem is solved by applying a specialized adaptive discretization algorithm of the continuous variables, developed in order to facilitate the use of MINLP solvers. In works such as [26] and [27] the SDO problem is solved for large scale CCHP and utility systems respectively, based again on superconfiguration concepts. The common aspect of these two works is the linearization of the problem, so that mixed integer linear programing (MILP) algorithms are used for the solution. A similar approach of using linear modeling of residential energy systems comprising heat pumps and photovoltaic subsystems in order to apply MILP optimization techniques appears in [28]. Except of linearization techniques of the complete SDO problem, other approaches can be found, such as in [29], where the synthesis and design part of the optimization problem of energy multi−generation systems is tackled with metaheuristics and only for the operation optimization linear solvers are used.

Certain other approaches concerning the optimal synthesis of energy systems have appeared in the literature. A theoretically based method for facilitating the synthesis of energy systems with heat transfer is presented in [30]. The synthesis problem is solved by considering the components in which no heat transfer is present separately from the components used for heat transfer. Two problems to be solved sequentially are thus formulated. In [31], this method is further used in an optimization algorithm that is applied for the synthesis and design optimization of thermal systems. The solution of the synthesis problem is not based on a superconfiguration of the system, but is determined in an evolutionary manner along with the intensive properties of the non−heat exchanging part of the system. The extensive properties of the heat transfer components are determined by deterministic optimization methods afterwards.

Another example of superconfiguration−free synthesis problem for distributed industrial energy supply systems is presented in [32]. The synthesis optimization is tackled with an ad hoc evolutionary algorithm and the use of a mutation operator, which is designed for deriving rules for the appropriate selection of components. The mutation operator is designed to follow certain “hierarchy rules”, in order to safeguard that the resulting synthesis is technically feasible and rational. The design and operation optimization problems are also taken into account on the synthesis level in a decomposed manner. The theoretical

framework presented in [32] has been extended for applications related to thermal power plants in [33].

Coming to the marine sector, the energy system of a ship has to cover all types of loads (propulsion, electric energy, thermal energy). In the past, each type of load was covered separately by dedicated machinery with very little room for optimization. The need to decrease fuel consumption and pollution of the environment has led to recovery of waste heat not only for serving thermal loads, but also for producing additional power by means of a steam bottoming cycle. A Diesel−Rankine combined cycle is studied in [34], while several options for exploitation of waste heat in marine Diesel engines are evaluated in [35]. A techno−economic analysis of single−pressure exhaust gas waste heat recovery on ship propulsion installations appears in [36], while a step further with optimization is taken in [37]. In [38], a system with exhaust gas recirculation and multi−stage waste heat recovery is optimized. In [39], the thermodynamic and economic performance of an organic Rankine cycle system operating on the exhaust gas thermal energy of a marine Diesel engine is first performed, followed by optimization of the system.

In the marine sector, systems with increasing integration are being proposed. The variety of feasible configurations, design specifications and operating states makes the application of optimization methods necessary in order to identify the configuration, the design specifications and the operating states with the best performance. Thus, works such as those in [40] and [41] appeared, which perform SDO optimization of the integrated system. The benefit derived from the application of optimization techniques in the decisions concerning the allocation of the loads in the various system components has also been recently demonstrated in [42], where, however, the waste heat recovery options for employing a mechanical power producing steam bottoming cycle are not considered.

A thorough review on the possibility of using gas turbine based combined cycles on merchant ships has been reported in [43−45]. The possibility of using such systems in place of the usually encountered Diesel engines is examined from the point of view of the need for decreasing the pollutants emissions and their environmental and health impacts, as also the continuously increasing strictness of emission regulations. It is indicated that gas turbine combined cycles can very well satisfy these regulations. Furthermore, the benefits of lower volume and weight of a ship power plant that uses such systems in commercial applications is assessed as an extra motive for their utilization.

In [46] a case study is conducted for the possibility of the application of a gas turbines based combined cycle power plant in a large containership instead of two−stroke Diesel engines, after optimization procedures for three different bottoming steam cycle designs have taken place. In addition to the benefits related to the overall weight and volume decrease of the machinery, a significant decrease in fuel consumption in comparison with the Diesel engines is achieved.

The majority of modern combined cycle applications usually consist of gas turbine configurations with compressors and/or turbines, the geometry of which varies along with the fuel flow in order to regulate the partial load power output. In [47−48] the effects that these complementary control strategies have on the thermal efficiency of the system during

partial load operation are studied for the cases of single−shaft and two−shaft marine gas turbines. The results suggest that even though the efficiency of the gas turbine itself tends to generally deteriorate (especially in low loads, in which any ship is going to be operating for a large portion of its service time), the use of variable geometry gas turbines is evidently beneficial for the thermal efficiency of an appropriately designed combined cycle.

Other possibilities of integrating gas turbines with other technologies for marine applications have also been reported. Besides the utilization of water/steam in bottoming cycles, alternative waste heat cycles and configurations, possibly more suitable for ship applications, have been proposed. In [49] a supercritical CO_2 recompression−regeneration cycle utilizing the exhaust gas thermal energy content is presented. A more advanced system in which a supercritical CO_2 recompression−regeneration cycle and a sole supercritical CO_2 regeneration cycle are cascaded is presented in [50]. Both studies suggest significant power enhancement and a very important increase of thermal efficiency of the overall power plant. The improved partial load performance of such cycles is also highlighted in [50]. Other works suggest the integration of gas turbines with fuel cells for marine applications [51−52]. In these systems, the waste heat of the exhaust gas is used to preheat the fuel used in the fuel cell to the required temperature of operation.

Apart from the cases where gas turbines are used in conjunction with steam bottoming cycles or other waste heat recovery configurations, important studies have also appeared in which gas turbine configurations are used solely for the production of mechanical power in ship energy systems. In a recent work [53], a comparison is made between the alternatives of using a) gas turbines as main engines, b) Diesel engines with no pollution abatement, and c) Diesel engines complemented with pollutant emission control devices (selective catalytic reaction or SCR, scrubber). These three different systems are simulated and optimized for a case study of a cruise ship with the aim of maximizing the overall energy efficiency in several operating conditions, while the pollutants emissions are afterwards quantified. The results show that the employment of gas turbines leads to important environmental benefits, comparable with the alternative of using emission control devices in a Diesel engine based system, while at the same time the complexity of the engine room is avoided. In [54] gas turbine based systems are assessed as an alternative for utilization in a RoPax fast ferry ship. Simple cycle and intercooled – recuperated configurations are studied. In the method presented, several technical, economic and environmental parameters concerning the operation of the system during the whole life cycle of the ship are taken into account. The study reports the benefits of using intercooled–recuperated gas turbines in comparison with simple cycle configurations. Natural gas is ideal for gas turbines and, as a consequence, gas turbines are very good candidates for liquefied natural gas (LNG) carriers, where they operate on the boil off gas. A techno−economic study is presented in [55], where the potential economic benefits of using a gas turbine based power plant burning LNG instead of reciprocating engines operating on heavy fuel oil (HFO) are demonstrated.

The SDO optimization problem for ship energy systems based on gas turbines as prime movers was first addressed in [40], while an application on LNG carries appeared in [41].

The success of applying heuristic optimization techniques such as genetic algorithms and/or particle swarm optimization in SDO optimization problems has been demonstrated in publications as for example in [56] and [57]. Other heuristic optimization techniques have been also successfully applied for problems of this type, such as ant colony optimization, simulated annealing, harmony search and Tabu search, as appeared in [58].

Independently of the choice of the optimization algorithm, in [40] and [41] as well as [40] and [41], nested optimization and time decomposition are applied, as described in [1−4]: for each given set of values of synthesis and design independent variables (level A), the operation optimization problem (level B) is solved for each time interval, one after the other. The level A optimizer updates the values of the synthesis and design independent variables based on the results derived by the solution of the level B problems, and the iterative procedure between levels A and B continues until convergence. As above mentioned, to the author's opinion, the complete SDO optimization problem has to be addressed in a unified approach so that the vast search space is more thoroughly explored.

1.3 Original Contribution of the Thesis

In the present work, a modeling procedure of the integrated energy system as a whole is developed, which permits for a more unified approach of the complete SDO optimization problem. In the few works appearing in the literature in which all the three levels of synthesis, design and operation optimization problem are tackled, nested optimization and time decomposition are applied: for each given set of values of synthesis and design independent variables (level A), the operation optimization problem (level B) is solved for each time interval, one after the other. The level A optimizer updates the values of the synthesis and design independent variables based on the results derived by the solution of the level B problems, and the iterative procedure between levels A and B continues until convergence.

With this bi−level iterative optimization procedure, if the conditions for decomposition are not strictly applicable there may be optimal solutions overlooked. In order to avoid such an incidence, a single−level approach is proposed and applied in the present work: the operation optimization is solved simultaneously for all time intervals, while the optimal synthesis and design specifications are derived together with the operation optimization results. This requires the development of a mathematical formulation of the simulation of the system as a whole which will be used for evaluating the optimization objective function in a single computational step, while taking into account the effects that the decisions on all the three levels of the problem will have on the value of the objective to be minimized or maximized. The single−level approach for the SDO optimization of energy systems inherently takes into account the effects that all the various operating conditions have on the synthesis of the system and the design characteristics of its components simultaneously. It also conversely takes into account the fact that the synthesis of the system and the design

characteristics of the components define the possibilities for the operating options at all of the instances of time during which the system is going to operate.

Attention has been directed more towards the need for simulating the integrated energy system in a manner that the single−level approach described in the preceding is achieved. The mathematical formulation of the problem has been carried out with the intention of developing a simulation procedure that can be used in conjunction with proven optimization algorithms. Thus, the outcome is a modeling procedure of the overall system, expressed on all the three levels of the SDO optimization problem, which is virtually independent of the choice of the optimization algorithm. The only requirement regarding the optimization algorithm used is that it must be able to handle mixed integer type of optimization problems.

The modeling of the integrated system as a whole is based on the modeling and simulation of the components appearing in the system. For the components of the steam bottoming cycle, specialized design procedures have been developed, which instead of being based only on first principles and empirical approaches, make use of dedicated numerical procedures which result in the detailed determination of their design characteristics and their internal structure. The off−design operating efficiency of these components is largely dependent on the internal structure and the corresponding off−design simulation algorithms are naturally based on these characteristics. With the single−level approach of the optimization procedure adopted in the present work, the detailed design of the steam bottoming cycle components is being carried out in a way that is most suitable for serving the purpose of the steam bottoming cycle throughout all of the life span of operation of the energy plant.

1.4 Thesis Outline

In the present chapter, the scope of the work has been briefly described. The literature review that follows indicates the need for a unified single−level approach to the SDO optimization problem of thermal energy systems and the chapter concludes with the beneficial contribution of such an approach.

In Chapter 2 the system to be optimized is presented in a descriptive manner. The superconfiguration[2] of the system is defined and the term *integrated* energy system is clarified. Explanations are given concerning the possible means that the different types of energy loads are to be covered by the overall system.

Chapter 3 presents the modeling and simulation procedures related to each of the individual components, which are developed keeping in mind that they will be used as building blocks of the modeling procedure of the overall system.

The single−level modeling approach of the integrated energy system is the subject of Chapter 4. In this chapter, the appropriate variables used for the evaluation of the optimization objective functions are defined. The appropriate mathematical interconnections

[2] The word ‘superstructure’ is usually used for land installations, but it is avoided here, because it has a different meaning on ships.

among the independent variables, as also among several other dependent quantities, which are required in order for all of the three levels of the SDO optimization problem to be simulated in a single computational step, are exposed.

In Chapter 5, the mathematical statement of the optimization problem is given, the set of independent variables is formally defined and the utilization of the genetic algorithm employed is described.

Numerical examples of the application of the method developed are presented in Chapter 6. More particularly, three numerical examples are presented, in which different types of prime movers are considered. Sensitivity analysis is performed for several of the important parameters of the problems posed, and the results derived by the application of the single−level unified simulation−optimization procedure are assessed.

In the final Chapter 7, concluding remarks as also recommendations for future work are stated.

References

1. Frangopoulos C.A. Optimal Synthesis and Operation of Thermal Systems by the Thermoeconomic Functional Approach. In *Analysis and Design of Energy Systems: Thermodynamic Analysis of Industrial Processes*, ASME Winter Annual Meeting, San Francisco, Ca., Dec. 10−15, RA Bajura, MR von Spakovsky, ES Geskin, eds., AES−Vol. 10−3, pp. 49−59, ASME, New York; 1989. Published also in the Journal of Engineering for Gas Turbines and Power 1992;114:707−714.
2. Frangopoulos C.A. Intelligent Functional Approach : A Method for Analysis and Optimal Synthesis−Design−Operation of Complex Systems. In *A Future for Energy*, Florence World Energy Research Symposium, Florence, Italy, May 28 − June 1, pp. 805−815, Pergamon Press, Oxford;1990. Published also in the International Journal of Energy, Environment and Economics 1991;1:267−274.
3. Frangopoulos C.A. Optimization of Synthesis−Design−Operation of a Cogeneration System by the Intelligent Functional Approach. In *A Future for Energy* [2], pp. 597−609. Published also in the International Journal of Energy, Environment and Economics, 1991;1:275−287.
4. Olsommer B, Favrat D, von Spakovsky MR. An Approach for the Time−Dependent Thermoeconomic Modeling and Optimization of Energy System Synthesis, Design and Operation Part I: Methodology and Results. Int J Applied Thermodynamics 1999;2:97−114.
5. Frangopoulos CA, von Spakovsky MR, Sciubba E. A Brief Review of Methods for the Design and Synthesis Optimization of Energy Systems. Int J Applied Thermodynamics 2002;5:151−160.
6. Muñoz JR, von Spakovsky MR. The Application of Decomposition to the Large Scale Synthesis/Design Optimization of Aircraft Energy Systems. Int J Applied Thermodynamics 2001;2:61−76.

7. Oyarzábal B, Ellis MW, von Spakovsky MR. Development of Thermodynamic, Geometric, and Economic Models for Use in the Optimal Synthesis/Design of a PEM Fuel Cell Cogeneration System for Multi−Unit Residential Applications. Journal of Energy Resources Technology 2004;126:21−29.
8. Calise F, Dentice d' Accadia M, Vanoli L, von Spakovsky MR. Single−level optimization of a hybrid SOFC–GT power plant. Journal of Power Resources 2006;159:1169−1185.
9. Pelster F, Favrat D, von Spakovsky MR. The Thermoeconomic and Environomic Modeling and Optimization of the Synthesis, Design, and Operation of Combined Cycles with Advanced Options. Journal of Engineering for Gas Turbines and Power 2001;123;717−726.
10. Mussati SF, Aguirre PA, Scenna NJ. A rigorous, mixed−integer, nonlineal programming model (MINLP) for synthesis and optimal operation of cogeneration seawater desalination plants. Desalination 2004;166:339−345.
11. Andiappan V, Ng DKS. Synthesis of tri−generation systems: Technology selection, sizing and redundancy allocation based on operational strategy. Computers and Chemical Engineering 2016;91:380−391.
12. Martelli E, Carpa F, Consonni S. Numerical optimization of Combined Heat and Power Organic Rankine Cycles – Part A: Design optimization. Energy 2015;90:310−328.
13. Martelli E, Carpa F, Consonni S. Numerical optimization of combined heat and power Organic Rankine Cycles – Part B: Simultaneous design & part−load optimization. Energy 2015;90:329−343.
14. Evins R. Multi−level optimization of building design, energy system sizing and operation. Energy 2015;90:1775−1789.
15. Arcuri P, Beraldi P, Florio F, Fragiacomo P. Optimal design of a small size trigeneration plant in civil users: A MINLP (Mixed Integer Non Linear Programming Model). Energy 2015;80:628−641.
16. Teichgraeber H, Brodrick PG, Brandt AR. Optimal design and operations of a flexible oxyfuel natural gas plant. Energy 2017;141:506−518.
17. Barberis S, Rivarolo M, Traverso A , Massardo AF. Thermo−economic optimization of a real polygenerative district. Applied Thermal Engineering 2016;97;1−12.
18. Zeng Q, Zhang B, Fang J, Chen Z. A bi−level programming for multistage co−expansion planning of the integrated gas and electricity system. Applied Energy 2017;200:192−203.
19. Ondeck A, Edgar TF, Baldea M. A multi−scale framework for simultaneous optimization of the design and operating strategy of residential CHP systems. Applied Energy 2017;205:1498−1511.
20. Fuentes−Cortés LF, Ponce−Ortega JM, Nápoles−Rivera F, Serna−González M, El−Halwagi M. Optimal design of integrated CHP systems for housing complexes. Energy Conversion and Management 2015;99:252−263.

21. Jing R, Wang M, Brandon N, Li N, Chen J, Zhao Y. Economic and environmental multi−optimal design and dispatch of solid oxide fuel cell based CCHP system. Energy Conversion and Management 2017;154:365−379.
22. Yan Y, Zhang C, Li K, Wang Z. An integrated design for hybrid combined cooling, heating and power system with compressed air energy storage. Applied Energy 2018;210:1151−1166.
23. Urbanucci L, Testi D. Optimal integrated sizing and operation of a CHP system with Monte Carlo risk analysis for long−term uncertainty in energy demands. Energy Conversion and Management 2018;157:307–316.
24. Sachs J, Sawodny O. Multi−objective three stage design optimization for island microgrids. Applied Energy 2016;165:798−800.
25. Goderbauera S, Bahlc B, Voll P, Lübbeckeb M, Bardow A, Koster AMCA. An adaptive discretization MINLP algorithm for optimal synthesis of decentralized energy supply systems. Computers and Chemical Engineering 2016;95:38−48.
26. Zhu Q, Luo X, Zhang B, Chen Y. Mathematical modelling and optimization of a large−scale combined cooling, heat and power system that incorporates unit changeover and time−of−use electricity price. Energy Conversion and Management 2017;133:385−398.
27. Sun L, Gai L, Smith R. Site utility system optimization with operation adjustment under uncertainty. Applied Energy 2017;186:450−456.
28. Beck T, Kondziella H, Huard G, Bruckner T. Optimal operation, configuration and sizing of generation and storage technologies for residential heat pump systems in the spotlight of self−consumption of photovoltaic electricity. Applied Energy 2017;604−619.
29. Lythcke−Jørgensen C, Ensinas AV, Münster M. A methodology for designing flexible multi−generation systems. Energy 2016;110:34−54.
30. Toffolo A, Lazzaretto A, Morandin M. The HEATSEP method for the synthesis of thermal systems: An application to the S−Graz cycle. Energy 2010;35:976−981.
31. Toffolo A. A synthesis/design optimization algorithm for Rankine cycle based energy systems. Energy 2014;66:115−127.
32. Voll P, Lampe M, Wrobel G, Bardow A. Superstructure−free synthesis and optimization of distributed industrial energy supply systems. Energy 2012;45:424−435.
33. Wang L, Voll P, Lampe M, Yang Y, Bardow A Superstructure−free synthesis and optimization of thermal power plants. Energy 2015;91:700−711.
34. Dimopoulos GG, Georgopoulou CA, Kakalis NMP. Modelling and optimisation of an integrated marine combined cycle system. *24th International Conference on Efficiency, Cost, Optimization, Simulation and Environmental Impact of Energy Systems, ECOS 2011*, M. Bojic et al., eds., Novi Sad, Serbia, 4−7 July, pp. 1283−1298.
35. Kakalis N, Dimopoulos G, Stefanatos I. Model−based techno−economic assessment and optimization of marine waste heat recovery options. Conseil International des Machines a Combustion (CIMAC) Congress 2013, Shanghai, China, Paper No. 183.

36. Theotokatos G, Livanos G. Techno−economical analysis of single pressure exhaust gas waste heat recovery systems in marine propulsion plants. J. of Engineering for the Maritime Environment 2013;227(2):83−97.
37. Benvenuto G, Trucco A, Campora U. Optimization of waste heat recovery from the exhaust of marine diesel engines. J. of Engineering for the Maritime Environment 2016;230(1):83−94.
38. Kyriakidis F, Sørensen K, Singh S, Condra T. Modeling and optimization of integrated exhaust gas recirculation and multi−stage waste heat recovery in marine engines. Energy Conversion and Management 2017;151:286−295.
39. Yang MH, Yeh RH. Thermodynamic and economic performances optimization of an organic Rankine cycle system utilizing exhaust gas of a large marine diesel engine. Applied Energy 2015;149:1−12
40. Dimopoulos GG, Kougioufas AV, Frangopoulos CA. Synthesis, design and operation optimization of a marine energy system. Energy 2008;33:180−188.
41. Dimopoulos GG, Frangopoulos CA. Synthesis, Design and Operation Optimization of the Marine Energy System for a Liquefied Natural Gas Carrier. Int. J. of Thermodynamics 2008;11:203−211.
42. Baldi F, Ahlgren F, Melino F, Gabrielii C, Andersson K. Optimal load allocation of complex ship power plants. Energy Conversion and Management 2016;124:344−356.
43. Hanglid F. A review on the use of gas and steam turbine combined cycles as prime movers for large ships. Part I: Background and design. Energy Conversion and Management 2008;49: 3458−3467.
44. Hanglid F. A review on the use of gas and steam turbine combined cycles as prime movers for large ships. Part II: Previous work and implications. Energy Conversion and Management 2008;49: 3468−3475.
45. Hanglid F. A review on the use of gas and steam turbine combined cycles as prime movers for large ships. Part III: Fuels and emissions. Energy Conversion and Management 2008;49: 3476−3482.
46. Altosole M, Benvenuto G, Campora U, Laviola M, Trucco A. Waste Heat Recovery from Marine Gas Turbines and Diesel Engines. Energies 2017;10:718.
47. Hanglid F. Variable geometry gas turbines for improving the part−load performance of marine combined cycles − Gas turbine performance. Energy 2010; 35:562−570.
48. Hanglid F. Variable geometry gas turbines for improving the part−load performance of marine combined cycles – Combined cycle performance. Applied Thermal Engineering 2011;31:467−476.
49. Sharma OP, Kaushik SC, Manjunath K. Thermodynamic analysis and optimization of a supercritical CO_2 regenerative recompression Brayton cycle coupled with a marine gas turbine for shipboard waste heat recovery. Thermal Science and Engineering Progress 2017;3:62−74.
50. Hou S, Wu Y, Zhou Y, Yu L. Performance analysis of the combined supercritical CO_2 recompression and regenerative cycle used in waste heat recovery of marine gas turbine. Energy Conversion and Management 2017;151:73−85.

51. Tse LKC, Wilkins S, McGlashana N, Urbanb B, Martinez−Botasa R. Solid oxide fuel cell/gas turbine trigeneration system for marine applications. Journal of Power Sources 2011;196;3149−3162.
52. Welaya YMA, Mosleh M, Ammar NR. Thermodynamic analysis of a combined gas turbine power plant with a solid oxide fuel cell for marine applications. Int. J. Nav. Archit. Ocean Eng. 2013;5:529−545.
53. Armellini A, Daniotti S, Pinamonti P, Reini M. Evaluation of gas turbines as alternative energy production systems for a large cruise ship to meet new maritime regulations. Applied Energy 2018;211;306–317.
54. Doulgeris G, Korakianitis T, Pilidis P, Tsoudis E. Techno−economic and environmental risk analysis for advanced marine propulsion systems. Applied Energy 2012;99:1–12.
55. El−Gohary MM. The future of natural gas as a fuel in marine gas turbine for LNG carriers. Proc IMechE Part M: J Engineering for the Maritime Environment 2012;226:371–377.
56. Dimopoulos GG, Frangopoulos CA. Optimization of energy systems based on Evolutionary and Social metaphors. Energy 2006;33:171−179.
57. Dimopoulos GG. Mixed−variable engineering optimization based on evolutionary and social metaphors. Computer Methods in Applied Mechanics and Engineering 2007;196:803−817.
58. Stojiljković MM, Stojiljković MM, Blagojević BD. Multi−Objective Combinatorial Optimization of Trigeneration Plants Based on Metaheuristics. Energies 2014;7:8554−8581

Chapter 2

Description of the System and the Optimization Problem

In the present work, the synthesis, design and operation optimization of integrated energy systems of ships is studied. The integration of the system is achieved with the inclusion of steam bottoming cycles, by which the overall system acquires the potential of covering the different types of the energy loads, that is, the different forms of propulsion, electric and thermal energy demands.

Figure 2.1 presents the superconfiguration of the energy system, which consists of the following:

- Main engines (two−stroke or four−stroke Diesel engines or gas turbines), which are mechanically coupled to the propeller.
- Heat recovery steam generators (HRSG), exploiting thermal energy of exhaust gases and cooling circuits of main engines.
- Steam turbines producing mechanical and/or, with the addition of electric generators, electric energy.
- Diesel−generator sets.
- Exhaust gas boiler.
- Auxiliary boiler.

The dots between the components of the same type imply that the number of components of each type is not predefined and is to be determined by the optimization. Of course, this characteristic has important implications on the overall modeling and optimization procedure developed.

As seen, the main engines are mechanically coupled to the propeller. The method developed in the present work is independent of the type of the prime mover and two-stroke, four-stroke Diesel engines or gas turbines can be used, each type of prime mover being connected to the propeller with the appropriate coupling (meaning that gearboxes are needed for the four-stroke Diesel engines and gas turbines). The concept of “all-electric ship”, in which the prime movers are coupled to electric generators and the propellers are moved by electric motors is not studied in the present work, however, the method can be conveniently applied to all−electric ships too. The exhaust gases from the prime movers are used for the production of steam in the Heat Recovery Steam Generators (HRSG). In Figure 2.1 this interconnection is symbolically represented by a simple connecting line, but in the method developed several possibilities about the way the HRSGs are connected to the prime movers are studied, as will be seen in Chapter 4 where the modeling and simulation of the overall system is presented.

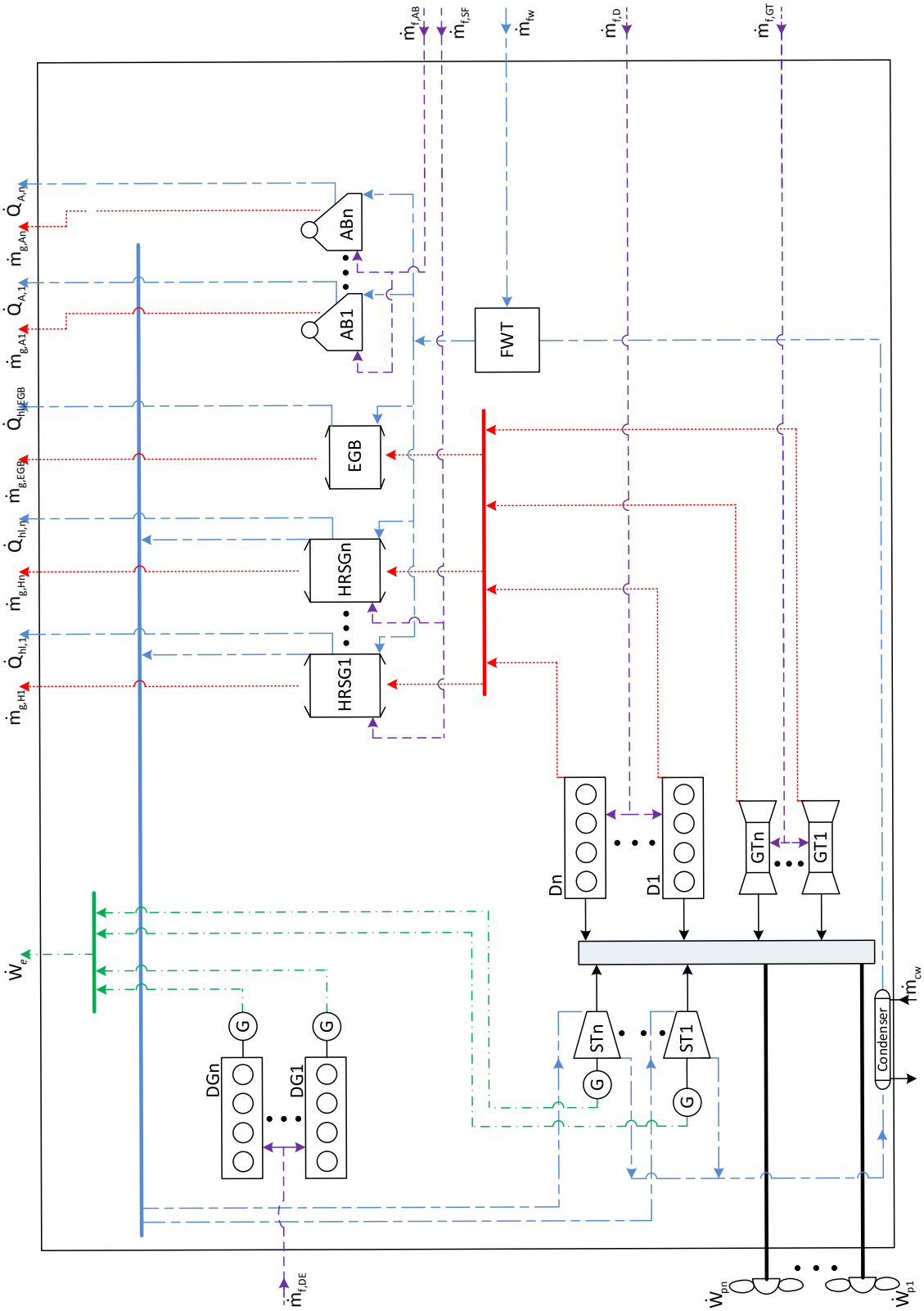

Figure 2.1: Superconfiguration of the ship energy system.

For the cases of the Diesel engines, the possibility of the waste heat recovery from the charge air and the jacket water are also used in the design and operation of the HRSGs. The HRSGs produce superheated steam for feeding steam turbines and saturated steam for serving thermal loads. Except of the HRSGs, another type of exhaust gas boiler is envisaged, producing steam for covering thermal loads only, which is symbolized as EGB (exhaust gas boiler) in Figure 2.1.

The steam turbines are mechanically coupled to the propellers, contributing to the propulsion load, but there is also the possibility that they can serve electric loads with the use of generators. It is considered that the power production of the steam turbines can be divided between these two different loads.

As aforementioned, apart from the bottoming cycle components, in the system superconfiguration there are also Diesel-generator sets and auxiliary boilers for potentially serving electric and thermal loads. It is important to note that these fuel consuming components are going to be present in each ship system either way, as there are energy consuming operating modes of ships (e.g. during harbor residence periods), in which the bottoming cycle of course does not operate. Furthermore, it is possible that the optimization may result in a system with no bottoming cycle. In such a case, these components are necessary again and will operate not only in harbor but also in other modes.

It is considered that the ship annual energy profile can be approximated with a predefined number of operating modes during which the three types of loads (propulsion, electric and thermal power) have constant values. These modes can be thought of as representative operating conditions for the expected actual modes of operation that will be encountered through the lifetime of the ship. The duration of each mode is also defined prior to the optimization problem solution.

The complete SDO optimization problem, as mentioned in the Introduction, is stated and solved for the system of Fig. 2.1. From the solution of the SDO optimization problem, the following decisions are taken, according to the three distinct levels:

Synthesis: On the synthesis level, the appropriate components that should be included in the system, as well as the functional relations that have to be established among them in order to cover the energy demands are sought. On this level, issues like the appropriate number of prime movers, number of HRSGs, interconnections between prime movers and HRSGs, number of steam turbines, number of Diesel−generator sets are addressed.

Design: On this level, the nominal characteristics of the present components are determined, as for example, the nominal power rating of the prime movers and the Diesel−generator sets. For the bottoming cycle components, the power ratings are determined, along with other intensive and extensive thermodynamic properties of the working fluids at design point operation. The design characteristics of the components have an important effect on off−design operating efficiency, and ultimately on the efficiency of energy resources utilization of the overall system during all of the operating modes of the ship.

Operation: The appropriate loading of each operating component in order for the energy loads to be covered is determined for each operating mode. This loading is dependent

upon several problem specific parameters, like the magnitudes of the loads to be covered, the time length of the different operating modes, the fuel and operating costs, and of course on the decisions made regarding the synthesis and the design of the system. On this level, decisions to be taken include the loading of the main engines, the allocation of the waste heat sources to the waste heat recovery appliances and the allocation of the useful power produced by the bottoming cycle among the various energy demands (e.g., the part of the power of a steam turbine used for propulsion, and the part used for feeding electric loads).

It can be argued that certain decisions to be taken on the operation level could also be thought of as being parts of the synthesis level. For example, the appropriate allocation of the power produced by a bottoming cycle steam turbine between the propulsion or electric loads in each of the operating modes, defines the relative magnitude of the power delivered to each of these loads, but at the same time also dictates the very inclusion of the steam bottoming cycle or the need for covering the electric loads with the use of fuel fed Diesel−generator sets, which should be included in the system.

References

1. Waste Heat Recovery System (WHRS) for Reduction of Fuel Consumption, Emissions and EEDI. MAN Diesel and Turbo, 5510-0136-03ppr, Aug 2014, Denmark.
2. Thermo Efficiency System for Reduction of Fuel Consumption and CO_2 Emission. MAN Diesel and Turbo, 5510-0030-03ppr. Oct 2014, Denmark.
3. Knudsen TS, Exhaust gas for power generation – How efficient are state–of−the–art methods? Ship Efficiency, 1st International Conference, Hamburg, October 8-9 2007.

Chapter 3

System Components Modeling

In the present chapter, design and off-design simulation models of individual components are presented, which have been developed so that the simulation of the whole system is synthesized and connected to the optimization software. The following prime movers are considered: (a) two−stroke Diesel engines, (b) four−stroke Diesel engines, (c) five configurations of gas turbines. The bottoming cycle components, that is the heat recovery steam generators and steam turbines, are modeled with detailed computational procedures that not only perform their performance simulation, but are based on detailed calculations the outcome of which includes the determination of their internal structure and several of their design details. Such an approach is of utmost importance for the evaluation of the off−design performance of these components. At the end of the chapter, the models related to auxiliary components are described. Apart from the technical aspects, capital cost estimations are given for each type of component.

3.1 Two−stroke Diesel Engines

From an integrated system's point of view, the most important technical quantities of interest concerning the prime movers (independently of their type) are their fuel consumption and the properties of their exhaust gases. The fuel consumption is expected to have a predominant contribution to the operational expenses, while the properties of the exhaust gases have an important effect on the potential for the utilization of their thermal energy content in steam bottoming cycles.

The models developed for two−stroke Diesel engines are based on regression analysis of data available from manufacturers and they are adequate for the SDO optimization Detailed thermodynamic and fluid flow models are computationally very heavy and, since they are called by the optimizer thousands of times, they would require extremely long time for the solution of the problem, that would detract from the main focus of the work.

The data were collected from the on line Computerized Engine Application System (CEAS) program of the MAN Diesel engines manufacturer [1], and are adequate for developing regression models for the quantities of interest (fuel consumption and exhaust gas properties) with only inputs the maximum continuous rating and the load factor of the engines. In this specific application, the user has to choose between official catalogue engines and replaced (or modified) ones, and for the present work only official catalogue data were used. Additionally, the data was confined to standard heavy fuel engines, and the case of dual fuel engines was not considered. Another important parameter is also the choice

of the compliance of the engine with the Tier II or Tier III regulations for emissions. Without restricting the generality of the optimization method, in the present modeling procedure only Tier II engines were considered.

The user is prompted to choose among several different engines with varying nominal power output. The power output is also a function of the number of cylinders of the engine, which is used as input to the CEAS program.

The data was collected for a maximum continuous rating (MCR) range of 10−83 MW, approximately. In the procedure of selecting engines, the main guideline was the choice of a set of MCR values appropriate for the regression to be performed. At the same time, consideration was taken in order to choose the minimum possible number of cylinders for a desired value of MCR (or a region close to this value).

For a successful regression analysis, it is important to collect data of Diesel engines of similar type and in particular of similar stroke to bore ratio. More specifically only super-long stroke engines were used. This type is also the most usually encountered in practice. All of the engines considered were of the latest electronically controlled technology. The results of the regression analysis are as follows.

The specific fuel oil consumption of the two−stroke Diesel engines is estimated with the equation

$$sfoc_{2-S,base} = a + b\ln f_l + c\left(\ln f_l\right)^2 + d\left(\ln f_l\right)^3 + e\left(\ln f_l\right)^4 + f\left(\ln f_l\right)^5 + \\ + g/MCR + h/MCR^2 + i/MCR^3 + j/MCR^4 + k/MCR^5 \tag{3.1}$$

where

MCR	maximum continuous rating of the engine in kW, range 10000−83000 kW
f_l	load factor given as percentage of the MCR, in the range 10 − 100%
$sfoc_{2\text{-}S,base}$	specific fuel oil consumption in gr/kWh.

The maximum absolute error of the regression with respect to the data of CEAS for Eq. (3.1) is ε = 0.93% occurring in a region with a rather low MCR, and the coefficient of determination is R^2=0.988. The regression coefficients are reported in Table 3.1.

Table 3.1: Coefficients for Equation (3.1).

a	-1295.47263397025	g	190821.995075997
b	2438.18952262072	h	-2862722896.71702
c	-1556.11464220056	i	21777694084450.5
d	483.951873881301	j	-7.09961304448649E+16
e	-73.9862532113159	k	8.21065459958556E+19
f	4.46320111809836		

The specific fuel oil consumption calculated with Eq. (3.1) is denoted as a *base* sfoc, because it represents the fuel consumption when the engine operates at specified

environmental conditions P_{env} = 1 bar, T_{env} = T_{sea} = 25°C and the fuel has LHV = 42700 kJ/kg. Thus, a correction is made according to Eq. (3.2)

$$sfoc_{2-S} = sfoc_{2-S,base}\frac{42700}{LHV_{actual}}\left[1+0.0002\left(25\text{-}T_{env}\right)-0.00002\left(1000-P_{env}\right)+0.006\left(25.0-T_{sea}\right)\right] \tag{3.2}$$

where:

LHV_{actual}	the LHV of the fuel actually used
T_{env}	atmospheric temperature in ^{o}C
T_{sea}	sea water temperature in ^{o}C
P_{env}	atmospheric pressure in mbar.

The exhaust gas mass flow rate of the two−stroke Diesel engines is given by the equation

$$\dot{m}_{g,2-S} = \exp\left(a+b/MCR+c\ln MCR\right)\times f_{mod}$$
$$f_{mod} = \begin{cases} f_l \Big/ \left(d_1+e_1 f_l+f_1\sqrt{f_l}\right), & \text{for} \quad f_l \le 30 \\ d_2 f_l + e_2 , & \text{for} \quad 30 < f_l < 35 \\ f_l \Big/ \left(d_3+e_3 f_l+f_3\sqrt{f_l}\right), & \text{for} \quad f_l \ge 35 \end{cases} \tag{3.3}$$

where $\dot{m}_{g,2-S}$ is the mass flow rate in kg/s and the inputs are set in the same way as for Eq. (3.1). The regression has ε = 0.84 % and R^2=0.9983 and the related coefficients are reported in Table 3.2. It is noted that the change of the equation in the load factors of 30% and 35% is due to the initiation of the operation of the engines blower in such low loading.

Table 3.2: Coefficients for Equation (3.3).

a	-5.67293497774115	d_2	-2.45616599999998E-03
b	-337.358555458333	e_2	0.508764598999999
c	0.956426808182649	d_3	99.2380932921421
d_1	-63.0637026295879	e_3	0.70666485205986
e_1	-4.31862595736187	f_3	-6.97669704062126
f_1	47.7672564816052		

The exhaust gas temperature of the two stroke Diesel engines is given by the equation

$$T_{g,2-S} = \begin{cases} a_1 b_1^{\,f_l} f_l^{\,c_1} , & \text{for} \quad f_l \le 30 \\ a_2 f_l + b_2 , & \text{for} \quad 30 < f_l < 35 \\ \exp\left(a_3+b_3 f_l+c_3 f_l^{\,2}\right) , & \text{for} \quad f_l \ge 35 \end{cases} \tag{3.4}$$

where $T_{g,2-S}$ is the exhaust gas temperature in ^{o}C and the inputs are set in the same way as for Eq. (3.1). For Eq. (3.4) it is ε=0.90%, R^2=0.989 and the related coefficients are presented in Table 3.3.

Table 3.3: Coefficients for Equation (3.4).

a_1	33.2515026494697	b_2	-11.9999999999999
b_1	0.962399049025347	a_3	6.08308573382902
c_1	0.919161259303835	b_3	-1.64281445770261E-02
a_2	8.4	c_3	1.12049849574961E-04

In recent years, a trend has appeared among the manufacturers towards building two−stroke engines the operation of which is more suitable for combined cycle applications [2,3]. The operation is modified with respect to a standard engine mainly by bypassing an amount of the exhaust gas past the turbochargers, from full load operation down to the load factor of 50%. Other modifications include the exhaust valves opening timing as well as the fuel injection timing, which have been possible recently due to the development of electronic control. The turbocharger bypass results in a lower exhaust gas mass flow rate and higher temperature, which is more suitable for heat recovery applications. Of course, a slight increase in the prime mover's fuel consumption is observed, but the overall mechanical power production is expected to be more efficient by employing power turbines and mainly double pressure steam cycles [2,3].

The resulting increase of the exhaust gas temperature ΔT_g is generally of the order of 65^{o}C. In the present work, ΔT_g is estimated with a regression analysis of confidential data and is a function of the load factor. The related mathematical formula is

$$\Delta T_g = a\, f_L^b \exp\left(c f_L\right) \tag{3.5}$$

with the related coefficients reported in Table 3.4a. This temperature difference is to be added to the temperature derived by Eq. (3.4) when the two−stroke Diesel engine is modified for combined cycle applications.

Table 3.4a: Coefficients for Equation (3.5).

a	10.3423912576824
b	0.497439646758772
c	-4.44656941315581*e*-03

The increase in fuel consumption is estimated with Eq. (3.6) and is at the order of 2 gr/kWh:

$$\Delta sfoc = a f_L^7 + b f_L^6 + c f_L^5 + d f_L^4 + e f_L^3 + f f_L^2 + g f_L + h \tag{3.6}$$

The related coefficients are reported in Table 3.4b. The appropriate data for developing Eq. (3.6) is derived from [4].

Table 3.4b: Coefficients for Equation (3.6).

a	1.18849972127075E-12	e	1.88617803562725E-02
b	−2.60814446082216E-09	f	−1.01723852643377
c	1.0674870988134E-06	g	28.8615937428503
d	−1.94231741300805E-04	h	−336.394237667221

The calculation of the exhaust gas mass flow rate $\dot{m}_{g,\Delta}$ is based on first law of Thermodynamics and certain assumptions, and is described in Appendix A. The resulting equation is

$$\dot{m}_{g,\Delta} = \dot{m}_{g,2-S} \frac{T_{g,2-S} - T_{ref}}{T_{g,2-S} + \Delta T_g - T_{ref}} + \frac{1}{c_{pg}\left(T_{g,2-S} + \Delta T_g - T_{ref}\right)} \frac{\dot{W}_D LHV}{3600000} \Delta sfoc \qquad (3.7)$$

where:

$\dot{m}_{g,\Delta}$	exhaust mass flow rate for modified operation (kg/s)
T_{ref}	reference temperature (typically 25^{o}C)
c_{pg}	exhaust gas specific heat capacity (kJ/kgK)
$\dot{W}_D$	brake power (kW)
LHV	fuel lower heating value (kJ/kg).

In Eq. (3.7), temperatures are given in ^{o}C.

3.2 Four−stroke Diesel Engines

As with the case of two-stroke engines, the regression models for the four-stroke Diesel engines take as inputs the MCR of the engine and the load factor f_l. The main differences are that the MCR is limited up to the value of 21 MW (due to the unavailability of engines with higher MCR), and the load factor is limited down to the value of 20 %. The base *sfoc* of the four-stroke engines is represented by Eq. (3.8) and the related coefficients are presented at Table 3.5

$$sfoc_{4-S,base} = a + b\ln MCR + c(\ln MCR)^2 + d(\ln MCR)^3 + e(\ln MCR)^4 + f(\ln MCR)^5 + gf_l + hf_l^2 + if_l^3 + jf_l^4 \qquad (3.8)$$

where

MCR	Maximum Continuous Rating of the engine in kW, range 5−21 MW
f_l	load factor in the range 20 to 100%
$sfoc_{4\text{-}S,base}$	specific fuel oil consumption in gr/kWh.

Table 3.5: Coefficients for Equation (3.8).

a	-678887.387229571	f	12.195741292492
b	383687.174062416	g	-12.5130349815109
c	-86467.7384338149	h	0.308163035452439
d	9719.36971772643	i	-3.3047702333155E-03
e	-544.977166168292	j	1.27515182648887E-05

The exhaust gas mass flow rate and temperature are given by the Eqs. (3.9) and (3.10), respectively, with the related coefficients presented in Tables (3.6) and (3.7)

$$\dot{m}_{g,4-S} = \left[aMCR^3 + bMCR^2 + cMCR + d \right] \times \left[ef_l^3 + ff_l^2 + gf_l + h \right] \tag{3.9}$$

where $\dot{m}_{g,4-S}$ is the mass flow rate in kg/s and the inputs are set in the same way as for Eq. (3.8).

Table 3.6: Coefficients for Equation (3.9).

a	-2.15333815223378E-12	e	-1.9614900920825E-06
b	9.36530362157392E-08	f	3.69303720484067E-04
c	1.02464367788971E-03	g	-1.30249958062006E-02
d	1.95718695165748	h	0.561755635436517

$$T_{g,4-S} = \left[a + bMCR + c/MCR^2 \right] \times \left[df_l^3 + ef_l^2 + ff_l + g \right] \tag{3.10}$$

In Eq. (3.10) $T_{g,4-S}$ is the exhaust gas temperature in ^{o}C and the inputs are set in the same way as for Eq. (3.8).

Table 3.7: Coefficients for Equation (3.10).

a	302.460757997832	e	-3.3937952254995E-04
b	4.61515815642556E-04	f	0.012694694942915
c	282274912.948458	g	1.04404874116135
d	2.08274512078117E-06		

3.3 Gas Turbines

For the simulation of gas turbines as prime movers of ships, a dedicated software has been developed in collaboration with the Laboratory of Thermal Turbomachines of the School of Mechanical Engineering, NTUA [5]. The software can be utilized for simulations of several configurations of gas turbines, such as single shaft, twin spool with no separate power turbine, single shaft with separate power turbine and twin spool with separate power turbine. Furthermore, combinations with intercooling between the two compressors, recuperation of the exhaust gases between the compressor and the burner and reheating

before the power turbine can be studied. A total of 22 configurations are simulated. In Figure 3.1, the most complicated configuration is depicted.

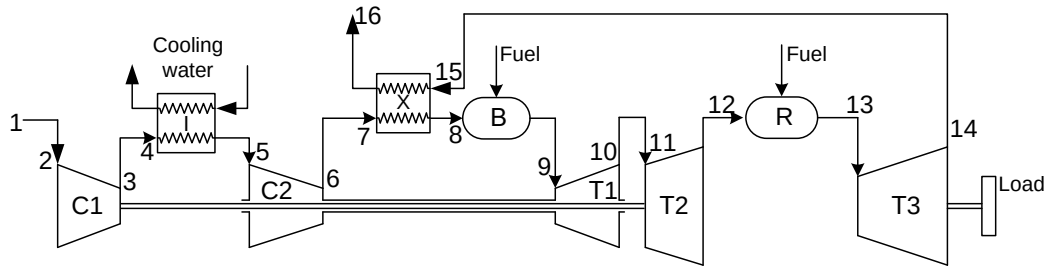

Figure 3.1: Schematic of the most advanced configuration of gas turbine simulated with software [5].

The software package requires that certain input data are defined by the user. With values defined for the inputs, the analysis of the performance is executed at the design point or at any off-design point defined by the user. The input data for the various configurations and the required data for off-design analysis are presented in Tables 3.8 and 3.9.

Table 3.8: Input data for the design point.

Atmospheric pressure
Atmospheric temperature
Atmospheric relative humidity
Exit pressure of the exhaust gas from gas turbine configuration
Rotational speed of power turbine
Power output of the gas turbine plant
Maximum temperature of the working medium
Pressure ratio of the first compressor
Pressure ratio of the second compressor (if applicable)
Polytropic efficiency of the compressors
Polytropic efficiency of the turbines
Effectiveness of the intercooler
Temperature of coolant
Effectiveness of recuperator

Table 3.9: Input data for off design simulation.

Atmospheric pressure
Atmospheric temperature
Atmospheric relative humidity
Exit pressure of the exhaust gas from gas turbine power plant
Rotational speed of power turbine
Power output of the gas turbine plant

The user can also select one of four different fuels and give its lower heating value. The fuels are the following: two different types of Diesel oil with equivalent chemical

formulas $C_{12.9}H_{22.9}$ and $C_{12.8}H_{23.7}S_{0.05}$, methane CH_4, and natural gas with the composition presented in Table 3.10.

Table 3.10: Compositions of natural gas used in the gas turbines simulation program.

Compound	Synthesis % v	Synthesis % w
CH_4	88.5	79.61
C_2H_6	4.7	7.93
C_3H_8	1.6	3.96
C_4H_{10}	0.2	0.65
N_2	5.0	7.85

With the definition of the fuel and the design point inputs, a thermodynamic analysis is executed throughout the configuration. This analysis determines the state of the working medium at all the points of interest inside the configuration and it also determines sizing parameters of the compressors and turbines. These quantities are required for creating performance maps for predicting the off−design operation of these components and, consequently, of the overall configuration.

Due to computational reasons, this software was not appropriate for being used with the optimization software. Instead, it has been used in order to produce sufficient results that have been used for development of regression equations that give fuel consumption and exhaust gas properties of the five selected configurations depicted in Figure 3.2 that operate either with Diesel oil with chemical formula $C_{12.8}H_{23.7}S_{0.05}$ or with natural gas with the composition reported in Table 3.10. Configurations 1 and 2 are considered operating only at constant rational speed of 3000 RPM, while configurations 3, 4 and 5 were simulated both for constant rotational speed of 3000 RPM and for variable rotational speed with 3000 RPM at full load and with variation according to the cubic propeller law at part load operation.

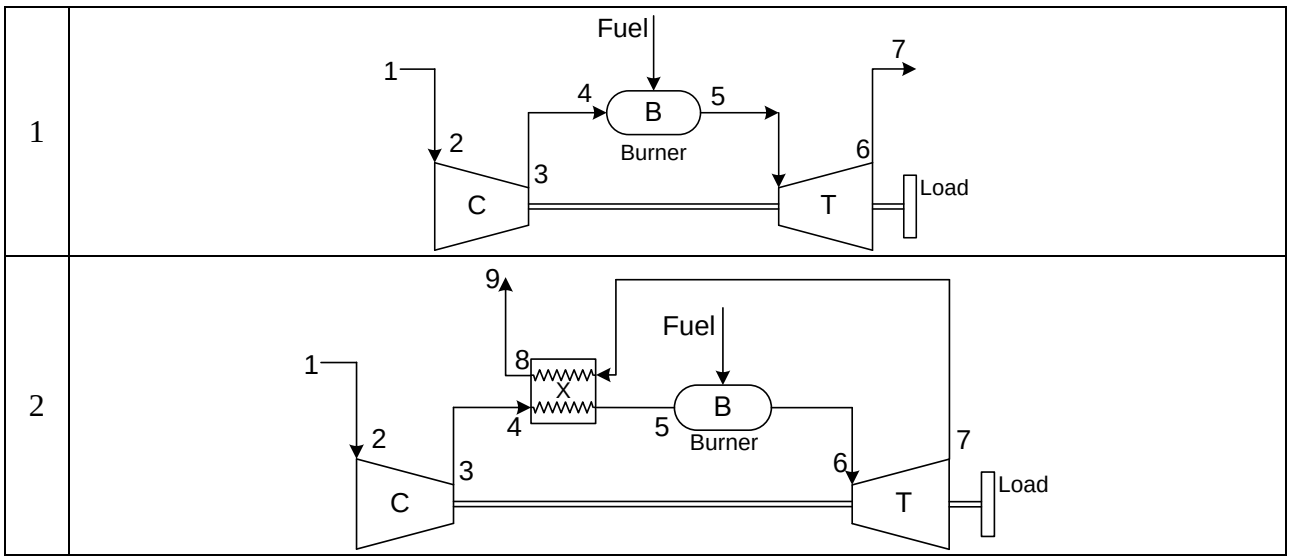

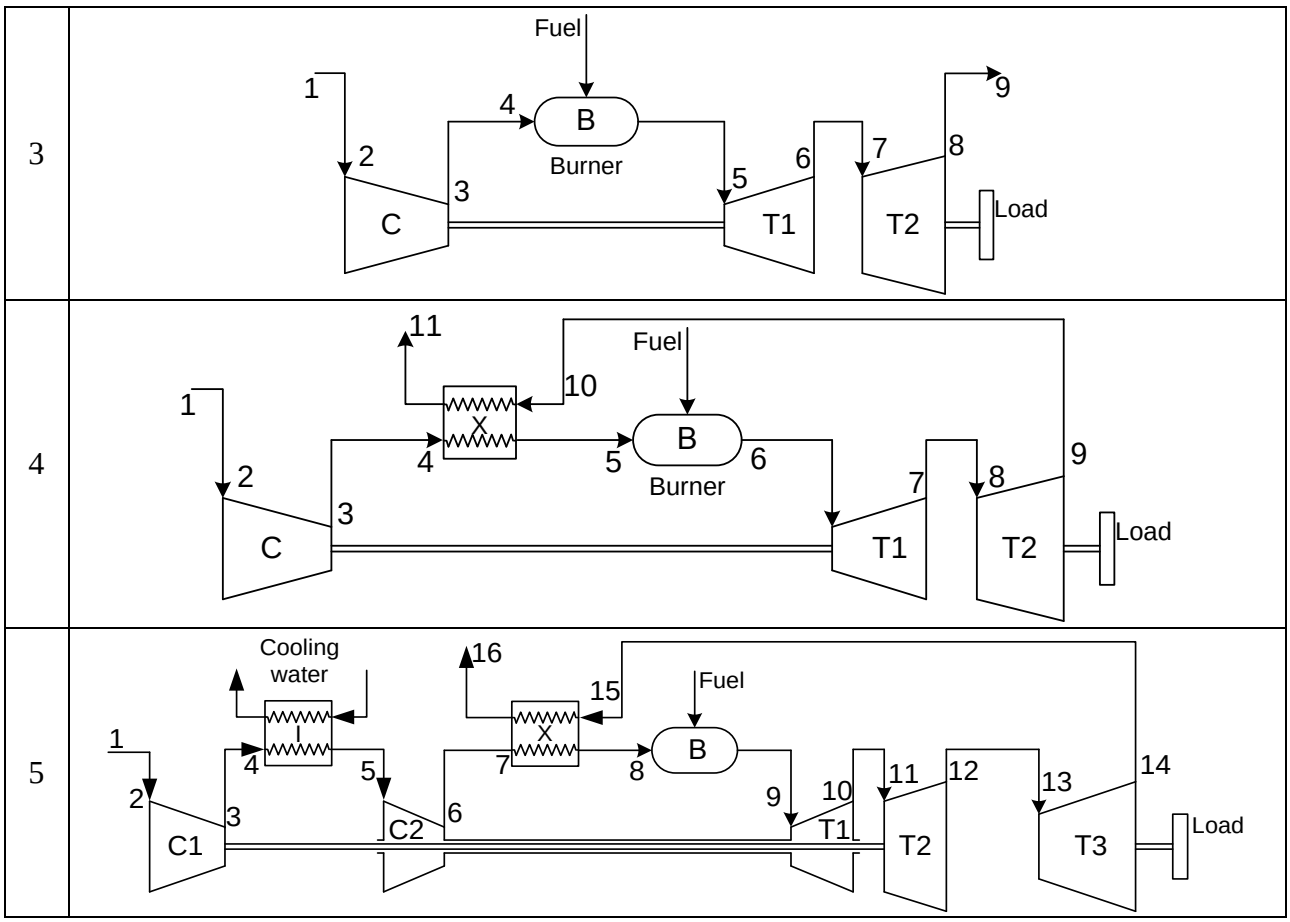

Figure 3.2: Schematics of the five types of gas turbines of specific interest for the present work.

In order to determine technically sound values of the overall pressure ratio and the maximum temperature of the cycle at the design, a two−variable exhaustive search was performed in which the thermal efficiency for each pair of these input variables was evaluated. The finally selected values were those that resulted in the highest thermal efficiency. At the same time, the specific power of the finally designed engine was monitored in order to be close to the values expected by the common practice, and also inside the limits suggested by the program developers. Restrictions were also posed on the maximum pressure ratio and the maximum temperature of the cycle to values that are technologically achievable at the current state of development. Thus, the maximum pressure ratio was confined to the value of 26 and the maximum temperature of the cycle was confined to the value of 1500°C.

For determining the polytropic efficiencies, data concerning the operation of actual existing marine gas turbines was collected, and the polytropic efficiencies used in the simulation program were tuned until an overall simulated cycle with the values of thermal efficiency, mass flow rates and maximum and outlet temperatures at nominal load operation were matched to the ones of actual engines. The finally used values for the polytropic efficiency are equal to 0.9 for compressors and 0.89 for turbines. These values are also very

close to the values suggested by the program developers for being in accordance to the present and the near future technological level of gas turbines development.

In Table 3.11 the input parameters used for the simulation are summarized and output data considering the fuel consumption and exhaust gas properties at design point operation are presented. It is noted that the mass flow rates presented in Table 3.11 are for a nominal power output of 20 MW for all the configurations.

Table 3.11: Input parameters and indicative outputs for the five gas turbine configurations.

Property	Configuration				
	1	2	3	4	5
Inputs					
r_{c1} (–)	26	10	26	10	3.5973
r_{c2} (–)	-	-	-	-	6.1159
T_{max} (°C)	1175	1225	1500	1275	1500
$\varepsilon_{intercooler}$ (–)	-	-	-	-	0.85
$\varepsilon_{recuperator}$ (–)	-	0.9	-	0.9	0.9
Outputs					
$\dot{m}_{g,MDO}$ (kg/s)	72.178	66.770	50.490	62.028	44.415
$T_{g,exh,MDO}$ (°C)	451	393	563	402	381
SFC_{MDO} (gr/kWh)	228.629	199.363	213.635	193.753	180.998
$\dot{m}_{g,NG}$ (kg/s)	69.469	65.029	48.930	60.368	43.280586
$T_{g,exh,NG}$ (°C)	453	395	568	405	385
SFC_{NG} (gr/kWh)	209.365	184.742	198.094	179.588	168.177

The nominal power rating has no effect on the calculation of the fuel oil consumption, as the results of the simulation program have indicated. However, the atmospheric temperature has an important impact on the fuel consumption, and the related equations are set up as functions of both the load factor and the atmospheric temperature.

Most of the equations derived for the fuel oil consumption from the regression analysis have the same form and only the coefficients are modified according to the gas turbine type and the choices of Marine Diesel Oil or natural gas and the constant or variable rotational speed. This general equation has the form

$$SFC_{GT} = a + b/f_l + cT_e + d/f_l^2 + eT_e^2 + f\frac{T_e}{f_l} + g/f_l^3 + hT_e^3 + i\frac{T_e^2}{f_l} + j\frac{T_e}{f_l^2} \quad (3.11)$$

where

T_e environmental temperature in the range -25 to 45°C (input in °C)
f_l load factor in the range 0.2 to 1
SFC_{GT} specific fuel oil consumption in gr/kWh.

The coefficients related to the gas turbine type, fuel and constant or variable rotational speed are tabulated in Appendix B.

For the cases of gas turbine type 5 with variable rotational speed and natural gas as well as of gas turbine type 3 with constant rotational speed and natural gas, Eq. (3.12) is valid:

$$\begin{aligned} SFC_{GT} = a + b\ln f_l + cT_e + d\left(\ln f_l\right)^2 + eT_e^2 + fT_e \ln f_l \\ + g\left(\ln f_l\right)^3 + hT_e^3 + iT_e^2 \ln f_l + jT_e\left(\ln f_l\right)^2 \end{aligned} \tag{3.12}$$

For the exhaust gas mass flow rates, Eqs. (3.13a) – (3.13d), have been derived, which are valid for nominal power rating of 20 MW. For different nominal power, Eq. (3.14) is used. The related coefficients are presented in Tables B5 – B8, that indicate also which equation is applicable for each combination of configuration, fuel and variable or constant rotational speed. The value of $\dot{m}_{g,GT,base}$ is given in kg/s.

$$\dot{m}_{g,GT,base} = a + bf_l + cT_e + df_l^{\,2} + eT_e^2 + fT_e f_l + gf_l^{\,3} + hT_e^3 + iT_e^2 f_l + jT_e f_l^{\,2} \tag{3.13a}$$

$$\begin{aligned} \dot{m}_{g,GT,base} = a + b\ln f_l + cT_e + d\left(\ln f_l\right)^2 + eT_e^2 + fT_e \ln f_l \\ + g\left(\ln f_l\right)^3 + hT_e^3 + iT_e^2 \ln f_l + jT_e\left(\ln f_l\right)^2 \end{aligned} \tag{3.13b}$$

$$\dot{m}_{g,GT,base} = a + bf_l + cf_l^{\,2} + df_l^{\,3} + ef_l^{\,4} + ff_l^{\,5} + gT_e + hT_e^2 + iT_e^3 + jT_e^4 + kT_e^5 \tag{3.13c}$$

$$\begin{aligned} \dot{m}_{g,GT,base} = a + b\ln f_l + c\left(\ln f_l\right)^2 + d\left(\ln f_l\right)^3 + e\left(\ln f_l\right)^4 + f\left(\ln f_l\right)^5 \\ + gT_e + hT_e^2 + + iT_e^3 + jT_e^4 + kT_e^5 \end{aligned} \tag{3.13d}$$

$$\dot{m}_{g,GT} = \dot{m}_{g,GT,base}\frac{\dot{W}_n}{20} \tag{3.14}$$

For the exhaust gas temperature, the equations derived were similar to the ones of the mass flow rate, and they will not be repeated therefore. The only difference is that $\dot{m}_{g,GT,base}$ in Eqs. (3.13) is replaced by $T_{g,GT}$. The related coefficients are also given in Appendix B.

3.4 Heat Exchangers

In engineering practice, the thermal problems involving heat exchangers can be categorized into one of two general groups of problems, namely the *rating problem* and the *sizing problem*, which can be formally defined as follows [6]:

Rating Problem: Determination of heat transfer and pressure drop of either an existing or an already sized heat exchanger. Inputs to the rating problem are the heat exchanger

construction, flow arrangement and overall dimensions, complete details on the materials and surface geometries on both sides, including their non-dimensional heat transfer and pressure drop characteristics (e.g. Nusselt number as function of Reynolds number), fluid flow rates, inlet temperatures, and fouling factors. The fluid outlet temperatures, total heat transfer rate, and pressure drops on each side of the exchanger are then determined in the rating problem.

Sizing Problem: Design of a new heat exchanger, i.e. the determination/selection of an exchanger construction type, flow arrangement, materials of tubes, plates and fins, and the physical size of an exchanger to meet the specified heat transfer and pressure drops within all specified constraints. The sizing problem is also referred to as the *design problem*.

Both of these types of problems are tackled with the appropriate computational procedures for the applications mentioned. The thermal analysis of problems involving heat exchangers has been carried out with the use of two widely used analytical methods, namely the ε−NTU and, mostly, the P−NTU method [6,7]. In this approach, dependent and independent dimensionless groups are formulated by the problem's variables and parameters of interest, and then the relationships between these dimensionless groups are determined for different flow arrangements. A brief description of these methods follows.

3.4.1 The ε−NTU method

In the ε−NTU method, the heat transferred between the two fluids is computed with the equation

$$\dot{Q} = \varepsilon C_{\min}(T_{h,i} - T_{c,i}) \tag{3.15}$$

where

ε	effectiveness of the heat exchanger,
C_{min}	the minimum of the heat capacity rates for the two fluid streams defined below,
$T_{h,i}$	inlet temperature of the hot fluid,
$T_{c,i}$	inlet temperature of the cold fluid.

The heat capacity rate is defined for each stream as

$$C = \dot{m}c_p \tag{3.16}$$

where

$\dot{m}$	mass flow rate of the fluid,
c_p	specific heat capacity of the fluid.

The C_{min} is an important parameter of the problem, determining the "ability" of the corresponding fluid to carry the heat transferred, the other one acting partially as a heat sink or source with a smaller temperature change.

The effectiveness ε is defined as the ratio of the heat actually transferred to the heat that would be transferred between the two fluids in a pure counter flow heat exchanger with heat transfer area large enough (theoretically infinite), so that the outlet temperature of the

C_{min} fluid to be equal to the inlet temperature of the other one. The effectiveness of a heat exchanger depends on the type of flow arrangement (counterflow, crossflow, etc.), the Number of Transfer Units (NTU) defined below and the ratio of the heat capacity rates:

$$\varepsilon = \varepsilon\left(NTU, C^*, \text{flow arrangement}\right) \tag{3.17}$$

$$C^* = C_{\min} / C_{\max} \tag{3.18}$$

The Number of Transfer Units is defined as the ratio of the overall thermal conductance *UA* to the C_{min}:

$$NTU = \frac{UA}{C_{\min}} \tag{3.19}$$

where

- A total area of the heat transfer surface,
- U overall heat transfer coefficient.

The product *UA* is given by the equation

$$\frac{1}{UA} = \frac{1}{(\eta_o hA)_h} + \frac{1}{(\eta_o h_f A)_h} + R_w + \frac{1}{(\eta_o h_f A)_c} + \frac{1}{(\eta_o hA)_c} \tag{3.20}$$

where

- η_o the (extended) surface overall heat transfer efficiency on the side of the hot (h) and cold (c) fluid,
- h convective heat transfer coefficient on the side of the hot (h) and cold (c) fluid,
- h_f inverse of the fouling resistance $(h_f = 1/r_f)$,
- R_w thermal resistance of the wall between the two streams.

In order to apply the ε−NTU method, in addition to the estimation of the *NTU* for a given heat exchanger, the type of flow arrangement has also to be specified. This can vary between counterflow, parallel and crossflow arrangements; whether each of the individual fluid streams is “mixed” or “unmixed” is also considered. The term “mixed” means that there are no temperature gradients in the bulk of the stream in directions other than the main flow direction.

Relationships for the computation of ε as a function of *NTU*, C^* and flow arrangement can be found in [6,7].

The main concern for the application of the ε−NTU method is the proper determination of the heat transfer coefficients for a given type of heat transfer surface. These surfaces are most of the times of the “extended” type, in the so called “compact heat exchangers”. The heat transfer coefficients are measured and determined experimentally for very specific geometric characteristics of the surface and the fins attached on it.

3.4.2 The P−NTU method

In the P−NTU method, the heat transferred between the two fluids is computed with the equation

$$\dot{Q} = P_1 C_1 \Delta T_{\max} = P_2 C_2 \Delta T_{\max} \tag{3.21}$$

where

C_j heat capacity rate of fluid *j*, Eq. (3.16),
$\Delta T_{\max}$ inlet temperature difference of the two streams, as in the ε−NTU method,
P_j temperature effectiveness of fluid *j*, defined by:

$$P_1 = \frac{T_{1,o} - T_{1,i}}{T_{2,i} - T_{1,i}}, \quad P_2 = \frac{T_{2,i} - T_{2,o}}{T_{2,i} - T_{1,i}} \tag{3.22}$$

with subscripts *i* and *o* referring to the inlet and outlet of the streams, respectively.

The main difference of the P−NTU from the ε−NTU method is that the computations with the P−NTU method can be carried out by considering each one of the two fluids for expressing the relationships between the non−dimensional groups, without concern on whether the fluid in mind is the one with the minimum heat capacity rate or not, or if it is the hot or the cold fluid.

In the P−NTU method, one can arbitrarily assume that the fluid 1 is the one that can facilitate the computations and then the temperature effectiveness P_1 is determined by relationships similar to those used in the ε−NTU method (Eq. (3.17))

$$P_1 = P_1\left(NTU_1, R_1, \text{flow arrangement}\right) \tag{3.23}$$

where

$$NTU_1 = UA/C_1 \tag{3.24}$$

$$R_1 = C_1 / C_2 \tag{3.25}$$

At a first glance, it may appear that the ε−NTU method is superior to the P-NTU, because the temperature effectiveness *P* has no physical significance and the P−NTU method seems to be simplistic compared to the ε-NTU. But the fact remains that most of the publications and works involving heat exchangers employ the P−NTU method. This is due to the fact that the researcher or engineer can work analytically or experimentally with each one of the two fluids without concern about whether the ratio of the two heat capacity rates is higher or lower than one.

One more important reason for the prevalence of the P−NTU method over ε−NTU is that by employing the P−NTU method, close form relationships of the form of Eq. (3.23) can be derived for heat exchangers that do not fall into any of the simple types of flow arrangement, namely counterflow, parallel flow or crossflow. This may include multipass

arrangements, which are the most usually encountered types in the practice of HRSGs as is reported in the related section. In the following, the additional theoretical analysis for simulating various types of heat exchangers needed for the purposes of the present work are described.

3.4.3 Fin and tube heat exchangers

The most important application of the fin-and-tube type of heat exchangers in the present study is the simulation and design of a heat recovery steam generator (HRSG). An example of a single pressure steam generator with one drum, depicting the various heat exchangers which it consists of is depicted in Figure 3.3. The economizer and superheater are treated as multipass heat exchangers. For the evaporator, a different approach needs to be followed, as will be seen in Section 3.5.1.

The feed water is supplied to the economizer in a subcooled state and is considered that it enters the drum as nearly saturated liquid at the design point of operation. In the evaporator, the mass flow rate in the tubes is higher than the mass flow rate in the economizer and the superheater. At the output of the evaporator, the water is in a two phase state, with quality 55-65%. This is demanded because at higher values of the mixture quality, the boiling heat transfer starts to diminish rapidly. The superheater receives saturated steam at its input and produces the superheated steam at the desired temperature.

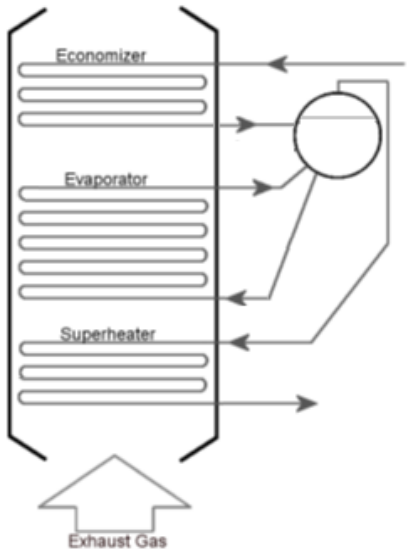

Figure 3.3: Schematic of a single pressure HRSG comprising multipass heat exchangers.

The arrangement selected for the HRSG is the multipass “serpentine” type. The tubes are individually finned and at a staggered arrangement, as depicted in Figures 3.4 and 3.5.

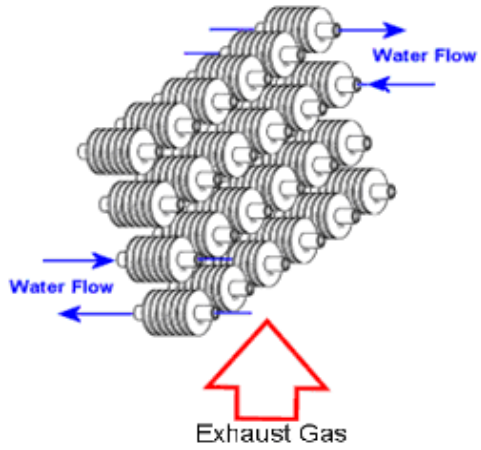

Figure 3.4: Cut view of the staggered arrangement.

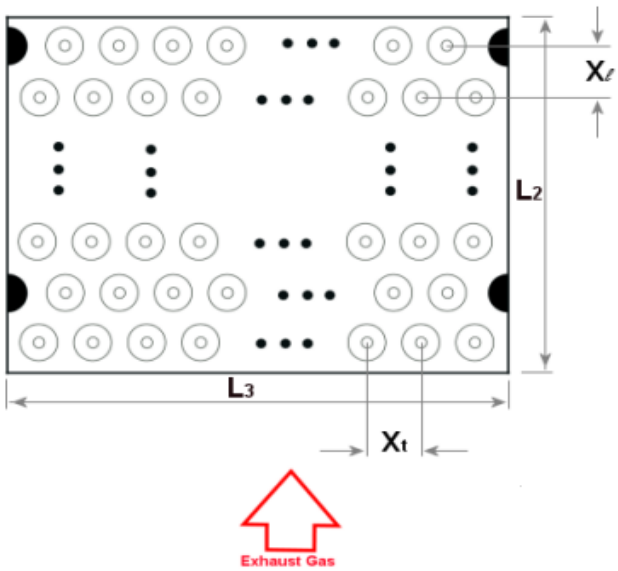

Figure 3.5: Geometric characteristics of fin and tube arrangement.

In Figure 3.5, an exchanger with staggered fin and tube arrangement is depicted, with the following geometric characteristics: X_t transverse pitch of the arrangement, X_l longitudinal pitch, L_3 width of the arrangement in the gas flow direction, and L_2 length in the gas flow direction.

For the application of the P-NTU method in a "serpentine" type heat exchanger, the fluid flowing outside the tubes (gas) is denoted as fluid 1. An appropriate expression for the temperature effectiveness P_1 has to be derived, considering the fact that it is a multipass heat exchanger with respect to the fluid 2 flowing inside the tubes. This type of exchanger can be considered as consisting of elementary crossflow exchangers, each one counting for every single pass of the fluid in the tubes. In these elementary heat exchangers, fluid 2 is considered mixed, while fluid 1 is unmixed due to the presence of the fins around the tubes. Fluid 1 though is considered as being mixed between successive passes [8].

For determining the P_1-NTU_1 relationship with the method of Domingos, as described in [9], one should take the $P_{1,ele}$ for each elementary heat exchanger given by the following equation:

$$P_{1,ele} = \frac{1-\exp(-KR_1)}{R_1}$$
$$K = 1-\exp(-NTU_{1,ele}) \tag{3.26}$$

An alternative way to derive the P_1-NTU_1 relationship is to consider the case of the flow arrangement depicted in Figure 3.6.

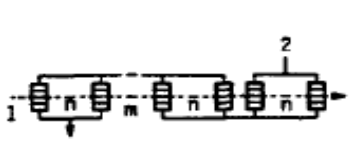

m-pass cross-counterflow exchanger; Fluid 2 mixed between passes, and within each pass, split into *n* streams individually mixed; Fluid 1 mixed between Fluid 2 streams, otherwise unmixed.

Figure 3.6: Coupling of elementary heat exchangers in an overall counterflow arrangement [9].

For this arrangement, it holds that:

$$\begin{gathered} P_1 = \left[(1-R_1B)^m - (1-B)^m \right] \Big/ \left[(1-R_1B)^m - R_1(1-B)^m \right] \\ B = 1-(1-A)^n \\ A = [1-\exp(-nKR_1)] / nR_1 \\ K = 1-\exp(-NTU_1 / nm) \end{gathered} \tag{3.27}$$

By setting n=1 in Eq. (3.27), the P-NTU formula is reduced to the appropriate expression for an m-pass serpentine arrangement. This has been verified by comparison to explicit formulas for 2-pass, 4-pass and 6-pass arrangements included in [10] and published in [11].

The heat transfer coefficient for the external side of the tubes is experimentally determined in [10]. Krupiczka's procedure is preferable, since the flow conditions resemble more closely to the serpentine arrangement, in contrast to the most works that involve experiments where the flow in the tubes is divided in parallel streams flowing in one direction.

The geometric characteristics of significance are the tube outer diameter d_o, the diameter of the fin d_e, the fin thickness t, the fin pitch p_t and tubes vertical pitch X_t (distance of tubes in the direction normal to the flow of gas). The arrangement of tubes has equilateral pitch, that is the longitudinal pitch X_l of the arrangement is such that the tubes pattern is a continuously repeated equilateral triangle, i.e. $X_l = 0.866025 * X_t$.

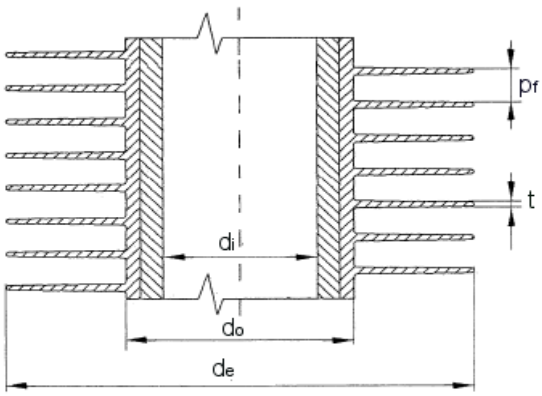

Figure 3.7: Geometric characteristics of the fin surface [10].

The Nusselt number of the specific arrangement has been experimentally determined and correlated with the aforementioned characteristics as follows

$$Nu = 0.182\,\mathrm{Re}_{\max}^{0.633}\,\mathrm{Pr}^{1/3}\left(\frac{p_f - t}{H}\right)^{0.2}\left(\frac{p_f - t}{t}\right)^{0.11}\left(\frac{p_f - t}{d_o}\right)^{-0.141} \tag{3.28}$$

which is valid for Re = 1000 – 10000.

In Eq. (3.28), H is the fin height:

$$H = (d_e - d_o)/2 \tag{3.29}$$

The relationship for the friction factor is:

$$\begin{aligned} f &= 840\,\mathrm{Re}_{\max}^{-0.9}\left(\frac{p_f - t}{d_o}\right)^{-0.82}\left(\frac{H}{d_o}\right)^{0.45}\left(\frac{X_t}{d_o}\right)^{-1} \quad \text{for } \mathrm{Re}_{\max} < 3500 \\ f &= 9.98\,\mathrm{Re}_{\max}^{-0.357}\left(\frac{p_f - t}{d_o}\right)^{-0.82}\left(\frac{H}{d_o}\right)^{0.45}\left(\frac{X_t}{d_o}\right)^{-1} \quad \text{for } \mathrm{Re}_{\max} > 3500 \end{aligned} \tag{3.30}$$

Equations (3.28) and (3.30) are valid for the following ranges:

$$\begin{gathered} 0.145 \le (p_f - t)/H \le 0.447 \\ 6.8 \le (p_f - t)/t \le 8.4 \\ 0.08 \le (p_f - t)/d_o \le 0.25 \\ 0.42 \le H/d_o \le 0.55 \\ 2.22 \le X_t/d_o \le 2.48 \end{gathered} \tag{3.31}$$

In the staggered arrangement of tubes, the Reynolds number definition is based on the outer diameter of tubes, and is equal to

$$\mathrm{Re}_{\max} = \frac{\dot{m}_1 d_o}{A_o \mu} \tag{3.32}$$

The Reynolds number is also dependent on the minimum flow area A_o which occurs in the space between the tubes. For equilateral arrangement it is

$$\begin{gathered} A_o = L_1\left[\left(\frac{L_3}{X_t} - 1\right)c_A + (X_t - d_o) - (X_t - d_o)tN_f\right] \\ c_A = (X_t - d_o) - (X_t - d_o)tN_f \end{gathered} \tag{3.33}$$

where L_1 is the length of the tubes and L_3 is the width of the arrangement with respect to the fluid flow direction.

With use of the friction factor defined as in Eq. (3.30), the pressure drop ΔP_{Nrs} over a total number of N_{rs} rows of tubes is [10]:

$$\Delta P_N = f N_{rs} \left(\frac{\dot{m}_1}{A_0} \right)^2 \Big/ 2\rho \tag{3.34}$$

where ρ is the fluid density.

The fin efficiency is computed with the equation [10]

$$\eta_f = \frac{\tanh\left(m\left(d_o/2\right)\phi_\eta\right)}{m\left(d_o/2\right)\phi_\eta}$$
$$m = \sqrt{\frac{2h_1}{tk_f}} \tag{3.35}$$
$$\phi_\eta = \left(\frac{d_e}{d_o} - 1\right)\left[1 + 0.35\ln\left(\frac{d_e}{d_o}\right)\right]$$

where

h_1 convective heat transfer coefficient on the gas side (W/m^{2}K)
k_f thermal conductivity of the fin material(W/mK)

The convective heat transfer coefficient for the fluid flowing inside the tubes is different for the economizer, evaporator and superheater. For the economizer and superheater it can be explicitly determined, but in the case of the evaporator it is not a trivial task, because the transfer properties of the boiling water change as a function of the heat input, which is still to be determined. The mixture quality (content in steam) and the flow conditions have also a strong influence on the convective heat transfer coefficient.

For the case of evaporator, the heat transfer coefficient has been determined with experiments and it is given by the equation [12]:

$$h_{2,eco} = K_w \frac{G^{0.8}}{d_i^{0.2}}$$
$$K_w = 5.86 + 0.018\frac{p}{100} + \left(9.41 - 0.63\frac{p}{100}\right)\frac{t_b}{100} - \left(1.542 - 0.3\frac{p}{100}\right)\left(\frac{t_b}{100}\right)^2 \tag{3.36}$$

where G is the mass velocity for each tube of the arrangement

$$G = \frac{4\dot{m}_{2.tube}}{\pi d_i^2} \tag{3.37}$$

p is the pressure in bar and t_b is the bulk temperature of the fluid in °C.

For the superheater, the equivalent relationship is [12]:

$$h_{2,\sup} = K_s \frac{G^{0.75}}{d_i^{0.25}}$$
$$K_s = 5.069 - 0.0529\,p + \left(4.467 + 0.169\,p\right)\frac{t_b}{1000} - \left(1.268 + 0.143\,p\right)\left(\frac{t_b}{1000}\right)^2 \tag{3.38}$$

The boiling heat transfer coefficient h_b for the case of evaporator was computed with the Liu-Winterton [13] approach described in [14]. The h_b is considered as averaged mean of the nucleate boiling heat transfer coefficient h_{nb} and the convection heat transfer coefficient h_L. The h_{nb} is computed according to the procedure published in [15] and h_L using the Dittus-Boetler correlation.

The set of equations for the computation of h_b is the following:

$$h_b = \sqrt{\left(Sh_{nb}\right)^2 + \left(Fh_L\right)^2} \tag{3.39}$$

$$h_L = 0.023\frac{k_2}{d_i}\mathrm{Re}_L^{0.8}\,\mathrm{Pr}_L^{0.4} \tag{3.40}$$

$$h_{nb} = 55\hat{q}^{0.67}P_{ratio}^{0.12}\left(-\log_{10}P_{ratio}\right)^{-0.55}M^{-0.5} \tag{3.41}$$

$$F = C_F\left[1 + x\,\mathrm{Pr}_L\left(\frac{\rho_l}{\rho_v} - 1\right)\right]^{0.35} \tag{3.42}$$

$$S = C_S\left(1 + 0.055F^{0.1}\,\mathrm{Re}_L^{0.16}\right)^{-1} \tag{3.43}$$

In Eqs. (3.39) to (3.43), the Reynolds and Prandtl numbers are computed for the properties of water, thus the L index. Especially, the Reynolds number is equal to:

$$\mathrm{Re}_L = \frac{4\dot{m}_{2,tube}(1-x)}{\pi d_i \mu_2} \tag{3.44}$$

Other symbols in the equations are: x is the mixture quality (mass percentage of steam), k_2 is the thermal conductivity of water, $\hat{q}$ is the heat flux density (in W/m^2), P_{ratio} is the ratio of the existing pressure to the critical pressure of the fluid, M is the molecular mass of the fluid and ρ_l and ρ_v are the densities of water and steam.

Because the tubes are in a horizontal orientation, the suppression and enhancement factors (S and F, respectively, in Eqs. (3.39) to (3.43)) have to be modified with the correction factors C_F and C_S appearing in Eqs. (3.42) and (3.43). These correction factors are dependent on the Froude number, which is defined as:

$$Fr = \frac{G}{\rho_l^2 g d_i} \tag{3.45}$$

with g the gravitational acceleration.

The correction factors are given as:

$$\begin{aligned} C_S = C_F = 1 &, \; Fr > 0.05 \\ C_S = \sqrt{Fr} &, \; Fr < 0.05 \\ C_F = Fr^{0.1-2Fr} &, \; Fr < 0.05 \end{aligned} \tag{3.46}$$

3.4.4 Shell and tube heat exchangers

This type of heat exchanger is used in the condenser of the steam bottoming cycle. The P−NTU method is applied, as described in [6]. A two−pass arrangement of the tube side fluid is considered (1-2 TEMA E Shell with shell fluid divided in two streams with a longitudinal baffle). Fluid 1 is the one flowing on the shell side and fluid 2 is flowing in the tubes. The mathematical expression of the P−NTU method is:

$$\begin{aligned} P_1 &= \frac{1}{R_1}\left[1 - \frac{(2-R_1)(2E+R_1B)}{(2+R_1)(2E-R_1/B)}\right] \\ E &= \exp(NTU_1) \\ B &= \exp\left(-\frac{NTU_1 R_1}{2}\right) \end{aligned} \tag{3.47}$$

In the special case of R_1=2, instead of Eq. (3.47) the following is valid:

$$P_1 = \frac{1}{2}\left[1 - \frac{1+E^{-2}}{2(1+NTU_1)}\right] \tag{3.47′}$$

Considering that the steam is condensed at the outer side of the tubes, the heat transfer coefficient is expressed as [14]:

$$h_c = 0.728\left[\frac{k_L^3 \rho_L (\rho_L - \rho_V) g \lambda}{\mu_L (T_V - T_W) d_o}\right]^{0.25} N_r^{-1/6} \tag{3.48}$$

where

h_c condensation heat transfer coefficient, Btu/h ft^2 ^{o}F
k_L thermal conductivity of the condensate, , Btu/h ft ^{o}F
ρ_L condensate density, lb/m^3
ρ_V vapor density, lb/m^3
g gravitational acceleration, 32.174 ft/s^2

λ latent heat of evaporation, Btu/lb
μ_L viscosity, cp
T_V vapor temperature, ^oF
T_W tube wall temperature, ^oF
d_o outer diameter of tubes, ft
N_r number of tube rows.

In the case of shell and tube heat exchangers, the definition of a "basic" heat transfer coefficient is not adequate for the calculations. This is due to the effect that the leakage and bypass flows have on the heat transfer, the effect that the flow distribution by baffles has on it also, and other factors specific to the shell and tube heat exchangers solely. For the determination of the heat transfer coefficients, special experiments have been conducted; the most widely known of them are known as the Bell method. In the present work this method is applied as described in [16].

The heat transfer coefficient in the internal side of the tube is calculated according to Eq. (3.36).

3.4.5 Plate heat exchangers

This type of heat exchanger is used in the jacket cooling water element of the HRSGs, which are used in conjunction with Diesel engines. A simple type of counterflow arrangement is considered, with the P-NTU relationship:

$$P_{1,c} = \frac{1-\exp\left[-NTU_1\left(1-R_1\right)\right]}{1-R_1\exp\left[-NTU_1\left(1-R_1\right)\right]} \quad , \quad P_{1,c} = \frac{NTU_1}{1+NTU_1} \text{ for } R_1 = 1 \tag{3.49}$$

The pure counterflow exchanger is the most favourable due to the better heat transfer properties

The plates considered in the present work are of the chevron type corrugation pattern. The geometric characteristics of a plate are depicted in Figure 3.8.

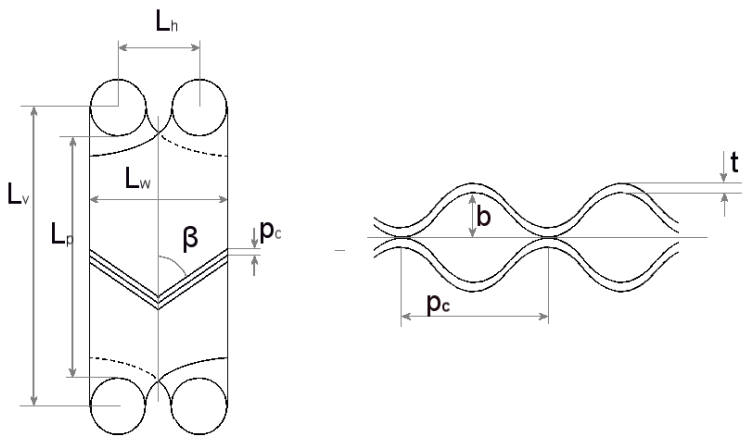

Figure 3.8: Geometric characteristics of the plate surface.

In Figure 3.8, t is the thickness of the plate, b is the height of corrugation from the central plane, p_c is the corrugation pitch, L_w and L_p are the plate width and length that make up the heat transfer area, and β is the chevron angle.

The hydraulic diameter of the channel created by two successive plates is defined as

$$D_h = \frac{4bL_w}{2\left(b+\phi L_w\right)} \approx \frac{2b}{\phi} \tag{3.50}$$

where ϕ is an enhancement factor, defined due to the fact that the actual surface is higher than the projected area $L_w \times L_p$. The last product must be multiplied by ϕ to compute the actual surface area, which is given by the relationship:

$$\phi(x) = \frac{1}{6}\left(1+\sqrt{1+x^2}+4\sqrt{1+x^2/2}\right)$$
$$x = \frac{2\pi(b+t)}{p_c} \tag{3.51}$$

Table 3.12: Coefficients for the determination of heat transfer and friction factors in plate heat exchangers.

	Heat Transfer			Pressure Drop		
β'	Re	C_h	n_h	Re	K_f	m_f
<=30	<10	0.718	0.349	<10	50	1
	>10	0.348	0.663	10-100	19.4	0.589
				>100	2.99	0.183
45	<10	0.718	0.349	<15	47	1
	10-100	0.4	0.598	15-300	18.29	0.652
	>100	0.3	0.663	>300	1.441	0.206
50	<20	0.63	0.333	<20	34	1
	20-300	0.291	0.591	20-300	11.25	0.631
	>300	0.13	0.732	>300	0.772	0.161
60	<20	0.562	0.326	<40	24	1
	20-400	0.306	0.529	40-400	3.24	0.457
	>400	0.108	0.703	>400	0.76	0.215
>=65	<20	0.562	0.326	<40	24	1
	20-500	0.331	0.503	40-400	2.8	0.451
	>500	0.087	0.718	>400	0.639	0.213

The Reynolds number is thus computed with the equation

$$\mathrm{Re}_x = \frac{\dot{m}_{x,channel} D_h}{\mu_x L_w b} \tag{3.52}$$

for each fluid '*x*'. $\dot{m}_{x,channel}$ is the mass flow rate for each individual channel.

For the determination of the heat transfer coefficient and the friction factor, the relationships found in [17] are used:

$$h = C_h \frac{k}{D_h} \mathrm{Re}^{n_h} \mathrm{Pr}^{1/3} \tag{3.53}$$

$$f = \frac{K_f}{\mathrm{Re}^{m_f}} \tag{3.54}$$

The coefficients C_h, n_h, K_f and m_f are given in Table 3.12. The angle β′ is the angle of corrugation with respect to the plate width (which means β′=90º–β):

3.5 Heat Recovery Steam Generators

Special attention has been given to the modeling of design and operation of the heat recovery steam generators (HRSG) possibly existing in the integrated energy system, as the potential for the exploitation of the exhaust gases thermal energy content relies on their appropriate design and operation. They actually are the central part of the overall system which relates functionally the mechanical power producing components of the system (prime movers and possibly existing steam turbines) in a combined cycle configuration, and may also have a major role in covering the thermal energy demands of the ship.

During the present work, several configurations of HRSGs were studied from the point of view of their internal structure, the individual heat exchangers relative succession in the exhaust gas path and the number of pressure levels. In the present chapter, two HRSGs are presented, the first one being appropriate for combined cycles with Diesel engines, and the second one for combined cycles with gas turbines as prime movers.

3.5.1 HRSGs for Diesel engines

The internal structure of the HRSGs for the utilization of waste heat of Diesel engines is presented in Figure 3.9. This HRSG is a dual pressure configuration which, apart from the exhaust gas, it also recovers heat from the engine's jacket cooling water and the charge air cooler. There are no economizers in the configuration and the water preheating before entering the drums is realized by the exploitation of these two heat sources. An important aspect of the lack of economizers is that, by an appropriate choice of the low pressure level, the sulfuric acid condensation on the heat exchange surfaces in the upper part of the HRSG can be readily avoided. This is because of the defined and constant temperature of the dual phase mixture inside the tubes of the low pressure evaporator (that is, the saturation temperature), which can be limited by posing a lower permitted value for the pressure level of the low pressure part. In this way, the last heat exchange area encountered by the flowing

exhaust gas can have a temperature high enough, so that exhaust gas temperature does not fall below the sulfuric acid dew point, even at the closest proximity and on the surface of the low pressure evaporator tubes. The minimum permitted temperature for Diesel fuels is generally set at about 160^{o}C (for the bulk flow) due to the relatively high sulfur content. This means that the internal flow cannot be permitted to acquire temperatures lower than about 135^{o}C.

One more important aspect of the lack of economizers is avoiding of steaming in these parts of the HRSG. When a HRSG operates at design point conditions, the designer has defined the extensive and intensive thermodynamic properties of the working fluids throughout the whole configuration and, in the general case of HRSG designs which incorporate economizers, the feed water delivered at their outlet is at a temperature usually slightly below the saturation temperature (this slight difference is called *"approach temperature"*).

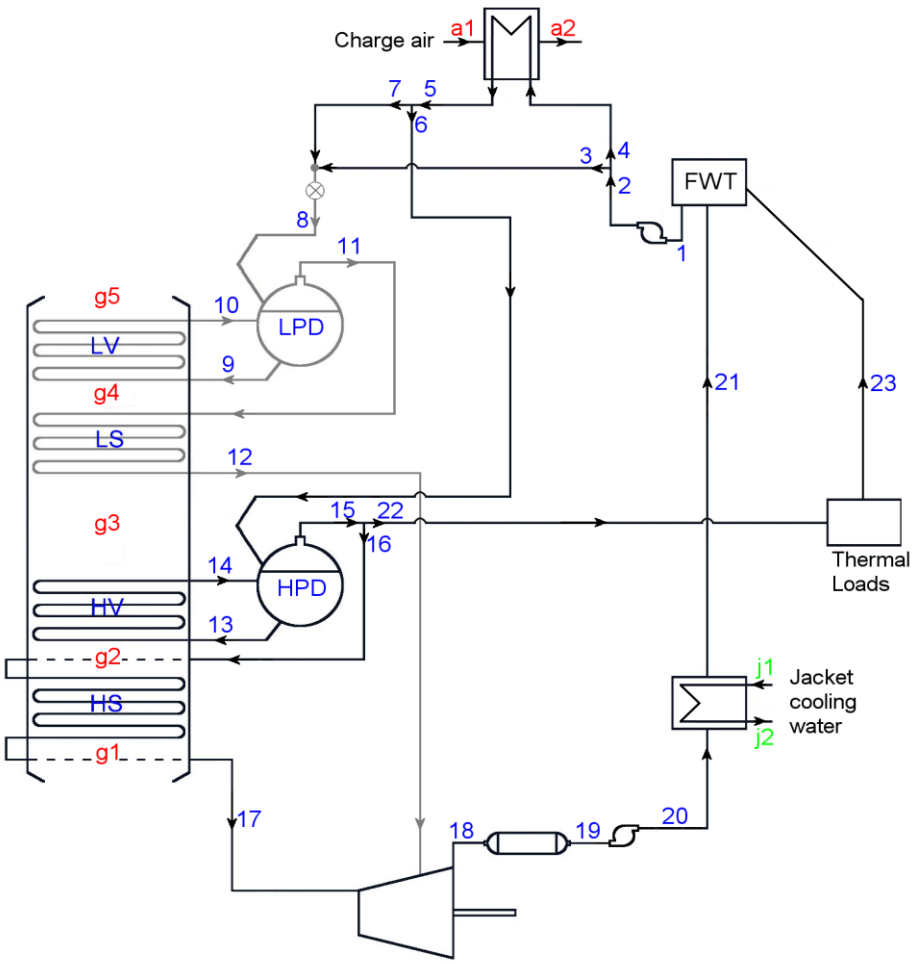

Figure 3.9: The heat recovery subsystem with the internal structure of the HRSG for the case of Diesel engines.

The change of flow characteristics (mass flow rate and temperature) of the exhaust gas during off−design operation of the prime movers may cause an operating condition which

results in the production of a dual phase mixture at the economizers water outlet, a condition that cannot be accepted as it is hazardous for the operation of the overall configuration. For avoiding such situations, partial bypassing of the exhaust gas outside of the HRSG could be employed, but this evidently results in lower exploitation of the exhaust gas thermal energy content, other than being an important technical complexity. Thus, the absence of the economizers makes the HRSG more versatile for operation in changing conditions of the exhaust gas inlet.

For the design of the HRSG, a dedicated computational procedure was developed. In this procedure, several of the operating parameters, crucial to the determination of the heat exchange areas of the heat exchange elements are used as inputs, with the intention to be used as independent variables of the optimization problem. Each HRSG is designed for given values of exhaust gas mass flow rate ($\dot{m}_g$) and temperature (T_g) at its exhaust gas inlet (point g1). For the high and low pressure levels of steam production, the design point steam mass flow rate, pressure and temperature, ($\dot{m}_{HP}$,P_{HP}, T_{HP} at point 17) and ($\dot{m}_{LP}$, P_{LP}, T_{LP} at point 12), are input variables. One additional input variable is the magnitude of thermal energy loads to be covered by the HRSGs, which are served by saturated steam delivered by the high pressure drum.

For the feed water preheating by the jacket cooling water of the engines, it is considered that

$$T_{21} = T_{j1} - \Delta T_j \tag{3.55}$$

The temperature T_{j1} depends on the operating point of the engine, while ΔT_j is a constant. The mass flow rate of the heating jacket water is externally determined by the properties of the prime movers.

For the design of the charge air−water heat exchanger, the following input variables are required: a) the charge air mass flow rate $\dot{m}_a$, b) the temperature T_{a1}, c) the heat exchanger temperature effectiveness P_a, and d) the bypass ratio of feed water ρ_m (defined as $\rho_m = \dot{m}_3 / \dot{m}_2$ with the numerical subscripts indicating the streams appearing in Figure 3.9). The water pressure in the charge air cooler is $P_{HP,}$ while the low pressure is obtained with a pressure reducing valve. The bypass flow (stream 3) is used for regulating the temperature at point 8 after the pressure reduction, so that it does not exceed the corresponding saturation temperature and can be varying in off-design operation, so that the low pressure drum receives subcooled water.

With the values of the aforementioned input variables given, heat balances are initially performed defining the exhaust gas, charge air and water/steam temperatures and enthalpies throughout the whole HRSG system. Furthermore, several checks are performed during the design calculations of the HRSG, the most important of them being the following: (a) the temperature difference between the heat exchanging fluids is not lower than a minimum value, (b) the exhaust gas temperature at the exit of the HRSG is not lower than a minimum

value, so that condensation of sulfuric acid is avoided as mentioned above, and (c) the feed water at points 5 through 8 does not attain enthalpies higher than the saturated water enthalpies at the corresponding pressure levels as also mentioned above. The heat balances are described with the set of Equations (3.56)

$$\dot{m}_g c_{pg1}\left(T_{g1}-T_{g2}\right)=\dot{m}_{HP}\left(h_{HP}-h_{ss,HP}\right) \tag{3.56a}$$

$$\dot{m}_g c_{pg2}\left(T_{g2}-T_{g3}\right)=\left(\dot{m}_{HP}+\dot{m}_{hl}\right)\left(h_{ss,HP}-h_5\right) \tag{3.56b}$$

$$\dot{m}_g c_{pg3}\left(T_{g3}-T_{g4}\right)=\dot{m}_{LP}\left(h_{LP}-h_{ss,LP}\right) \tag{3.56c}$$

$$\dot{m}_g c_{pg4}\left(T_{g4}-T_{g5}\right)=\dot{m}_{LP}\left(h_{ss,HP}-h_8\right) \tag{3.56d}$$

$$\dot{m}_{LP}h_8=\dot{m}_7h_5+\dot{m}_3h_2 \tag{3.56e}$$

$$\left(\dot{m}_{HP}+\dot{m}_{LP}\right)\left(h_{21}-h_{20}\right)=\dot{m}_{jw}\left(h_{j1}-h_{j2}\right) \tag{3.56f}$$

$$\dot{m}_{hl}\left(h_{ss,HP}-h_{23}\right)=\dot{Q}_{hl} \tag{3.56g}$$

$$\left(\dot{m}_{HP}+\dot{m}_{LP}+\dot{m}_{hl}\right)h_1=\left(\dot{m}_{HP}+\dot{m}_{LP}\right)h_{21}+\dot{m}_{hl}h_{23} \tag{3.56h}$$

and an additional equation relating the enthalpy rise in the feed water pump is required:

$$h_2=h_2\left(h_1,P_{FWT},P_{HP}\right) \tag{3.57}$$

It is noted that a set of inputs for the design procedure of each HRSG may lead to an infeasible design, i.e. to a solution of the design point operation in which one or more of the aforementioned constraints are not satisfied. These constraints may also be considered as constraints of the SDO optimization problem for each of the possibly existing HRSGs.

Afterwards, each individual heat exchanger is designed using the properties of the fluids that have already been determined. A computational design procedure was developed for this purpose, in which the dimensions and the total surface area of each heat exchanger are calculated. Geometric parameters such as the internal and external diameters of the tubes and the fins characteristics are taken into account. The superheaters and charge air coolers are considered as multi−pass heat exchangers, and they are sized by applying the P−NTU method, which is described in Section 3.3.3. In this procedure, the Reynolds number of the exhaust gas flow is used as an input parameter and, along with the geometric characteristics of the tubes and fins, determines the footprint of each heat exchanger. Passes are added in the exchanger until the desired temperature effectiveness at design point is achieved, while the length of the tubes is slightly modified during this procedure in a repetitive manner until

the exchanger is sized according to the exact value of the required temperature effectiveness. Thus, the total heat exchange surface area is determined for each heat exchanger.

The evaporators of the HRSGs are designed with a different approach. Each of the passes of the evaporator is considered as individual heat exchanger and the total heat transferred is the sum of the individuals. The $\varepsilon - NTU$ method is applied in each pass. The effectiveness and the heat transferred are given by the following equation [6]:

$$\dot{Q}_{pass,eva} = \varepsilon \dot{m}_g c_{pg} \left(T_{g,pass,in} - T_{sat} \right) = \left(1 - \exp\left(-NTU \right) \right) \dot{m}_g c_{pg} \left(T_{g,pass,in} - T_{sat} \right) \tag{3.58}$$

and the same procedure of adding passes and modifying the length of the tubes is used until the sum of the heat transferred from all passes is equal the total heat exchanged at the evaporator, as calculated with the Equations (3.56b) and (3.56d).

The design specifications of the individual heat exchangers are then used to determine the off−design operation of the HRSG. As off−design operation can be considered any condition in which the exhaust gas, charge air and jacket water properties differ from the nominal ones used for the sizing of the heat exchangers. An algorithm has been developed for the simulation of the off−design performance of the HRSGs. The mass flow rates and temperatures of the water/steam throughout each heat exchanger of the HRSG and thus the characteristics of the steam streams produced by the HRSG are ultimately calculated. The same principal equations for the heat transfer coefficients and the effectiveness of the exchangers as in the design procedure are used, with the difference that the heat transferred is one of the calculated quantities, according to the predetermined heat exchange areas. There is the possibility that the available off−design exhaust gas mass flow rate and temperature may have values that lead to an infeasible operation, i.e. one or more technical constraints cannot be met; for example, the exhaust gas temperature at the HRSG outlet may be too low, or the water streams at points 5 or 8 (Figure 3.9) may start to evaporate. In such cases, it is considered that the HRSG cannot operate. Such off−design operation constraints are also considered as constraints of the SDO optimization problem.

It is noted that for HRSGs used in conjunction with Diesel engines, a deaerating condenser appliance is used [2,3].

3.5.2 HRSGs for gas turbines

In the case of the HRSGs to be used in conjunction with gas turbines, the general rationale for the sizing procedure is the same as for the HRSGs for Diesel engines described above. The important changes are found in the internal structure of HRSGs, as gas turbines do not provide additional heat sources for recovery except of the exhaust gas. The use of economizers is thus inevitable, as also, due to the larger expected mass flow rates of water/steam, a deaerator utilizing exhaust gas thermal energy for its operation is also included. The structure of this type of HRSGs is depicted in Figure 3.10.

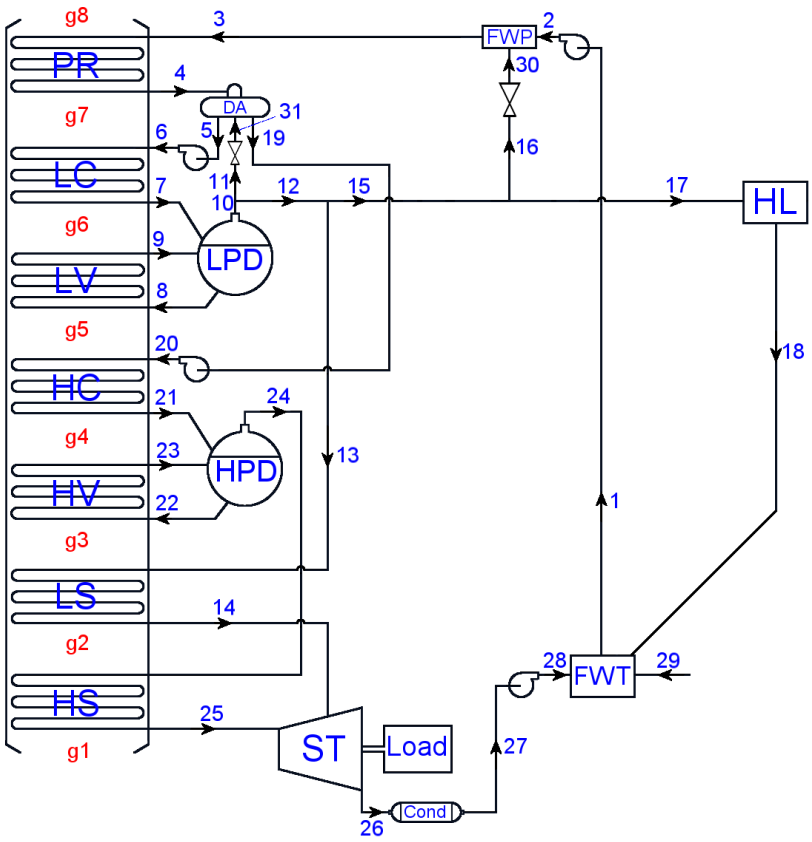

PR: Preheater, LPD: Drum LP, HPD: Drum HP
LC: Economizer LP, LV: Evaporator LP, LS: Superheater LP
HC: Economizer HP, HV: Evaporator HP, HS: Superheater HP
HL: Heat load, FWP: Feed Water Preheater, Cond: Condenser
ST: Steam Turbine, FWT: Feed water tank, DA:Deaerator

Figure 3.10: Internal structure of a gas turbine HRSG.

Thus, the HRSG consists of a water preheater, low pressure economizer, evaporator and superheater, and high pressure counterparts, which are all multi−pass heat exchangers. The HRSG feeds the steam turbine (points 14 and 25 with mass flow rates $\dot{m}_{LP}$ and $\dot{m}_{HP}$, respectively), while a fraction of the saturated low pressure steam is used for thermal loads (point 17 with mass flow rate $\dot{m}_{hl}$). For the deaerator integrated with the HRSG, a heating stream (point 31, $\dot{m}_{da}$) originating from the low pressure drum is used, if necessary, for heating the feed water to the appropriate conditions for deaeration.

As mentioned in Section 3.5.1, the inclusion of the economizers and the preheater poses an additional restriction on the HRSG's operation, which is that the evaporation in these parts must be avoided during any operating conditions. Other important constraints are the minimum permitted temperature of the exhaust gases (specified at 130°C for MGO and 100°C for natural gas), and the minimum temperature of water at the inlet of the HRSG (specified at 105°C for MGO and 75°C for natural gas). Due to the fact that the feed water temperature will generally be quite lower that the limits mentioned above, a feed water

preheater must be included in the system, which is a mixing preheater that uses saturated steam from the low pressure drum.

After the determination of the design characteristics, the calculation of the appropriate heat transfer surface areas and generally the geometric characteristics of the heat exchangers, an off−design simulation algorithm developed can be used for determining the feasibility of the HRSG operation with exhaust gas properties other than the nominal and for quantifying the magnitude of the steam mass flow rate production and the temperatures of the pertaining streams feeding the steam turbines.

3.6 Steam turbines

Steam turbines potentially used in marine energy systems are important components that have to be synthesized in a way that will be able to contribute to the requirements for propulsion and electricity. Steam turbines can contribute an important part of the overall power produced by the power plant when used in bottoming Rankine cycles.

During the present work, several configurations of steam turbines were examined with variations regarding the number of pressure levels (one, two or three pressures for the inlet streams), the number of sections of reaction stages, the possibility of extraction points for serving thermal loads, etc. The HRSGs that finally were used in the later parts of the work were decided to be of the double pressure type with no reheat circuits. Thus, the structure of the steam turbines that were finally considered is the one presented in Figure 3.12.

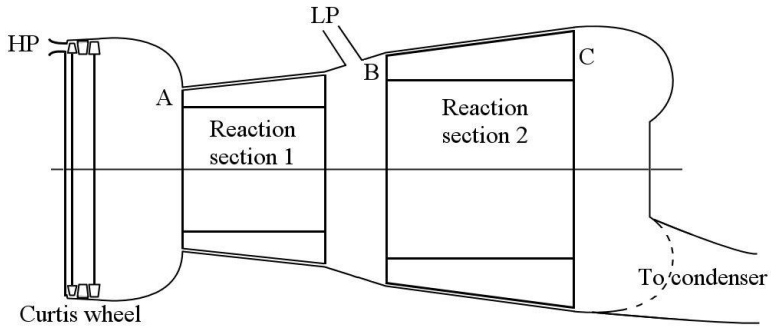

Figure 3.12: Schematic of the structure of the steam turbines considered.

The steam turbine consists of a Curtis wheel and two reaction sections with bladings of constant inner radii.

The design of steam turbines is based on the determination of their most important design characteristics, which are intended to be used as independent variables of the optimization problem of the energy system as a whole. The design procedure of the steam turbines is based on the underlying principles for the simulation of the individual stages, and the following section is referred to this subject for the case of reaction stages. The Curtis wheel is treated in a different way and follows afterwards.

3.6.1 Reaction stages modeling

Throughout the turbine, the concept of one-dimensional analysis of turbomachinery is used. The analysis is also based on the consideration of the steam turbine as an ensemble of "stage groups" which facilitates the simulation at off-design operation, as will be seen in the related subsections to follow. Even though one dimensional analysis is used, the usual "repeating stage" assumption was not considered, as it resulted in unrealistic designs of the stage groups. The performance simulation of individual stages is the primary procedure on which the whole design and simulation are based. The size and other important properties of each stage group (e.g. the order of the axial component of steam velocity) are determined by the first stage of the group which, for this reason, is subjected to a special treatment that differs from the procedure for the subsequent stages, and which will be explained in a separate subsection.

3.6.1.1. Individual stages with upstream stage

For the reaction stage groups, the mass flow rate $\dot{m}$ and rotational speed N of the shaft are used as input variables. It is assumed that throughout each group the mass flow rate is constant. These parameters are considered as input to the procedure regarding any individual stage.

The stages will always be considered as consisting of a stator followed by a rotor, and the "stations" denoted with the numbers 1 to 3 are as follows:

1. inlet of stator
2. outlet of stator – inlet of rotor
3. outlet of rotor.

When the stage at hand is preceded by another one, the steam properties and the geometrical and other characteristics at the inlet are defined by the predetermined outlet values of these parameters of the preceding stage. These are the following:

- Inlet pressure p_1
- Inlet specific enthalpy h_1
- Inlet specific entropy s_1
- Inlet steam quality x_1
- Inlet density ρ_1
- Inlet flow angle α_1
- Inlet velocity c_1
- Inlet axial velocity c_{x1}
- Inner radius at the inlet r_i (constant throughout stage)
- Inlet mean radius r_{m1}
- Inlet outer radius r_{o1}

- Inlet peripheral speed U_1
- Inlet height of the blading H_1.

Two more geometrical characteristics are required for the estimation of losses:

- Ratio of blade height to blade axial width
- Clearance of rotor tip.

The height to width ratio is needed for the implementation of the Sodeberg's method for the computation of flow losses through turbine bladings, described in a later paragraph.

For the computations of thermodynamic properties changes in the stage, two more design parameters are input to the procedure, namely:

- Stage reaction degree r
- Stage loading factor ψ .

According to the theory of steam turbines, the reaction degree is defined by the equation

$$r = \frac{h_2 - h_3}{h_1 - h_3} \tag{3.59}$$

where h_i is the specific enthalpy at the corresponding station i.

The stage loading is defined as

$$\psi = \frac{h_{t1} - h_{t3}}{U^2} \tag{3.60´}$$

where the total enthalpies are used and the peripheral speed is constant throughout the stage. However, for simplification of computations in the present work, the stage loading is defined as

$$\psi = \frac{h_1 - h_3}{U_1^2} \tag{3.60}$$

For the analysis of turbine stage performance, there is need to define explicitly the sign conventions for the flow angles of the velocity triangles. The convention used is as in [18] and the positive angles are depicted in Figure 3.13.

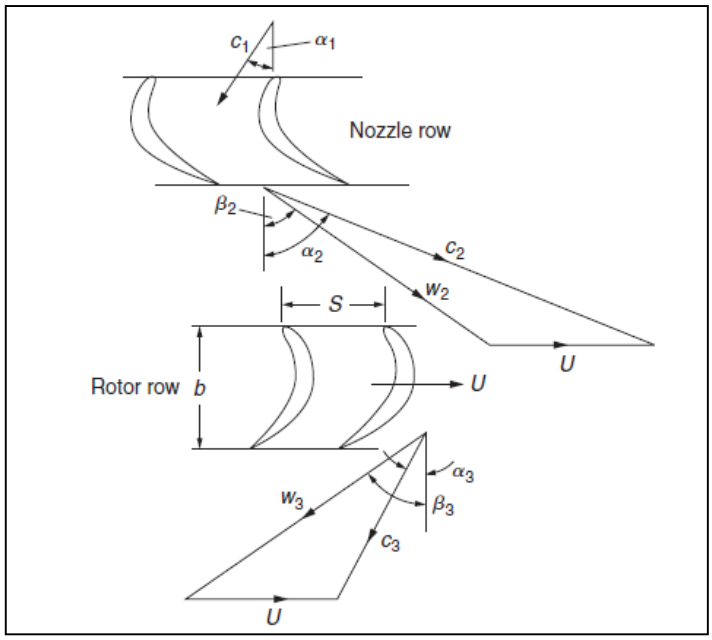

Figure 3.13: Turbine stage velocity diagrams [18].

The following parameters are depicted in Figure 3.13:

c	absolute velocity of the flow
w	relative velocity of the flow
U	peripheral speed at the mean radius
a	absolute flow angle
β	relative flow angle.

The relation between the absolute and relative velocities in each position is given by the vector addition:

$$\vec{c} = \vec{w} + \vec{U} \tag{3.61}$$

The purpose of simulation is to determine the expansion line as depicted in Figure 3.14 together with the thermodynamic properties, geometrical characteristics, work produced and efficiency.

The simulation begins with the computation of the exit specific enthalpy h_3 directly from Eq. (3.60), which is a basic thermodynamic property in the whole procedure and remains unaltered throughout a series of computations during which the loading coefficient and the mean radius are not changed. The specific enthalpy h_2 can be computed subsequently from Eq. (3.59).

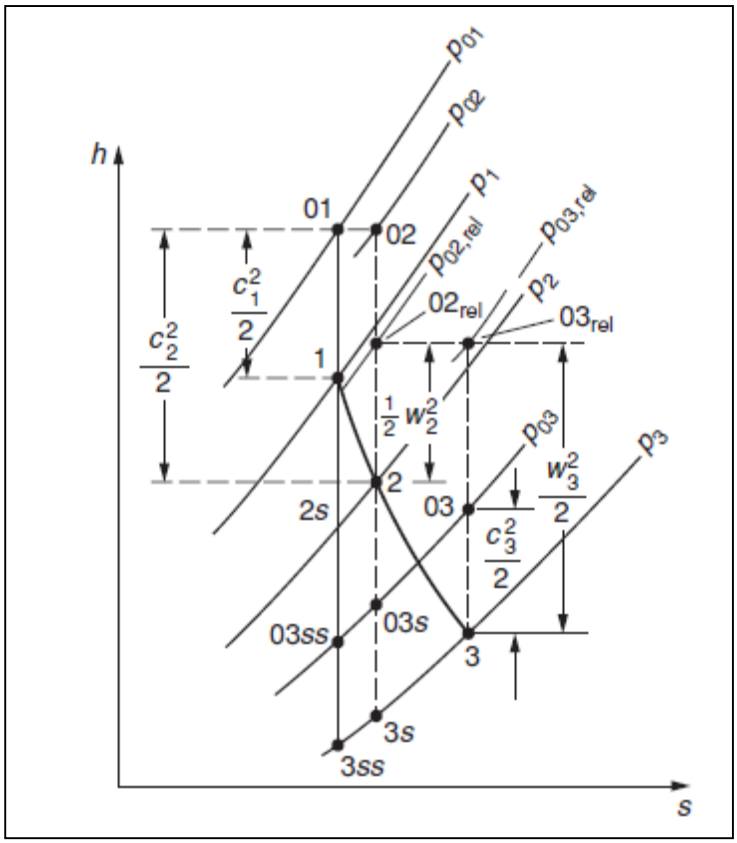

Figure 3.14: h-s diagram for a turbine stage [18].

The mean radius of a stage at any of the three stations is considered as the radius that divides the flow annulus in two annuli of equal area, which means that

$$r_m^2 = \frac{r_o^2 - r_i^2}{2}$$
$$A = 2\pi(r_m^2 - r_i^2) \tag{3.62}$$

where

r_m mean radius
r_o outer radius of blading
r_i inner radius of blading
A flow area of stage

for the three stations.

The peripheral speed is computed with

$$U_i = \frac{\pi N r_{mi}}{30} \quad i = 1,2,3 \tag{3.63}$$

and the mass flow rate is computed with

$$\dot{m} = \rho_i A_i c_{xi} \quad i = 1,2,3 \tag{3.64}$$

Combining the preceding equations, the following expression for the axial velocity is obtained:

$$c_{xi} = \frac{\dot{m}}{2\rho_i \pi \left(\frac{900}{\pi N^2} U_i^2 - r_i^2 \right)} \qquad i = 1, 2, 3 \tag{3.65}$$

The axial velocity of steam generally increases as the pressure drops in the direction of the flow, along with the increase as the radius of the stages. In the simulations, the stage flow coefficient, ϕ, is used:

$$\phi_i = \frac{c_{xi}}{U_i} \quad i = 1, 2, 3 \tag{3.66}$$

The flow coefficient is considered equal at the inlet and outlet of an individual stage, so that succeeding stages have the same value of ϕ:

$$\frac{c_{x1}}{U_1} = \frac{c_{x3}}{U_3} \tag{3.67}$$

Combining Eqs. (3.65) and (3.67), the following expression for the peripheral speed at station 3 is obtained :

$$U_3 = \frac{\dot{m}}{2\pi\rho_3 \frac{c_{x1}}{U_1} \left(\frac{900}{\pi N^2} U_3^2 - r_i^2 \right)} \tag{3.68}$$

The last equation can be solved for U_3 with a repetitive or other numerical procedure, if the value of density ρ_3 is known. For starting the computations, ρ_3 is set equal to the value that would be obtained if the expansion were isentropic and ended at a hypothetical point on the h−s diagram which has entropy equal to point 1 in Figure 3.13 and specific enthalpy equal to the known value of h_3. Later on, the actual value of ρ_3 is computed and the whole procedure that will be described from now on is repeated until there is no change in the value of U_3.

With the preliminary values for U_3 and c_{x3}, the axial velocity at station 2 is set as:

$$c_{x2} = c_{x3} + r\left(c_{x1} - c_{x3}\right) \tag{3.69}$$

where r is the reaction of the stage. With the use of Eq. (3.69), c_{x2} is set equal to c_{x3} for impulse or zero reaction stages and equal to $0.5\left(c_{x1}+c_{x3}\right)$ for reaction stages with degree of reaction equal to 0.5. In this way it is ensured that the acceleration of the flow occurs in the stator for impulse stages and is equally divided between the stator and rotor in reaction stages, following the trend of the pressure drops in both cases.

The absolute velocity of flow at station 2 can be computed with

$$c_2 = \sqrt{2\left(h_1 - h_2\right) + c_1^2} \tag{3.70}$$

which is a direct interpretation of energy conservation through the stator.

The flow angle α_2 can be now computed with

$$a_2 = \arccos\left(\frac{c_{x2}}{c_2}\right) \tag{3.71}$$

At this point, the Soderberg loss estimation method is used to find the static pressure at station 2. The method is described in Section 3.5.4. In this method, a loss coefficient of specific enthalpy ζ is defined as:

$$\zeta = \frac{h_x - h_{xs}}{\frac{1}{2}c_x^2} \tag{3.72}$$

where h_x is the actual value of specific enthalpy at the exit of the blading, h_{xs} its isentropic expansion counterpart (e.g. the point *2s* in Figure 3.14 for the case of stator and *3s* for the rotor) and c_x is the exit velocity from the blading. The application of Soderberg method determines the loss coefficient ζ_N for the stator. Equation (3.72) is then solved for h_{2s}. The pressure p_2 can now be determined in terms of the known values of h_{2s} and specific entropy $s_{2s}=s_1$:

$$p_2 = p_2\left(h_{2s}, s_{2s}\right) \tag{3.73}$$

With point 2 of expansion line determined, the entropy is calculated from known values of pressure and enthalpy:

$$s_2 = s_2\left(p_2, h_2\right) \tag{3.74}$$

as also the density ρ_2 :

$$\rho_2 = \rho_2\left(h_2, s_2\right) \tag{3.75}$$

Next the geometrical characteristics of the blading at station 2 are determined

$$\begin{aligned} r_{m2}^2 &= \sqrt{r_i^2 + \frac{\dot{m}}{2\pi c_{x2}\rho_2}} \\ r_{o2}^2 &= \sqrt{r_i^2 + \frac{\dot{m}}{\pi c_{x2}\rho_2}} \\ H_2 &= r_{o2} - r_i \end{aligned} \tag{3.76}$$

and the peripheral speed U_2 at station 2 from Eq. (3.63). The relative flow angle β_2 is determined by

$$\beta_2 = \arctan\left(\tan(\alpha_2) - \frac{U_2}{c_{x2}}\right) \tag{3.77}$$

and the measure of relative velocity w_2 by

$$w_2 = \frac{c_{x2}}{\cos(\beta_2)} \tag{3.78}$$

The computations considering the rotor of the stage can now be executed. Firstly, the value of the relative velocity is computed with

$$w_3 = \sqrt{2\left(h_2 - h_3\right) + w_2^2 + U_3^2 - U_2^2} \tag{3.79}$$

The above equation is an expression of the fact that the relative enthalpy in the rotating system of reference attached to the rotor (or the so called rothalpy) remains unchanged upstream and downstream the rotor. The value used for U_3 is the one computed with Eq. (3.68). The relative flow angle β_3 is determined by

$$\beta_3 = \arccos\left(\frac{w_{x3}}{w_3}\right) \tag{3.80}$$

With the values of β_3 and w_3 the Soderberg method can be used this time for the rotor, to determine p_3, in the same way that pressure p_2 was determined. The difference is that in the case of the rotor, the relative flow velocities and angles are used. The procedure continues in the same way as was described for the stator, and equations equivalent to Eqs. (3.73) –

(3.76) are used for the computation of s_3, r_{m3}, r_{o3}, H_3 and ρ_3. The importance of the determination of the value of density ρ_3 is that it is now possible to use Eq. (3.63) to compute U_3, as the new mean radius is depended on the density. The new value for U_3 will generally be different from the one found using Eq. (3.68), which is used only for the initial estimation of U_3, and in which the density ρ_3 is considered to have the same value as the density at point 3ss depicted in the diagram of Figure 3.14. From now on, only Eq. (3.63) is used for the determination of U_3 in a repetitive procedure, which stops only when U_3 remains virtually unchanged.

After the new value for U_3 is found, the flow angle α_3 is determined by:

$$a_3 = \arctan\left(\tan(\beta_3) - \frac{U_3}{c_{x3}}\right) \tag{3.81}$$

and the absolute velocity c_3 is:

$$c_3 = \frac{c_{x3}}{\cos(a_3)} \tag{3.82}$$

Now, it is possible to determine the point 3ss in Figure 3.14, and the total-to-total and total-to-static efficiencies of the stage:

$$\begin{aligned} \eta_{t-t} &= \frac{h_{o1} - h_{o3}}{h_{o1} - h_{o3ss}} \\ \eta_{t-s} &= \frac{h_{o1} - h_{o3}}{h_{o1} - h_{3ss}} \end{aligned} \tag{3.83}$$

The power of the stage is also found as:

$$\dot{W}_{stage} = \dot{m}\left(h_{o1} - h_{o3}\right) = \dot{m}\left(h_1 + \frac{1}{2}c_1^2 - h_3 - \frac{1}{2}c_3^2\right) \tag{3.84}$$

The drop of enthalpy is finally computed, along with the pressure drop and the pressure ratio of the stage, which are useful measures of the performance of each stage, when the design of the whole turbine is considered. Generally, a turbine that is ‘well’ designed must have increasing enthalpy drops and pressure ratios as the steam proceeds to lower pressure stages.

In the next section, the case of the first stage on a stage group is described.

3.6.1.2 First stage of a group of stages

The first stage of a group has a significant effect on the whole performance and design of a stage group for various reasons. The most important one is that, with the blade height given upstream of the first stator of a group, the axial velocity component is determined for a given mass flow rate and steam properties, thereby having later a strong effect on the changes of radial dimensions and the number of stages in a group (the 'bigger' the stage, the higher pressure drop and the lower the number of stages). In this particular problem, the mass flow rate and steam properties are intended to be used as 'inputs' for the design of the steam turbine, because they are intended to be variables of the more general problem of optimization (moreover, the steam mass flow rate and its properties cannot be decided independently of each other in the case of combined cycles, because the heat supply is determined by specific processes). Actually, in a design procedure of a steam turbine where these parameters are predetermined, there is a great complication due to the reduction of freedom of the design. The blade heights must not be smaller than about 2 cm, for manufacturing reasons and because of the high flow losses. On the other hand, the axial velocities must also not be too small, because they result in very large absolute and relative flow angles in the velocity triangles. Furthermore, lower axial velocities in the first stages of a group will generally result in low axial velocities for the last stages also and this would result in higher blade heights at the lower pressure sections and to the increase of the physical dimensions of the turbine.

When a stage is the first one after a Curtis wheel or a steam inlet point, it is considered as 'first stage' of the group. For these stages the required inputs are the following:

- Stage reaction r
- Stage loading coefficient ψ
- Steam mass flow rate $\dot{m}$
- Rotational speed N
- Blade height to width ratio
- Rotor clearance κ
- Inner radius of blading r_i
- Height of the blading upstream the first stator H_1
- Total inlet specific enthalpy h_{o1}
- Inlet specific entropy s_1.

The inlet angle is considered to be zero, because no guiding of the flow is present. This holds especially in the case of the first stage after the reaction chamber that follows a Curtis wheel. The flow between the Curtis wheel and the initial stage is assumed to be lossless and consequently isentropic and with constant total energy.

The flow area of the annulus upstream of the first stator A_1 is readily determined by the aforementioned input variables. The axial velocity c_{x1} can be computed with

$$c_{x1} = \frac{\dot{m}}{A_1 \rho_1} \tag{3.85}$$

but the value of density ρ_1 is unknown. An initial estimation for ρ_1 is made by assuming the total enthalpy is equal to the static one and the value of s_1 is known; then ρ_1 and c_{x1} are determined. The static enthalpy h_1 is computed with:

$$h_1 = h_{o1} - \frac{1}{2} c_{x1}^2 \tag{3.86}$$

thus obtaining a new value of h_1. With this new value combined with s_1 in the same way as before, new values for ρ_1 and c_{x1} are obtained and the procedure continues until there is no change in any value. When the final value of h_1 is found, the static pressure p_1 can be determined by

$$p_1 = p_1(h_1, s_1) \tag{3.87}$$

The mean radius r_{m1} can be defined as in Eq. (3.62) and the peripheral speed U_1 is given by Eq. (3.63). The procedure continues as in the case of the stage preceded by another one, because nothing is different from the station 2 of the stage up to station 3 between the two types of stages. That is, h_3 is determined by Eq. (3.60) and so on, until the pressure ratio and enthalpy and pressure drops are found.

3.6.2 Curtis wheel

The Curtis wheel consists of an inlet nozzle section of partial admission, followed by a series of fixed and moving bladings, which are configured in a way so as to produce work by the reduction of the high kinetic energy of the steam acquired by the expansion in the nozzles. In the whole procedure, the flow of steam is assumed to be isenthalpic after the inlet nozzles.

The input variables related to the Curtis wheel are the following:

- Inlet pressure p_{in}
- Inlet temperature T_{in}
- Steam mass flow rate $\dot{m}$
- Rotational speed N
- Maximum number of stages $stages_{max}$
- Ratio of static pressure at the exit of the nozzle to inlet pressure λ_p
- Nozzle efficiency η_N
- Axial velocity ratio through rotor blading λ_c

- Mean radius of blading r_m
- Rotor clearance κ
- Blade height to width ratio $r_{H/b}$
- Blade height upstream of the first rotor H_{first}
- Partial Admission ratio r_{pa} .

The steam inlet conditions and mass flow rate are considered as variables of the more general system to be subjected to optimization, together with the rotational speed of the turbine. The nozzle efficiency is used for the determination of the enthalpy at the nozzle exit. The velocity of the steam is reduced in the Curtis wheel moving bladings and the associated design parameter defined is the ratio of the axial component of velocity outlet over the inlet. The mean radius of blading is the design parameter primarily defining the size of the Curtis wheel and in conjunction the capability for work production. The rotor clearance and the height-to-width ratio are used in the computation of steam flow losses in the blading, as are required parameters for the Soderberg method for estimation of losses. The blade height upstream the first moving row encountered and the partial admission ratio virtually define the initial axial velocity and the potential for work production.

Figure 3.15 is a schematic of the presumed configuration and the related velocity triangles.

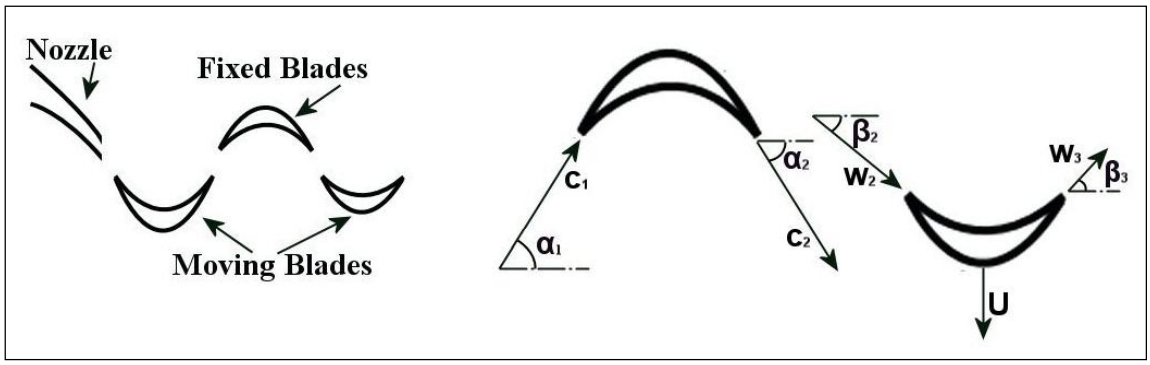

Figure 3.15: Curtis wheel with two moving bladings schematic and velocity triangle with positive flow angles.

The simulation begins with the computations of the enthalpy specific h_{in}, specific entropy s_{in} and density ρ_{in} at the nozzle inlet, with the known input values of pressure and temperature:

$$h_{in} = h_{in}\left(p_{in}, T_{in}\right) \qquad s_{in} = s_{in}\left(p_{in}, T_{in}\right) \qquad \rho_{in} = \rho_{in}\left(p_{in}, T_{in}\right) \tag{3.88}$$

The steam velocity is essentially zero in the chamber before the nozzle and the input values are considered to be the stagnation conditions.

The pressure at the nozzle exit p_2 is readily computed, since the pressure ratio λ_p of the nozzle is provided among the input parameters. From the known values of p_2 and s_{in}, the specific enthalpy of the assumed isentropic expansion h_{2s} can be computed. By using the input for the nozzle efficiency, the actual value of enthalpy at the nozzle exit is computed

$$h_2 = h_{in} - \eta_N \left(h_{in} - h_{2s} \right) \tag{3.89}$$

where η_N the nozzle efficiency. The value of h_2 is the value of specific enthalpy that remains constant throughout the subsequent blade rows as mentioned in the preceding.

The pressure drops are only due to losses. In Figure 3.16 the pressure values p_3, p_4, p_5 are referred to the outlet of the first moving blading, to the outlet of the first fixed blading and to the outlet of the second moving blading, respectively. The pressure drops through the bladings of a Curtis wheel may be large, due to the high steam velocities.

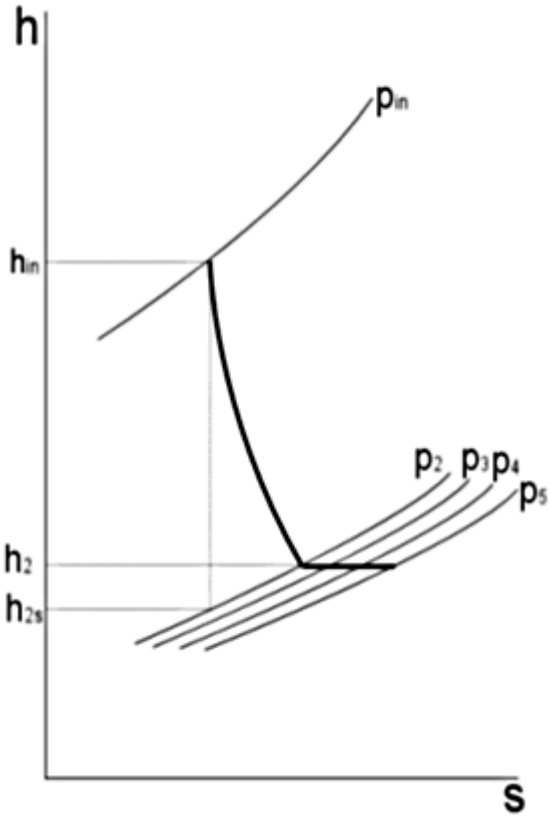

Figure 3.16: h-s diagram for a Curtis wheel with three blade rows.

With p_2 and h_2 known, the specific entropy s_2 and density ρ_2 are computed:

$$s_2 = s_2 \left(p_2, h_2 \right) \qquad \rho_2 = \rho_2 \left(p_2, s_2 \right) \tag{3.90}$$

The total enthalpy remains constant through the nozzle and the absolute velocity at the nozzle exit is computed with:

$$c_2 = \sqrt{2\left(h_{in} - h_2\right)} \tag{3.91}$$

The flow area downstream the nozzles is computed with

$$A_2 = a_r \pi H_{first} \sqrt{4r_m^2 - H_{first}^2} \tag{3.92}$$

where a_r is the partial admission ratio, H_{first} the blades height at the inlet of the first moving blading and r_m is the mean radius, which is constant throughout the Curtis wheel.

The outer and inner radii at the same point are:

$$\begin{aligned} r_{o2} &= \frac{1}{2}\left(H_{first} + \sqrt{4r_m^2 - H_{first}^2}\right) \\ r_{i2} &= r_{o2} - H_{first} \\ \lambda_2 &= \frac{r_{i2}}{r_{o2}} \end{aligned} \tag{3.93}$$

The axial velocity upstream the first moving blading is:

$$c_{x2} = \dot{m} / \left(\rho_2 \mathrm{A}_2\right) \tag{3.94}$$

where $\dot{m}$ is the mass flow rate.
The flow angle a_2 is given by

$$a_2 = \arccos\left(\frac{c_{x2}}{c_2}\right) \tag{3.95}$$

and subsequently the peripheral speed U and the flow angle β_2 by:

$$U = \frac{\pi r_m N}{30} \tag{3.96}$$

$$\beta_2 = \arctan\left(\tan a_2 - \frac{U}{c_{x2}}\right) \tag{3.97}$$

At the present point there is a check in the program about the sign of the β_2 flow angle. If it is negative, the program displays a warning message and the simulation stops. This situation may arise because the user may have placed input parameters that result in a negative β_2, but this possible fact cannot be known before the simulation has reached this point.

The flow angle β_3 is set equal to β_2, since the purpose of the moving blading is to reverse the flow as at the same time reduces the kinetic energy of the stream. The axial velocity c_{x3} at the exit of the moving blading is readily computed with the input of the axial velocity ratio λ_c as $c_{x3} = c_{x2}\lambda_c$. The flow angle a_3 can be computed with:

$$a_3 = \arctan\left(\tan a_2 - U \frac{\lambda_c + 1}{\lambda_c c_{x2}} \right) \tag{3.98}$$

A second check is now performed concerning the sign of a_3. If a_3 is negative, the design is acceptable with no more stages in the Curtis wheel.

The flow velocities c_3, w_2, w_3 are computed with:

$$\begin{aligned} c_3 &= c_{x3} / \cos(a_3) \\ w_2 &= c_{x2} / \cos(\beta_2) \\ w_3 &= c_{x3} / \cos(\beta_3) \end{aligned} \tag{3.99}$$

With known values of the flow angles and velocities, the Soderberg method can be used to find the pressure drop through the moving blading. For the application of the Soderberg method the "inputs" required are the flow angles β_2 and β_3, the height of the blading H_{first}, the width of the blading b, the velocity w_3 and the density ρ_3 and viscosity at the exit of the moving blading. The values of ρ_3 and viscosity are initially estimated as in the case where the flow was isentropic and a repetitive procedure is used to find the pressure p_3.

With known values of pressure and enthalpy at the exit of the moving blades, the thermodynamic properties of steam are defined, and with known c_{x3} the blades height is computed along with the inner and outer radii.

The power produced by the first moving blading is:

$$\dot{W} = \dot{m}\left(h_{in} - h_3 - \frac{1}{2} c_3^2 \right) \tag{3.100}$$

At this point, if the flow angle a_3 is positive and the input for maximum number of stages is higher than 1, the simulation continues for the second fixed blading. The thermodynamic properties and geometric characteristics at the inlet of the fixed blading, (to which the index 1 is assigned in conjunction with the notation adopted for the stator and rotor of a usual turbine stage) are set equal to the ones denoted with index 3 above.

Indices 1, 2 and 3 refer now to the inlet of the first fixed blading, outlet of fixed blading and outlet of the second moving blading. The axial velocity is assumed not to change in the fixed blading, because the purpose of the last is only to reverse the flow angle of the steam so it can rotate the second moving blading in the same direction as the first moving blade. In other words, no thermodynamic change is attempted to be done on the steam through the fixed blading, as in the case of the moving blading, and the pressure drop is only due to the losses. So for the pair "first fixed blading – second moving blading", it holds that:

$$\begin{aligned} c_{x2} &= c_{x1} \\ c_{x3} &= \lambda_c c_{x2} \end{aligned} \tag{3.101}$$

The flow angle a_2 is also set equal to a_1, thus resulting in the computation of c_2:

$$\begin{aligned} a_2 &= a_1 \\ c_2 &= c_{x2} / \cos(\alpha_2) \end{aligned} \tag{3.102}$$

The Soderberg method can now be applied as in the case of usual stages to find h_{2s} and pressure p_2, as described in the Section 1.2, concerning the simulation of individual stages. The specific entropy s_2 and density ρ_2 can also be determined.

An important point of the whole design procedure is the computation of the flow angle β_2, in the same way as it was for the first moving blading. If it is found negative, the simulation stops and a message warns that only one moving blading is feasible by using the specific input values that have led to this point. Again, it is not possible to know beforehand whether a second moving blading is feasible or not.

The computations continue in the same manner as for the first moving blading. At the end of the computations for the second moving blading, the total work of the two bladings and efficiency can be determined.

If required by the inputs, the procedure continues to a second pair of fixed blading – moving blading and so on.

At the end of computations, the values of entropy and total enthalpy are among the outputs of the simulation subroutine concerning the Curtis wheel, because they are required inputs for the design procedure of the first of the following stage groups.

3.6.3 Estimation of energy losses based on Soderberg method

Soderberg's method is a relatively simple method for the estimation of kinetic energy losses, which, as mentioned in [18], is quite accurate and has been applied extensively. Its great advantage for the purposes of the present work is that the determination of losses is based on a small number of geometric characteristics of the turbine blade rows. One more advantage of this method is that it is based on experiments on steam turbines [18] and is therefore more apropriate for the present application. Soderberg has also extended his method to be valid for small turbines with low aspect ratio blading (small height to chord ratio).

The required geometrical characteristics, except of the flow angles, are:

H height of the blade
b width of blading in the axial direction (projection of the chord in that direction)
s distance between successive blades (blade pitch).

In fact, of these three parameters only two can be treated as independent variables, because the design must satisfy Zweifel's criterion, as it is expressed by Eq. (3.103) [18].

For turbine cascade blades there is an optimal space to chord ratio that gives a minimum overall loss. Figure 3.17 illustrates the way the velocity distribution varies around the surface of a turbine blade in a cascade at three values of space to chord ratio. If the spacing between the blades is made small, the fluid receives the maximum amount of guidance from the blades, but the friction losses will be large. On the other hand, with the same blades spaced well apart, friction losses are small but, because of poor fluid guidance, the losses resulting from flow separation are high. These considerations led Zweifel to formulate his criterion for the optimal space-to-axial chord ratio of turbine blades.

According to Zweifel, the optimal space to axial chord width ratio is:

$$\frac{s}{b} = \frac{0.4}{\cos^2 \omega_2 \left(\tan \omega_1 + \tan \omega_2 \right)} \tag{3.103}$$

where ω_1 and ω_2 are the flow angles in the entrance and exit planes, coinciding with flow angles α_1 and α_2 in the stator row and β_2 and β_3 in the rotor.

The loss coefficient is initially computed as:

$$\zeta^* = 0.04 + 0.06 \left(\frac{\varepsilon}{100} \right)^2 \tag{3.104}$$

where $\varepsilon = \omega_1 + \omega_2$ is the deflection angle.

The loss computed with Eq. (3.104) can be considered as the basic "profile" loss.

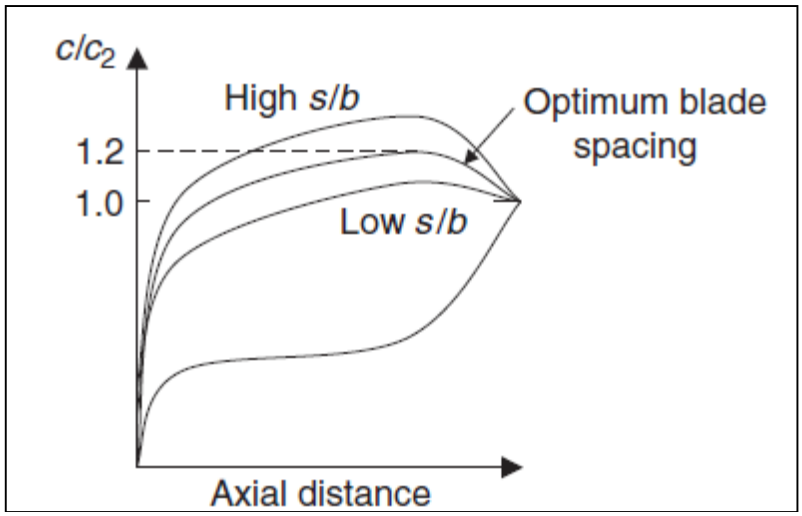

Figure 3.17 Optimal space–chord ratio for a turbine cascade. c_2 is the velocity at the exit plane [18].

For the cases where the ratio of blade height to width is $H/b \neq 3$, the following corrections are applied:

$$\zeta_{1N} = \left(1+\zeta^*\right)\left(0.993+0.021\frac{b}{H}\right)-1$$
$$\zeta_{1R} = \left(1+\zeta^*\right)\left(0.975+0.075\frac{b}{H}\right)-1 \tag{3.105}$$

With the inclusion of the ratio *H/b* in Eq. (3.105), the last one can be considered as a correction for the "secondary" loss, which is strongly affected by the aforementioned ratio.

One more correction for the Reynolds number effects is

$$\zeta_2 = \zeta_1\left(\frac{10^5}{\mathrm{Re}}\right)^{1/4} \tag{3.106}$$

applied when $\mathrm{Re} \neq 10^5$.

The Reynolds number is defined as

$$\mathrm{Re} = \frac{\rho_2 c_2 D_h}{\mu} \tag{3.107}$$

where

ρ_2 density of steam at exit of blade row
μ dynamic viscosity of steam at exit of blade row
D_h hydraulic diameter of the flow defined as follows

$$D_h = \frac{2sH\cos a_2}{s\cos a_2 + H} \tag{3.108}$$

One more correction can be made for the effect of the tip leakage loss in the rotor blades. According to [19], the drop of isentropic efficiency due to the tip leakage can be estimated by multiplying the isentropic efficiency computed without considering the particular loss by the ratio of "blade area" to the sum of "blade area + clearance space". In that case, the enthalpy difference at the stage outlet is expressed as

$$h_3 - h_{3s} = \frac{1}{2} w_3^2 \zeta_R \left(\frac{H + \kappa}{H} \right) \tag{3.109}$$

where κ is the height of the clearance space.

3.6.4 Design procedure of the steam turbines

The theoretical analysis regarding the parts comprising the steam turbine described in the previous sections is used in a design algorithm for the determination of their structural characteristics. The related inputs required, which are also intended to be used as independent variables of the optimization problem, are the high and low pressure levels of steam (P_{HP}, P_{LP}) and the corresponding mass flow rates ($\dot{m}_{HP}$, $\dot{m}_{LP}$) and temperatures (T_{HP}, T_{LP}). All other quantities described throughout the Sections 3.6.1 to 3.6.3 are given as parameters or calculated with the equations included.

For the Curtis wheel, the nozzle pressure ratio, isentropic efficiency and mean radius of the rotor are the most important of the required parameters. The main parameters that need to be defined for the reaction sections are approximate values of the inner radii of the bladings (the exact values are derived with a numerical procedure, as is described in the following), the stage loading coefficients ψ_s and the stage reaction degree *r*. The total and static enthalpy drops through each stage are related to the flow angles in the stator and rotor through the set of trigonometric and thermodynamic equations described in the Sections 3.6.1 and 3.6.3, so that the expansion through every stage in the *h*−*s* diagram and the corresponding velocity triangles are calculated, along with the corresponding thermodynamic properties.

The design procedure for each reaction section begins with the known pressure at its inlet. Stages are added to the section and their performance is simulated with the aforementioned set of equations. Among all the other thermodynamic and geometric quantities resulting from the stage simulation, the pressure drop is calculated for each stage. Stages are added to each one of the reaction sections until the pressures at points B and C (Figure 3.12) drop below the prescribed design values. When this is accomplished, the last stage added is excluded from the section and the inner radius of the reaction section is

slightly increased with a numerical repetitive procedure, until the outlet pressure from the section matches the prescribed value. It is noted that the internal radius is constant throughout the bladings of a section, with the mean and outer radii increasing as the pressure falls downstream the section. In this way, the number of stages at each section is defined, along with the internal and external radii of the bladings and other geometric characteristics (e.g. blade angles). The power output at the design point is also determined, as the steam thermodynamic states are known throughout the expansion line.

The determination of the structural characteristics of the steam turbines is required for the calculation of the turbine performance at off−design operating conditions.

3.6.5 Off−design performance of steam turbines

In the off−design operation of a turbine, there are two important attributes that differ from the design point operation: the isentropic efficiencies of the sections, and the pressure levels posed upstream and downstream the sections, which depend on the sections flow capacity and the steam mass flow rates. A computational algorithm was developed for evaluating the off−design performance of steam turbines, which, on one hand is based on the determined (by the design procedure already executed) geometrical characteristics, and on the other hand on computational approaches addressing the changes in the isentropic efficiency and the flow capacity

3.6.5.1 Off−design flow capacity

The off−design simulation procedure begins with the determination of the pressure levels upstream the two reaction sections. An extended form of the Stodola ellipse found in [20] is used, in which the effect of the finite number of stages is taken into account along with the possibility of operation at choking conditions. The condenser pressure P_C (point C in Figure 3.12) is assumed to be constant at the design−point value. With the mass flow rate of steam in the reaction section 2 known, the pressure P_B (point B in Figure 3.12) at off−design operation is determined by the following procedure: If $P_{C,d} - P_{B,d} a_{BC} \geq 0$, then Eq. (3.110b) is solved for P_B. If $P_{C,d} - P_{B,d} a_{BC} < 0$, which indicates choking conditions at design point, then Eq. (3.110c) is solved for P_B. In both cases, ϕ_{BC} is substituted from Eq. (3.110a). Then, if $P_C - P_B a_{BC} \geq 0$, the value of P_B is retained. If, however, $P_C - P_B a_{BC} < 0$, which indicates choking conditions at off−design, then P_B is calculated with Eq. (3.110d).

$$\phi_{BC} = \frac{\dot{m}_{BC} \sqrt{\upsilon_B}}{\sqrt{P_B}} \tag{3.110a}$$

$$\text{If } P_{C,d} - P_{B,d}a_{BC} \geq 0 \Rightarrow \frac{\phi_{BC}}{\phi_{BC,d}} = \frac{\sqrt{1-\left(\dfrac{P_C - P_B a_{BC}}{P_B - P_B a_{BC}}\right)^2}}{\sqrt{1-\left(\dfrac{P_{C,d} - P_{B,d} a_{BC}}{P_{B,d} - P_{B,d} a_{BC}}\right)^2}} \tag{3.110b}$$

$$\text{If } P_{C,d} - P_{B,d}a_{BC} < 0 \Rightarrow \phi_{BC} = \phi_{BC,d}\sqrt{1-\left(\frac{P_C - P_B a_{BC}}{P_B - P_B a_{BC}}\right)^2} \tag{3. 110c}$$

$$\text{After } (3.110\text{b}) \text{ or } (3.110\text{c}), \text{ if } P_C - P_B a_{BC} < 0 \text{ then } P_B = P_{B,d}\left(\frac{\dot{m}_{BC}^2 \upsilon_B}{\dot{m}_{BC,d}^2 \upsilon_{B,d}}\right) \tag{3. 110d}$$

In these equations, subscript *d* denotes the design point properties and subscript *BC* the second reaction section from point B to point C. The parameter υ_B is the specific volume of steam at point B. The parameter ϕ_{BC} is known as the mass flow constant and a_{BC} is the effective choking pressure ratio of the reaction section *BC*, which depends on its number of stages [20]. The pressure at point A is calculated according to the respective procedure for reaction section 1.

3.6.5.2 Off−design isentropic efficiency

The approach used for the estimation of isentropic efficiency change, is based on the publications [21, 22]. From the results of the specific works, one can predict the effect on the efficiency due to the alteration of pressures in the inlet and exit of stage groups and also of rotational speed. The main distinction for applying the results of these works is whether it is about impulse or reactions stage groups, which is in accordance with the procedures described in the previous sections. In the present section, the steps for using these results are described. The impulse type will be considered first.

The isentropic efficiency η is considered as a function of the pressure ratio of the stage group and a dimensionless index for the rotational speed:

$$\eta = \eta\left(\varepsilon, \bar{N}\right) \tag{3.111}$$

where

ε the outlet to inlet pressure ratio for the stage group p_ω/p_α

$\bar{N}$ speed index defined as $\bar{N} = \dfrac{N}{N_n}\sqrt{\dfrac{\left(p_\alpha v_a\right)_n}{p_\alpha v_a}}$

v_α specific volume

n index for nominal or design conditions.

When both ε and $\bar{N}$ are changing, the change in isentropic efficiency is also dependent on the number of stages comprising the group. This can be seen in Figure 3.18, for the cases of three stages.

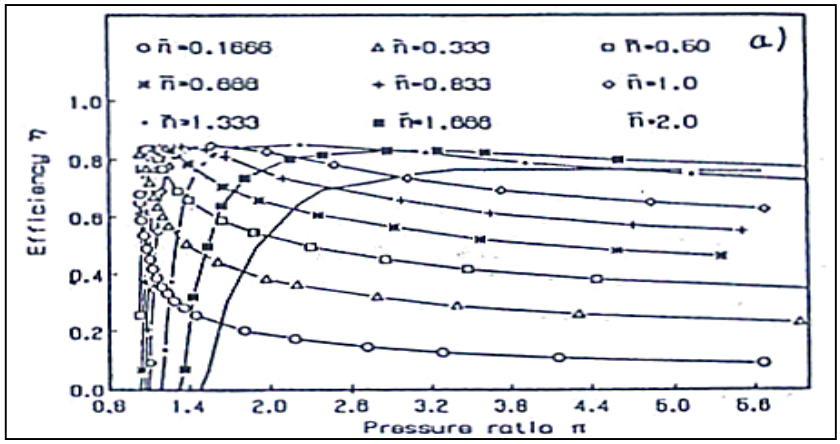

Figure 3.18: Change of isentropic efficiency of a 3-stage reaction group under off-design conditions. The x axis is pressure ratio ε [21].

What is also noticed in the Figure 3.18 is that the curves of efficiency have a quite irregular form, making any generalization impossible. More regular forms seem to be obtainable by introducing some changes in the variables ε and $\bar{N}$. The first step is to transform the characteristics to a form proposed by Traupel using the following variables:

$$\bar{\eta} = \frac{\eta}{\eta_n} = \bar{\eta}\left(\bar{N}, X\right) \tag{3.112}$$

where:

$$X = \frac{\pi - 1}{\pi_0 - 1} \tag{3.113}$$

and $\pi = 1/\varepsilon$.

Thus the curves of Figure 3.18 are transformed to those in Figure 3.19. Similar shape of all curves is obtained in this way, with diversified location of their peak and extensions along the $\bar{N}$ axis can be observed.

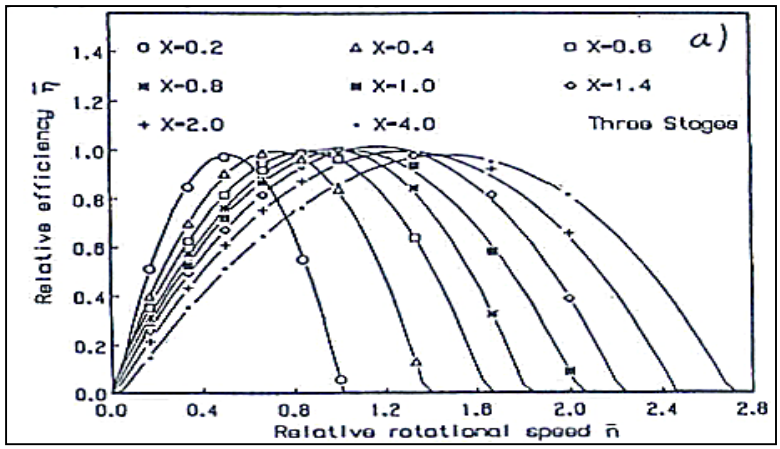

Figure 3.19: Alternative representation of stage efficiency for constant X [21].

This implies introducing the new variables:

$$\bar{\bar{\eta}} = \frac{\bar{\eta}}{\bar{\eta}_{\max}}, \qquad \bar{\bar{N}} = \frac{\bar{N}}{\bar{N}_{opt}} \tag{3.114}$$

associated with the following reduction of the value of the relative efficiency $\bar{\bar{\eta}}$ and reduced rotational speed $\bar{\bar{N}}$, this time to the peak coordinates $\bar{\eta}_{\max}$ and $\bar{N}_{opt}$ for each curve *X*=const. In this case $\bar{\eta}_{\max}$ and $\bar{N}_{opt}$ are functions of *X*. The curves for $\bar{\eta}_{\max}$ and $\bar{N}_{opt}$ as in Figure 3.20 are then obtained.

The $\bar{\eta}_{\max}$ i.e. the maximum values of the efficiency as depicted can be considered as a function of *X* and the number of stages *ns*.

$$\bar{\eta}_{\max} = 1 + a\left(X - 1\right)^{1.24} \tag{3.115}$$

with α defined as

$$\begin{aligned} a &= -0.00466 - 0.00655ns \quad \text{for} \quad X < 1 \\ a &= -0.000558 - 0.000922ns \quad \text{for} \quad X \geq 1 \end{aligned} \tag{3.115´}$$

Similarly, for the value of $\bar{N}_{opt}$ it holds that:

$$\begin{aligned} \bar{N}_{opt} &= 1 + \beta\left(1 - X\right)^{1.3}, \quad \text{where} \quad \beta = 0.762 - 0.0392ns^2 \quad \text{, for} \quad X < 1 \\ \bar{N}_{opt} &= 1 + \beta\left(1 - X\right)^{0.77}, \quad \text{where} \quad \beta = 0.25 - 0.017ns^2 \quad \text{, for} \quad X \geq 1 \end{aligned} \tag{3.116}$$

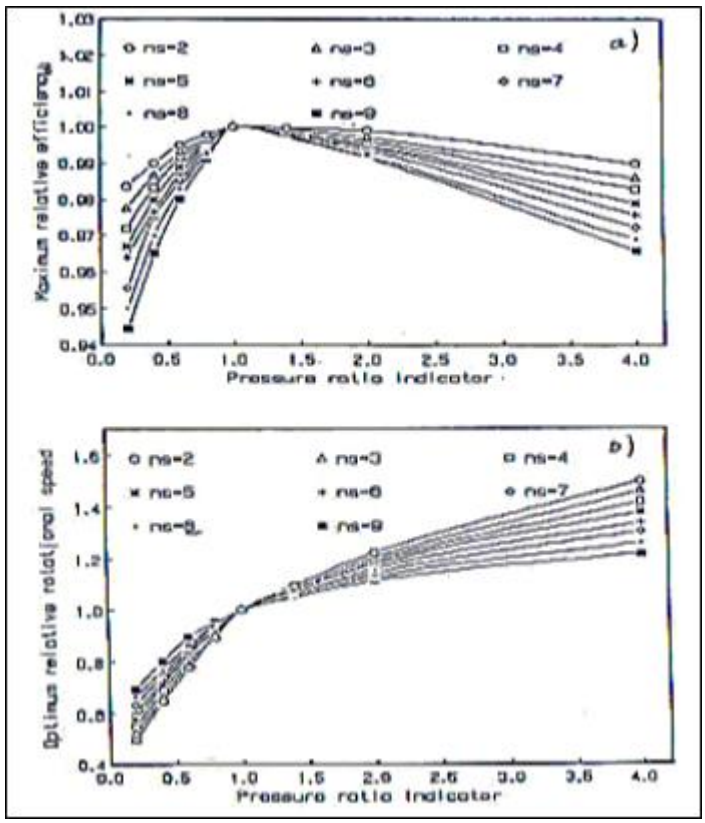

Figure 3.20: The values of $\bar{\eta}_{\max}$ and $\bar{N}_{opt}$ as function of ns and X [21].

Statistical tests of curves in Figure 3.21 proved that there is no need to indicate the influence of the number of stages in the group in the relation. Therefore, the relation can be regarded as below:

$$\begin{aligned} \bar{\bar{\eta}} &= 1-\left(1-\bar{\bar{N}}\right)^{1.94}, \quad \text{for} \quad \bar{\bar{N}} < 1 \\ \bar{\bar{\eta}} &= 1-0.885\left(1-\bar{\bar{N}}\right)^{2.42}, \quad \text{for} \quad \bar{\bar{N}} \geq 1 \end{aligned} \tag{3.117}$$

To summarize, with determined X and $\bar{N}$ the steps to compute $\bar{\eta}$ of Eq. (3.112) are:

- $\bar{N}_{opt}$ is calculated with Eq. (3.116)
- $\bar{\bar{N}}$ is calculated with Eq. (3.114)
- $\bar{\bar{\eta}}$ is calculated with Eq. (3.117)
- $\bar{\eta}_{\max}$ is calculated with Eq. (3.115)
- $\bar{\eta}$ is calculated with Eq. (3.114).

It should be noted that the results for the impulse stage groups are related to a typical impulse stage blade design, as referred by the authors of [21] and are applicable in similar cases. Therefore, they can be used in place of a “generalized” map as the ones used for gas turbines.

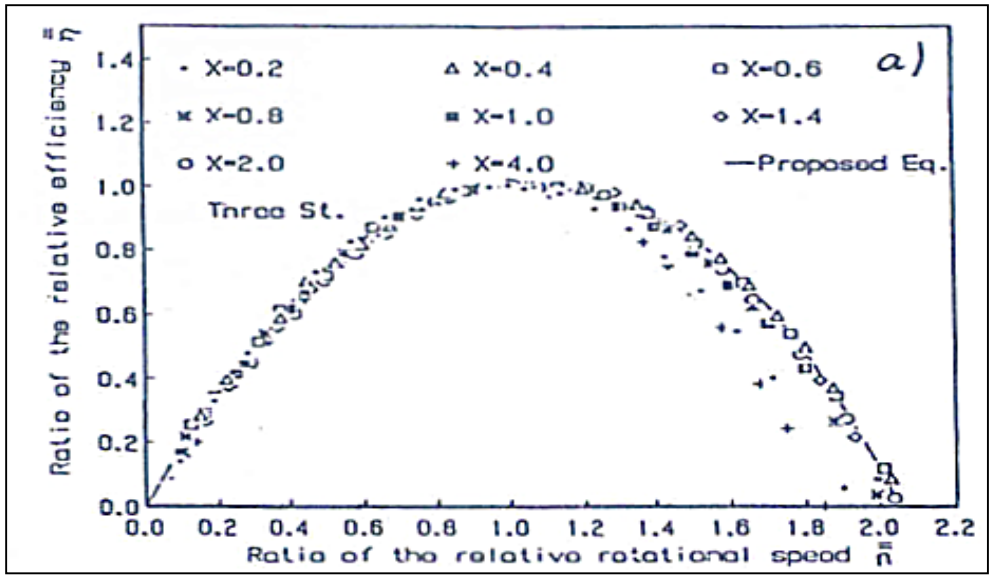

Figure 3.21: Dimensionless efficiency $\bar{\bar{\eta}}$ as a function of X and $\bar{\bar{n}}$ [21].

The reaction stage groups are treated in a similar way, where the definitions of variable reductions are the same as in the case of impulse stage groups, meaning that Eqs. (3.121) – (3.124) are also used in this context. One noticeable difference from the impulse stage group results is that the dimensionless efficiency $\bar{\bar{\eta}}$ seems to be a function of number of stages of the group. Two different types of reaction stage groups are considered, the one being a Brown Boveri design (1K12) and one based on "traditional" design concepts (TN-2).

The stage group efficiency at off design operating conditions can again be expressed as:

$$\eta = \eta_n \bar{\bar{\eta}} \bar{\eta}_{\max} \tag{3.118}$$

The peak dimensionless efficiency $\bar{\eta}_{\max}$ is dependent on the variable *X* of Eq. (3.113), the number of stages and on the type of turbine. Its value can be obtained with regression of the curves on the diagram of Figure 3.22.

The same are also applicable for the dimensionless speed ratio $\bar{N}_{opt}$ which can be derived from the curves of Figure 3.23.

The dimensionless efficiency is expressed with the following relations:

$$\begin{aligned} \bar{\bar{\eta}} &= 1-\left(1-\bar{\bar{N}}\right)^{\alpha_1}, \quad \text{for} \quad \bar{\bar{N}} < 1 \\ \bar{\bar{\eta}} &= 1-\alpha_3\left(\bar{\bar{N}}-1\right)^{\alpha_2}, \quad \text{for} \quad \bar{\bar{N}} \geq 1 \end{aligned} \tag{3.119}$$

The coefficients α_1, α_2, α_3 are taken from Table 3.13.

Table 3.13: Coefficients for Eq. (3.119). z is the number of stages in the group.

Turbine type 1K12				Turbine type TN-2			
z	α_1	α_2	α_3	z	α_1	α_2	α_3
3	2.7	1.8	0.165	3	2.6	1.7	0.202
6	3.5	1.7	0.147	6	3.0	1.6	0.179
9	4.3	1.7	0.140	9	3.4	1.6	0.163
12	5.0	1.8	0.173	12	3.5	1.7	0.159

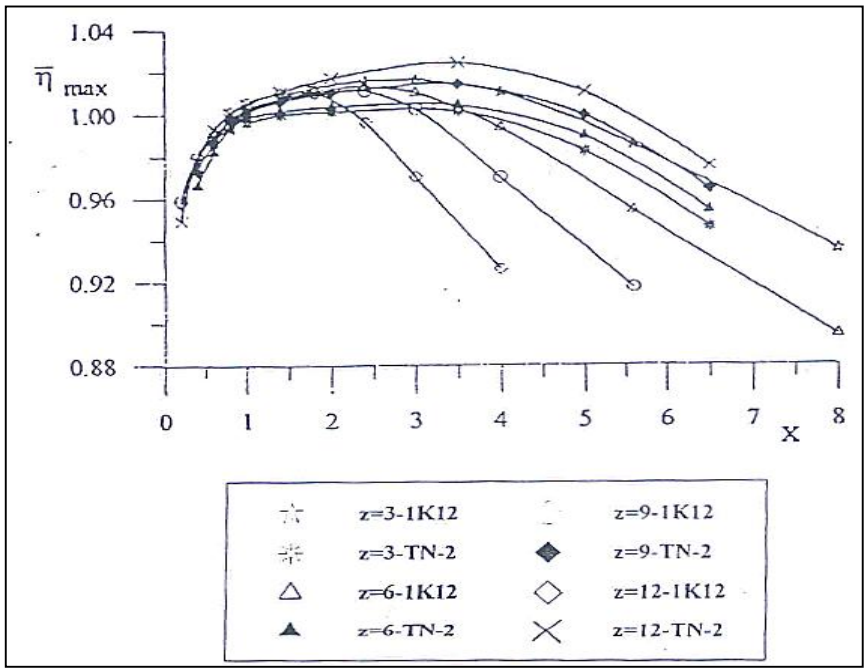

Figure 3.22: Variation of $\bar{\eta}_{\max}$ of reaction stage groups as function of design type, pressure index X and number of stages [22].

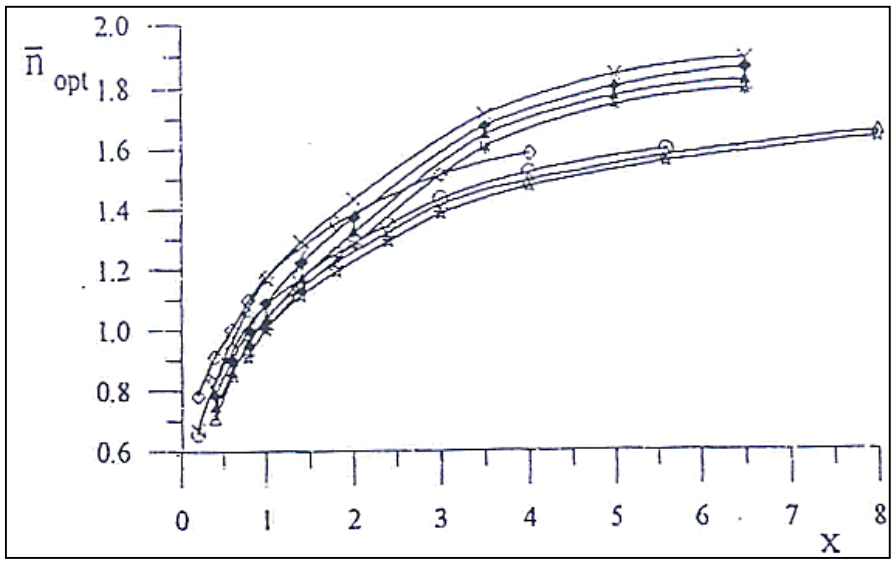

Figure 3.23: Variation of $\bar{N}_{opt}$ of reaction stage groups as function of design type, pressure index *X* and number of stages ([22]).

Thus, to compute the change in efficiency by means of Eq. (3.118) the procedure is as follows:

- $\bar{N}_{opt}$ is found from Figure 3.23
- $\bar{\eta}_{\max}$ is found from Figure 3.22
- In the case of $X<1$ it is

$$\eta = \eta_n \left[1 - \left(1 - \frac{N}{N_n} \sqrt{\frac{(p_a v_a)_n}{p_a v_a}} \frac{1}{\bar{N}_{opt}(z, X)} \right)^{a_1} \right] \eta_{\max}(z, X)$$

- In the case of $X \geq 1$ it is

$$\eta = \eta_n \left[1 - a_3 \left(\frac{N}{N_n} \sqrt{\frac{(p_a v_a)_n}{p_a v_a}} \frac{1}{\bar{N}_{opt}(z, X)} - 1 \right)^{a_2} \right] \eta_{\max}(z, X)$$

3.7 Diesel−Generator Sets

The Diesel gen-sets that may appear in the energy system are modelled by regression analysis performed on available manufacturers' data. The SFOC is calculated with the Eq. (3.120) and the related coefficients are presented in Table 3.14. It is noted that for engines with MCR higher than 4800 kW, the MCR input is set equal to 4800 kW.

$$\begin{aligned} SFOC_{GS,base} = a + b \ln MCR + c \ln f_l + d (\ln MCR)^2 + e (\ln f_l)^2 + f \ln MCR \ln f_l + \\ + g (\ln MCR)^3 + h (\ln f_l)^3 + i \ln MCR (\ln f)^2 + j (\ln MCR)^2 \ln f_l \end{aligned} \quad (3.120)$$

where

MCR: Maximum Continuous Rating of the engine in kW, range 400−11000 kW

f_l: load factor is input in the range 20 to 100% (numerical values given in the range 20 - 100)

$SFOC_{GS,base}$: specific fuel oil consumption in gr/kWh.

Table 3.14: Coefficients for Equation (3.120).

a	1863.36174080984	f	84.7884631761691
b	-549.571305719787	g	-2.02488401570365
c	-112.333372381162	h	11.3791269650595
d	53.0073600751809	i	-5.41645772696988
e	-77.2503323160516	j	-2.68200939081895

The exhaust gas mass flow rate (in kg/s) and temperature (in ^{o}C) are calculated with Eqs. (3.121) and (3.122), respectively, and the related coefficients are presented in Tables 3.15 and 3.16.

$$\dot{m}_{g,GS} = \left[aMCR^{b} \exp\left(cMCR\right) \right] \times \left[df_l^{3} + ef_l^{2} + ff_l + g \right] \tag{3.121}$$

Table 3.15: Coefficients for Eq. (3.121).

a	3.64405450057258E-03	d	-1.9614900920825E-06
b	0.918105441305709	e	3.69303720484067E-04
c	1.0209750314211E-05	f	-1.30249958062006E-02
		g	0.561755635436517

$$T_{g,GS} = \left[aMCR^{b/MCR} \right] \times \left[cf_l^{3} + df_l^{2} + ef_l + f \right] \tag{3.122}$$

Table 3.16: Coefficients for Eq. (3.122).

a	303.713609889053	d	-3.3937952254995E-04
b	9.47014136611228	e	0.012694694942915
c	2.08274512078117E-06	f	1.04404874116135

3.8 Properties of Working Fluids

In the present section the calculations of the thermodynamic and thermo−physical properties of the working fluids flowing in the steam cycle components are presented. These are essentially the exhaust gas in the HRSGs and the water/steam flows in the HRSGs and the steam turbines. The presentation begins with the exhaust gas properties.

3.8.1 Exhaust gas properties

The exhaust gases delivered by the prime movers are mixtures of gases, and their thermodynamic and thermo−physical properties required for the calculations (specific heat, thermal conductivity and viscosity) are estimated as explained in the following. For the analysis to follow, it is assumed that the mass and molar fraction of each of the major component gases is given. These are assumed to be the chemical elements or the compounds of N_2, O_2, H_2O (gaseous), CO_2 and SO_2.

The properties of the component gases are dependent on the temperature. In the present work, the related formulas contained in [23] are used. For the specific heat, the equation used is the following:

$$f_T = \frac{T}{A+T}$$
$$\frac{c_p}{R} = B + (C-B) f_T{}^2 \left[1 - \frac{A}{A+T} \left(D + E f_T + F f_T{}^2 + G f_T{}^3 \right) \right] \tag{3.123}$$

where T is the temperature of the gas in K, and R is the gas constant in kJ/kgK. The related coefficients are presented in Table 3.17.

Table 3.17: Coefficients for Eq. (3.123) [23].

	N_2	O_2	H_2O	CO_2	SO_2
A	432.2027	2122.2098	706.3032	514.5073	848.4734
B	3.516	3.5302	5.1703	3.4923	4.1379
C	2.8021	-7.1076	-6.0865	-0.9306	-0.0601
D	-4.1924	-1.4542	-6.6011	-6.0861	-4.0449
E	42.0153	30.6057	36.2723	54.1586	56.0276
F	-114.25	-83.6696	-63.0965	-97.5157	-109.335
G	111.1019	79.4375	46.2085	70.9687	76.84

The dynamic viscosity of the gases is calculated as:

$$\mu = A + BT + CT^2 + DT^3 + ET^4 \tag{3.124}$$

where μ is the dynamic viscosity in Pa·s, and the related coefficients are presented in Table 3.18.

Table 3.18: Coefficients for Eq. (3.124) [23].

	N_2	O_2	H_2O	CO_2	SO_2
A	-0.0102e-5	-0.10257e-5	0.64966e-5	-0.18024e-5	-0.13559e-5
B	0.74785e-7	0.92625e-7	-0.15102e-7	0.65989e-7	0.5123e-7
C	-0.59037e-10	-0.80657e-10	1.15935e-10	-0.37108e-10	-0.11626e-10
D	0.0323e-12	0.05113e-12	-0.10080e-12*	0.01586e-12	0
E	-0.00673e-15	-0.01295e-15	0.031e-15	-0.003e-15	0

*This is a validated value, the minus sign *"–"* is correct. In [23] the minus sign is missing.

The thermal conductivity is calculated as a fourth order polynomial:

$$k = A + BT + CT^2 + DT^3 + ET^4 \tag{3.125}$$

where *k* is the thermal conductivity in W/mK, and the related coefficients are presented in Table 3.19.

Table 3.19: Coefficients for Eq. (3.125) [23].

	N_2	O_2	H_2O	CO_2	SO_2
A	-0.133e-3	-1.285e-3	13.918e-3	-3.882e-3	0.358e-3
B	.101e-3	0.107e-3	-0.047e-3	0.053e-3	0.013e-3
C	-0.060650e-6	-0.052630e-6	0.258066e-6	0.071460e-6	0.069520e-6
D	0.033610e-9	0.025680e-9	-0.183149e-9	-0.070310e-9	-0.032070e-9
E	-0.007100e-12	-0.005040e-12	0.055092e-12	0.018090e-12	-0.008300e-12

Equations (3.123) – (3.125) give the properties of the gaseous components of the exhaust gas. For the case of the specific heat, the pertaining property of the gas mixture is readily calculated as an average of the specific heat of the components weighted by the mass ratio of each component. For the cases of thermal conductivity and the dynamic viscosity more sophisticated approaches are required when calculating the mixture's respective properties.

The dynamic viscosity μ_m of a gaseous mixture is calculated with the individual components viscosities μ_i as [24]:

$$\mu_m = \sum_{i=1}^{n} \frac{\mu_i}{1 + \frac{1}{x_i} \sum_{\substack{j=1 \\ j \neq i}}^{n} x_j \phi_{ij}}$$

$$\phi_{ij} = \frac{\left[1 + \sqrt{\frac{\mu_i}{\mu_j}} \left(\frac{M_j}{M_i} \right)^{\frac{1}{4}} \right]}{\frac{4}{\sqrt{2}} \sqrt{1 + \frac{M_i}{M_j}}} \tag{3.126}$$

where x_i is the mole fraction and M_i is the molecular weight of each component *i*.

The thermal conductivity is calculated as [25]:

$$k_m = \sum_{i=1}^{n} \frac{k_i}{1 + \frac{1}{x_i} \sum_{\substack{j=1 \\ j \neq i}}^{n} A_{ij} x_j} \tag{3.127a}$$

$$A_{ij} = \frac{1}{4} \left\{ 1 + \sqrt{\frac{\mu_i}{\mu_j} \left(\frac{M_j}{M_i} \right)^{\frac{3}{4}} \left(\frac{T + S_i}{T + S_j} \right)} \right\}^2 \left(\frac{T + S_{ij}}{T + S_i} \right) \tag{3.127b}$$

$$S_{ij} = S_{ji} = C\sqrt{S_i S_j} \qquad S_{i,j} = 1.5T_{bi,j} \tag{3.127c}$$

where C is a constant which is equal to unity when both elements i and j are non-polar molecules (cases of N_2, O_2, CO_2 for the specific application) or takes the value of 0.73 if either of the elements i or j is polar (as H_2O and SO_2 are), and T_{bi} is the normal boiling point of the element i in K (for the cases of hydrogen, helium and neon, not present in the specific application, the parameter S_i is simply S_i=79 K)

3.8.2 Water – steam properties

All the water and steam properties are evaluated with the direct and inverse thermodynamic propertied functions reported in [26].

References

1. MAN, Computerized Engine Application System (CEAS) http://marine.mandieselturbo.com/two-stroke/ceas
2. Waste Heat Recovery System (WHRS) for Reduction of Fuel Consumption, Emissions and EEDI. MAN Diesel and Turbo, 5510-0136-03ppr, Aug 2014, Denmark.
3. Thermo Efficiency System for Reduction of Fuel Consumption and CO2 Emission. MAN Diesel and Turbo, 5510-0030-03ppr. Oct 2014, Denmark.
4. Knudsen TS, Exhaust gas for power generation – How efficient are state–of−the–art methods? Ship Efficiency, 1st International Conference, Hamburg, October 8-9 2007.
5. Software MarineGTs, Laboratory of Thermal Turbomachines, NTUA, https://www.ltt.ntua.gr/index.php/en/softwaremn/marine-gts .
6. Shah RK, Sekulić DP. Fundamentals of Heat Exchangers. John Wiley and Sons Inc., 2003, ISBN: 0-471-32171-0.
7. Kays MW, London AL. Compact Heat Exchangers. McGraw Hill Book Company, 3rd ed. 1984, ISBN: 0-07-033418-8.
8. Domingos JD (1969). Analysis of Complex Assemblies of Heat Exchangers. Int. Journal of Heat Mass Transfer 1969; 12: 537−548.
9. Pignotti A, Shah RK (1992). Effectiveness - Number of Transfer Units Relationships for Heat Exchanger Complex Flow Arrangements. Int. Journal of Heat Mass Transfer 1992;35: 1275−1291.
10. Krupiczka R, Rotkegel A, Walczyk H, Dobner L. An Experimental Study of Convective Heat Transfer from Extruded Type Helical Finned Tubes. Chemical Engineering and Processing 2003; 42:29−38.
11. Schlünder EU. Heat Exchanger Design Handbook, Hemisphere Publishing Corporation, 1983, ISBN: 0-891-16-125-2.
12. Annaratone D. Steam Generators, Description and Design. Springer-Verlag, Berlin-Heidelberg, 2008, ISBN: 978-3-540-77714-4.

13. Liu Z, Winterton RHS. A General Correlation for Saturated and Subcooled Boiling in Tubes and Annuli, Based on a Nucleate Pool Boiling Equation. Int. Journal of Heat Mass Transfer 1991; 34: 2759–2766.
14. Serth RW. Process Heat Transfer, Principles and Applications. Academic Press 2007, ISBN: 978-0-12-373588-1.
15. Cooper MG. Saturation Nucleate Pool Boiling: A Simple Correlation. I. Chem. Eng. Symposium Ser., 86, No. 2 1984, 785–793.
16. Cao E. Heat Transfer in Process Engineering. McGraw Hill Book Company, 2010, ISBN 978-0-07-162408-4.
17. Kakaç S, Liu H. Heat Exchangers, Selection, Rating and Thermal Design, 2nd ed., CRC Press, 2002, ISBN: 0-8493-0902-6.
18. Dixon SL, Hall CA. Fluid Mechanics and Thermodynamics of Turbomachinery, 6th Ed. Butterworth-Heinemann, 2010, ISBN: 978-1-85617-793-1.
19. Horlock JH. Losses and Efficiencies in Axial-Flow Turbines. International Journal of Mechanical Sciences 1960;2:48-75.
20. Cooke DH. On Prediction of Off−Design Multistage Turbine Pressures by Stodola's Ellipse. Journal of Engineering for Gas Turbines & Power 1985;107:596−606.
21. Miller A, Lewandowski J, Abed KA. A Contribution to the Flugel's−Stodola's Law for Flow Capacity of Turbine Stages Group. VDI Berichte 1995;1185:391−405.
22. Miller A, Lewandowski J, Trzcinska Z, Abed KA. Generalized performance characteristics of turbine stage groups, An attempt to supplement the Flugel's−Stodola's law. Archive of Mechanical Engineering 2000;XLVII:33−52.
23. VDI Heat Atlas, 2nd Edition. VDI–Gesellschaft Verfahrenstechnik und Chemieingenieurwesen. Springer-Verlag Berlin Heidelberg, 2010, ISBN 978-3-540-77876-9.
24. Bromley LA, Wilke CR. Viscosity Behaviour of Gases. Industrial and Engineering Chemistry 1951; 43:1641−1648.
25. Lindsay AL, Bromley LA. Thermal Conductivity of Gas Mixtures. Industrial and Engineering Chemistry 1950; 42:1508−1511.
26. Wagner W, Kretzschmar HJ. International Steam Tables, Properties of Water and Steam Based on the Industrial Formulation IAPWS-IF97, 2nd Ed. Springer-Verlag Berlin Heidelberg, 2008, ISBN 978-3-540-21419-9.

Chapter 4

Integrated System Modeling

In the present chapter, the simulation procedure regarding the overall integrated energy system is presented. The modeling of the system is on one hand based on the modeling and design procedures of the individual components, which is presented in Chapter 3. On the other hand, the modeling of the system as a whole is based on the definition of appropriate variables concerning the technical and functional interconnections of the components of the system. Generally, the intention of the present work is to identify the optimal synthesis, design and operational characteristics of the components of the energy system, with the mathematical optimization objective function expressed in a way the it takes into account the design point characteristics and the performance of the components during the various operating modes in a single and unified simulation step. This is a main difference in comparison with other works in the field mentioned in the Introduction, where the optimization is executed on two levels, the first one determining the optimal synthesis and design of the energy system and the operational optimization is performed on a second level, for the synthesis and design of the energy system determined on the first level.

For this reason, the simulation of the energy system as a whole had to be developed having in mind that the input variables should be able and adequate to determine the synthesis, design and operational performance of the components during the various modes of ship operation and, finally, to reach the value of the objective function in a single computational step.

According to the way the whole system is modeled, a mixed integer nonlinear optimization problem is formulated. The use of optimization algorithm employed is described in Chapter 5.

4.1 Integrated System Modeling based on the System Superconfiguration

The superconfiguration of the system is presented in Chapter 2. In Figure 2.1, it is observed that there is the possibility of using Diesel engines or gas turbines as prime movers. The initial intention was that the type of the prime movers was to be determined by the optimization algorithm. This intention was later abandoned mainly for the following reason. The order of magnitude of the steam bottoming cycle components and their intensive and extensive thermodynamic properties vary largely between systems with Diesel engines or gas turbines as prime movers. It turned out that the solution of the optimization problem was much more efficient and effective when the two types of engines were examined in separate.

As a consequence, the superconfiguration of the system is reduced to the one depicted in Figure 4.1. The difference is that the alternative types of prime movers are replaced by the generic type of *Main Engine* (ME), which implies that the prime movers can be either Diesel engines or gas turbines.

The procedure for modeling the integrated system is independent of the type of prime mover, with only one minor modification for the case of gas turbines which will be mentioned in Section 4.3.

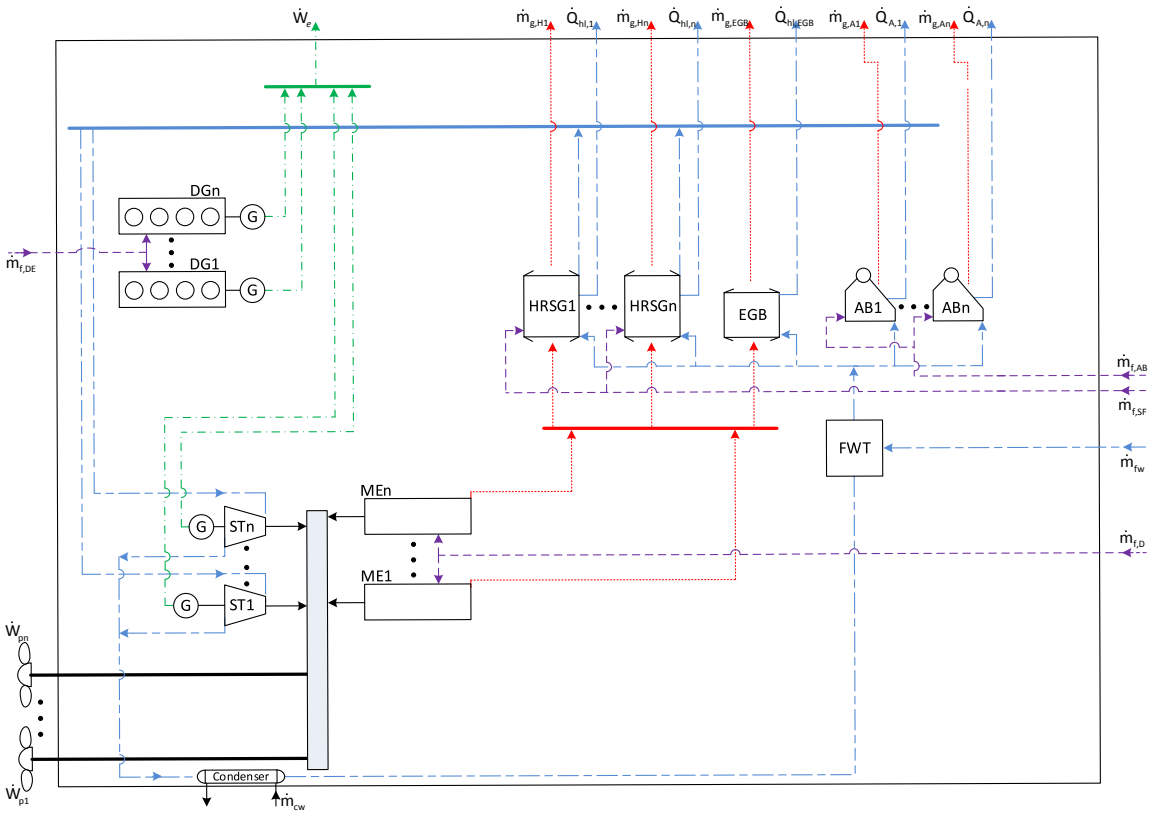

Figure 4.1: Superconfiguration used for the integrated system modeling.

4.2 Modeling Equations for the Single−level Approach of Optimization

In the superconfiguration depicted in Fig. 4.1, the numbers of the prime movers, the HRSGs, the steam turbines, the auxiliary boilers and the Diesel generator sets are depicted as unknown variables to be determined. The fact that the number of components present is not known before the application of the optimization algorithms has a very important effect on the rationale on which the development of the single level approach for the integrated system modeling as a whole is based.

For the formulation of the problem, it is assumed that the number of operating modes N_T of the ship is predefined. Each mode has duration $t_{D,y}$, while the propulsion, electric and thermal power requirements (symbolized as $\dot{W}_{p,y}$, $\dot{W}_{e,y}$ and $\dot{Q}_{th}$, respectively) are constant

during each of these modes, and may be of a predefined magnitude or not. That is, the only requirement for the formulation of the method, is that the magnitude of the loads must be considered as constant during the span of each operating mode.

The requirements that every type of energy demand (propulsion, electric or thermal energy) is covered by the system are stated as equality constraints of the optimization problem:

$$\sum_{x=1}^{x=n_{ME,y}} \dot{W}_{ME,x,y} + \sum_{v=1}^{v=n_{ST,y}} \dot{W}_{STp,v,y} = \dot{W}_{p,y} \quad , \qquad y = 1,...,N_T \tag{4.1}$$

$$\sum_{x=1}^{x=n_{DG,y}} \dot{W}_{DGx,y} + \sum_{v=1}^{v=n_{ST,y}} \dot{W}_{STev,y} = \dot{W}_{e,y} \quad , \qquad y = 1,...,N_T \tag{4.2}$$

$$\sum_{z=1}^{z=n_{HRSG,y}} \dot{Q}_{hlz,y} + \sum_{u=1}^{u=n_{AB,y}} \dot{Q}_{AB,u,y} + \dot{Q}_{EGB,y} = \dot{Q}_{hl,y} \quad , \quad y = 1,...,N_T \tag{4.3}$$

where

$n_{ME,y}, n_{DG,y}, n_{ST,y}, n_{HRSG,y}, n_{AB,y}$ numbers of main engines, Diesel−generator sets, steam turbines, heat recovery steam generators and auxiliary boilers operating in mode y

$\dot{W}_{ME,x,y}$ power supplied by main engine x ($x = 1,...,n_{ME,y}$) to the propeller

$\dot{W}_{STp,v,y}$ mechanical power of steam turbine v ($v = 1,...,n_{ST,y}$) supplied for propulsion

$\dot{W}_{DG,x,y}$ electric power output of Diesel−generator set x ($x = 1,...,n_{DG,y}$)

$\dot{W}_{STe,v,y}$ electric power of steam turbine−generator v

$\dot{Q}_{hlz,y}$ thermal power supplied by the heat recovery steam generator z ($z = 1,...,n_{HRSG,y}$)

$\dot{Q}_{AB,u,y}$ thermal power of auxiliary boiler u ($u = 1,...,n_{AB,y}$)

$\dot{Q}_{EGB}$ thermal power of the exhaust gas boiler.

The first step in the simulation procedure is the computations concerning the operation of the prime movers. The procedure is similar for all the cases where the prime movers may be two−stroke or four−stroke Diesel engines or gas turbines.

The prime movers are assumed to be mechanically coupled to the propeller. The number of prime movers that operate at each mode, $n_{ME,y}$, is an independent variable of the optimization problem.

As already mentioned, the steam turbine of the bottoming cycle (if present and operating) may contribute to the propulsion in any of the operating modes. Thus, the sum of the brake power of the prime movers may be lower than the propulsion power prescribed and this is expressed by Eq. (4.4)

$$\sum_{x=1}^{n_{ME,y}} \dot{W}_{ME,x,y} = \lambda_{ME,y} \dot{W}_{p,y} \qquad \lambda_{ME,y} \leq 1 \tag{4.4}$$

where $\dot{W}_{ME,x,y}$ is the brake power of the prime mover x in mode y and $\lambda_{ME,y}$ is an independent variable of the problem

The propulsion power produced by the prime movers must be allocated among the prime movers operating in each mode y. For this reason, the variables $\tilde{W}_{ME,x,y}$ are introduced as independent variables of the optimization problem, and their use in determining the brake power of each prime mover x with the equation

$$\dot{W}_{ME,x,y} = \tilde{W}_{ME,x,y} \left(\lambda_{ME,y} \dot{W}_{p,y} - \sum_{i=1}^{x-1} \dot{W}_{ME,i,y} \right) \quad , \quad \tilde{W}_{ME,x,y} \leq 1 \quad , \quad 1 < x < n_{ME,y} \tag{4.5}$$

For the engine with $x=n_{ME,y}$, the brake power is computed with the equation

$$\dot{W}_{ME,n_{ME,y},y} = \lambda_{ME,y} \dot{W}_{p,y} - \sum_{i=1}^{n_{ME,y}-1} \dot{W}_{ME,i,y} \quad , \quad x = n_{ME,y} \tag{4.6}$$

After the brake powers of the prime movers are calculated, the maximum value of the power of each prime mover is set as a temporary value of its nominal power rating $\dot{W}_{MEx,N,temp}$. This is a temporary value for two reasons. The first reason has to do with the general requirement of the installed power to be higher than the maximum propulsion power demand, for reasons of gradual degradation of the machinery and their performance and the hull fouling. For this reason, in the case of Diesel engines as prime movers, the value of $\dot{W}_{MEx,N,temp}$ is divided by a factor μ_s, resulting in the new temporary value $\dot{W}_{MEx,N,temp,sm} = \dot{W}_{MEx,N,temp} / \mu_s$. The factor μ_s is lower than unity (with a typical value of 0.85) and results in an excess of propulsive power generally known as *sea margin*.

Up to this point, the nominal power rating of each prime mover x is set with the aforementioned procedure, with no application of optimization. In order to leave room for optimization, the variables $\dot{W}_{N,x,mult}$ are introduced as independent variables of the optimization problem, and the final value for the nominal power rating of each prime mover is calculated with the equation

$$\dot{W}_{ME,x} = \dot{W}_{N,x,mult} \dot{W}_{MEx,N,temp,sm} \tag{4.7}$$

After the application of the multipliers $\dot{W}_{N,x,mult}$, the load factors of the engines can be calculated in each mode. At this point the functions given in Chapter 3 can be applied, so that the specific fuel oil consumption $SFOC_{x,y}$ and the exhaust gas mass flow rates $\dot{m}_{gx,y}$

and temperatures $T_{gx,y}$ can be calculated for each engine *x* and each mode *y*. With the exhaust gas data calculated in the previous step, the HRSGs intended to be present in the system can be designed (in terms of nominal flows and temperatures of steam production) and their performance in the various modes can be evaluated.

Before designing each HRSG, decisions have to be made concerning their number and the way the prime movers are connected to them. For this reason, the independent variables $g_{x,y}$ are introduced. The values of $g_{x,y}$ are integer and they designate the number of HRSG *z* where the engine *x* delivers the exhaust gas in operating mode *y*. For example, $g_{2,3}$=1, means that the prime mover numbered 2 delivers the exhaust gas to HRSG numbered 1 in mode 3. These variables are independent variables of the optimization problem. Their use has a double significance: (i) they define which HRSG operates in each mode and with what exhaust gas inlet, and (ii) they define the number of the HRSGs present in the system. It is noted that the maximum allowed number of HRSGs, $n_{HRSG,max}$, is equal to the number of prime movers in the system, which is calculated in the step concerning the prime movers (that is, the number of HRSGs cannot be higher than the number of prime movers). Furthermore, it is assumed that the exhaust gas stream from each engine cannot be divided between two HRSGs, i.e. each engine *x* can deliver its exhaust gas to only one HRSG in a defined mode *y*.

It is considered that any of the HRSGs possibly present in the system will be operating at a common pressure level, or two common pressure levels in the case of double pressure HRSGs and the steam produced is fed to a common collector, before it is delivered to the steam turbines. Pressures, P_{HP} and P_{LP}, are independent variables of the optimization problem.

When the exhaust gas streams intended to be used in HRSG *z* are defined in operating mode *y*, a mass and an energy balance is performed to define the inlet mass flow rate and temperature resulting from the mixing procedure (if any), symbolized as $\dot{m}_{gz,y}$ and $T_{gz,y}$, respectively. At this point, the design characteristics of each HRSG can be calculated. For establishing a formal relationship between the design point calculations of the HRSGs and the characteristics of the exhaust gas streams actually used at their inlets, two intermediate dependent variables are calculated for each HRSG, the time mean values of the exhaust gas mass flow rate and temperature, defined with the equations

$$\dot{m}_{gz,mean} = \frac{\sum_{y=1}^{N_T} \dot{m}_{gz,y} t_{D,y}}{\sum_{y=1}^{N_T} t_{D,y}} \tag{4.8a}$$

$$T_{gz,mean} = \frac{\sum_{y=1}^{N_T} T_{gz,y} t_{D,y}}{\sum_{y=1}^{N_T} t_{D,y}} \tag{4.8b}$$

The values of $\dot{m}_{gz,mean}$ and $T_{gz,mean}$ are used to calculate the *design* or *nominal* mass flow rates $\dot{m}_{g,z}$ and temperatures $T_{g,z}$ of the HRSGs. This is achieved by defining values of two variables for each HRSG, namely $\dot{m}_{gz,mult}$ and $T_{gz,mult}$, the use of which is as seen in the equations

$$\dot{m}_{gz} = \dot{m}_{gz,mean} \times \dot{m}_{gz,mult} \tag{4.9a}$$

$$T_{gz} = T_{gz,mean} \times T_{gz,mult} \tag{4.9b}$$

The variables $\dot{m}_{gz,mult}$ and $T_{gz,mult}$ are independent variables of the optimization problem. In addition to the exhaust gas properties at the design point of the HRSGs, variables concerning the steam mass flow rates produced and the pertaining temperatures are required for designing the HRSGs. For each HRSG, the design point mass flow rates of steam, $\dot{m}_{HP,z}$ and $\dot{m}_{LP,z}$ are independent variables of the optimization problem, which means that they are directly used as inputs to the simulation procedure (variable $\dot{m}_{LP,z}$ is used only when double pressure HRSGs are considered). For the design point temperatures of the high pressure and low pressure steam produced, $T_{HP,z}$ and $T_{LP,z}$, the related independent variables are the variables $\Delta T_{HP,z}$ for the high pressure and $\Delta T_{LP,z}$ for the low pressure. Their use is seen below:

$$T_{HP,z} = T_{gz} - \Delta T_{min,gg} - \Delta T_{HP,z} \tag{4. 10a}$$

$$T_{LP,z} = T_{sat,LP} + \Delta T_{LP,z} \tag{4. 10b}$$

In Eq. (4.10a), the term $\Delta T_{min,gg}$ refers to the minimum allowed temperature difference required for heat transfer between the exhaust gas and superheated steam (this is a parameter of the problem). In Eq. (4.10b), $T_{sat,LP}$ is the saturation temperature at the pertaining low pressure level of the HRSGs.

At this point, the design or nominal characteristics of the exhaust gas and steam streams produced are defined. The HRSG design algorithm is employed for calculating the water/steam properties and exhaust gas temperatures throughout the HRSG and for determining the heat exchange areas of the individual components. The determination of the heat exchange areas is required for simulating the performance of the HRSG at off-design

operation. In fact, as the exhaust gas properties of the prime movers are previously determined along with the determination of the heat exchange areas, the properties of the steam produced are also determined in all modes by using the appropriate HRSG off-design simulation algorithm. It is noted that the values of the mass flow rates of the steam production as set by the related input variables and the properties of the exhaust gases available may be incompatible to each other, which means that the HRSG cannot be designed or operated at an off-design mode and must therefore be excluded from the system (either completely or assumed not to be operating in certain modes). This is a possibility that must be examined by the HRSG design algorithm or the off-design simulation algorithm and cannot be predicted before the required inputs are set.

At this point the design procedure for the steam turbines can be applied and the simulation of their off-design performance can be performed, as the available steam in all the operating modes has been quantified in terms of both mass flow rates and energy content.

The superheated steam produced by each HRSG is fed to a common collector for each pressure level of steam production. The resulting streams will have mass flow rates $\dot{m}_{HP,COL,y}$, $\dot{m}_{LP,COL,y}$ and temperatures $T_{HP,COL,y}$, $T_{LP,COL,y}$ in each mode, which are determined by applying mass and energy balances.

As in the case of the prime movers, the number of steam turbines $n_{ST,y}$ operating in each mode *y* is set as an input variable to the simulation procedure. The mass flow rate delivered to each steam turbine is defined by setting values to the input variables $\tilde{m}_{STHPv,y}$ and $\tilde{m}_{STLPv,y}$, which are the proportion of the total steam mass flow rates $\dot{m}_{HP,COL,y}$, $\dot{m}_{LP,COL,y}$ delivered to steam turbine *v* in each mode *y*. At this point the steam mass flow rates and temperatures, $\dot{m}_{HPv,y}$, $\dot{m}_{LPv,y}$ and $T_{HPv,y}$, $T_{LPv,y}$ respectively, delivered to each steam turbine are quantified.

The design mass flow rates and temperatures of the steam streams , $\dot{m}_{HPv}$, $\dot{m}_{LPv}$ and T_{HPv}, T_{LPv}, are defined for each steam turbine in way similar to the determination of the design exhaust gas mass flow rates and temperatures of the HRSGs from the exhaust streams available. The mean values of steam mass rates and temperatures are given by:

$$\dot{m}_{HPv,mean} = \frac{\sum_{y=1}^{N_T} \dot{m}_{HPv,y} t_{D,y}}{\sum_{y=1}^{N_T} t_{D,y}} \tag{4.11a}$$

$$T_{HPv,mean} = \frac{\sum_{y=1}^{N_T} T_{HPv,y} t_{D,y}}{\sum_{y=1}^{N_T} t_{D,y}} \tag{4.11b}$$

Input variables $\dot{m}_{HPv,mult}$ and $T_{HPv,mult}$ are used as in Eqs. (4.12a) and (4.12b) in order to relate these mean values to the design point values:

$$\dot{m}_{HPv} = \dot{m}_{HPv,mean}\dot{m}_{HPv,mult} \tag{4.12a}$$

$$T_{HPv} = T_{HPv,mean}T_{HPv,mult} \tag{4.12b}$$

Equations (4.11) and (4.12) are also applicable to the low pressure streams, if double pressure bottoming cycle is examined.

After the design steam streams are defined, the steam turbine design procedure is applied to define the internal steam turbine characteristics (namely number of stages, blading diameters, etc.), in order for the simulation procedure to be able to quantify the power production from the steam turbines $\dot{W}_{ST,y}$ in each operating mode *y*, by applying the off-design simulation algorithms.

For the operation of the steam turbine as a component of the integrated system, two constraints are imposed: (i) the steam at the outlet of the Curtis wheel should not be a two-phase mixture, and (ii) the steam quality at the steam turbine outlet to the condenser should not be below a prescribed limit. These limitations apply both at design and off-design operation. As mentioned, the power produced by the steam turbines can be used for partially covering the propulsion demand in each mode, with the remaining power being used for serving electric loads. In case a steam turbine contributes to the propulsion of the ship, its rotational speed depends on the propeller's rotational speed.

For the propulsion part, the following equation is derived:

$$\dot{W}_{STp,y} = \sum_{v=1}^{v=n_{ST,y}} \dot{W}_{STpv,y} = \left(1-\lambda_{ME,y}\right)\dot{W}_{p,y} \tag{4.13}$$

If more than one steam turbine operate in mode *y*, the total steam turbine propulsion power is distributed to the steam turbines in proportion to their total power output:

$$\frac{\dot{W}_{STpv,y}}{\sum_{v=1}^{v=n_{ST,y}} \dot{W}_{STpv,y}} = \frac{\dot{W}_{STv,y}}{\sum_{v=1}^{v=n_{ST,y}} \dot{W}_{STv,y}} \tag{4.14}$$

The remaining power, if any, drives the electricity generators.

For the electric power produced by the steam turbine generators, the following equation is applicable:

$$\dot{W}_{STe,y} = \sum_{v=1}^{v=n_{ST,y}} \dot{W}_{STev,y} = \eta_G \left(\sum_{v=1}^{v=n_{ST,y}} \dot{W}_{STv,y} - \sum_{v=1}^{v=n_{ST,y}} \dot{W}_{STpv,y} \right) = \eta_G \left(\sum_{v=1}^{v=n_{ST,y}} \dot{W}_{STv,y} - \left(1-\lambda_{ME,y}\right)\dot{W}_{p,y} \right) \tag{4.15}$$

where η_G is the efficiency of the generator, a parameter considered the same for all generators.

If $\dot{W}_{STe,y}$ is lower than the electric load $\dot{W}_{e,y}$, the Diesel−generator sets supplement with the power $\dot{W}_{DG,TOT,y}$:

$$\dot{W}_{DG,TOT,y} = \dot{W}_{e,y} - \dot{W}_{STe,y} \tag{4.16}$$

The number of Diesel−generator sets operating during mode *y* is $n_{DG,y}$. If $n_{DG,y} > 1$, the power output of the Diesel−generator set *x*, $\dot{W}_{DG,x,y}$, is determined by the equations

$$\dot{W}_{DG,1,y} = \tilde{W}_{DG,1,y} \dot{W}_{DG,TOT,y}, \quad \tilde{W}_{DG,1,y} \le 1 \tag{4.17a}$$

$$\dot{W}_{DG,x,y} = \tilde{W}_{DG,x,y} \left(\dot{W}_{DG,TOT,y} - \sum_{i=1}^{x-1} \dot{W}_{DG,i,y} \right), \quad \tilde{W}_{DG,x,y} \le 1, \quad 1 < x < n_{DG,y} \tag{4.17b}$$

$$\dot{W}_{DG,n_{DG,y},y} = \dot{W}_{DG,TOT,y} - \sum_{i=1}^{n_{DG,y}-1} \dot{W}_{DG,i,y} \quad , \quad x = n_{DG,y} \tag{4.17c}$$

where the number of sets operating in each mode, $n_{DG,y}$, and the values of the multipliers $\tilde{W}_{DG,x,y}$ are inputs to the model for all modes.

The nominal power rating of the Diesel−generator set *x*, $\dot{W}_{DGx,N}$, is determined by multiplying the maximum power output of the set among the operating modes by a variable $\dot{W}_{DGN,x,mult}$, as in the case of the main engines. The variables $\dot{W}_{DGN,x,mult}$ are also inputs to the model.

The last step in the system modeling is the determination of the thermal power of each heat recovery steam generator and auxiliary boiler. It is considered that the total thermal power of the HRSGs and the ABs is given by the equations

$$\dot{Q}_{hl,HRSG,TOT,y} = \lambda_{Q,y} \dot{Q}_{hl,y} \qquad 0 \le \lambda_{Q,y} \le 1 \tag{4.18}$$

$$\dot{Q}_{AB,TOT,y} = \left(1-\lambda_{Q,y}\right) \dot{Q}_{hl,y} \qquad 0 \le \lambda_{Q,y} \le 1 \tag{4.19}$$

where the value of $\lambda_{Q,y}$ is an input to the model. The allocation of $\dot{Q}_{hl,HRSG,TOT,y}$ among the operating HRSGs is determined with the equations

$$\dot{Q}_{hl1,y} = \tilde{Q}_{hl1,y}\dot{Q}_{hl,HRSG,TOT,y}\ , \quad \tilde{Q}_{hl1,y} \le 1, \tag{4.20a}$$

$$\dot{Q}_{hlz,y} = \tilde{Q}_{hlz,y}\left(\dot{Q}_{hl,HRSG,TOT,y} - \sum_{i=1}^{z-1}\dot{Q}_{hli,y}\right), \quad \tilde{Q}_{hlz,y} \le 1, \quad 1 < z < n_{HRSG,y} \tag{4.20b}$$

$$\dot{Q}_{hln_{HRSG,y},y} = \dot{Q}_{hl,HRSG,TOT,y} - \sum_{i=1}^{n_{HRSG,y}-1}\dot{Q}_{hli,y} \quad , \quad z = n_{HRSG,y} \tag{4.20c}$$

where the values of $\tilde{Q}_{hlz,y}$ are also inputs to the model.

With the procedure described in the preceding, the number of each of the components present and operating in each mode *y* and their functional interconnections are determined. It is noted that the number of operating components as also their functional interconnections are allowed to differ among the various operating modes. Thus, the final outcome concerning the overall synthesis of the system and the nominal characteristics of components present is affected by the synthesis and functional interconnections required for all operating modes as well as by the magnitude of the loads to be covered.

4.3 Modification for the Case of Gas Turbines as Prime Movers

In a gas turbine combined cycle, the steam turbine power production is expected to be, in general, much higher than in the case of combined cycle with Diesel engines, due to the favorable exhaust gas characteristics. By an appropriate design of the bottoming cycle, it is thus possible that the steam turbine may have a quite significant contribution to the propulsion load, affecting in this way the optimal operational and nominal characteristics of the main engine. The need for sea margin (extra power for hull fouling and weather adverse conditions) is taken into consideration in determining the nominal power output of the system in the following way.

Among the operational modes, one of them presents the highest propulsion load, which is symbolized with $\dot{W}_{p,max}$. The sea margin excess power requirement is herein expressed with the inequality (4.21), which relates the sum of the nominal power rating of the gas turbines and the sum of steam turbine propulsion powers symbolized with $\dot{W}_{ST,p,ml}$

$$\sum_{i=1}^{n_{GT}}\dot{W}_{GTi,N} + \dot{W}_{ST,p,ml} \ge \dot{W}_{p,max}\big/\mu_s \tag{4.21}$$

where the index *ml* implies the aforementioned operating mode in which $\dot{W}_{p,max}$ appears, and μ_s is the sea margin factor (usually taken equal to 0.85).

For the sum of the steam turbine propulsion powers in mode *ml*, the following equation is valid

$$\dot{W}_{ST,p,ml} = \left(1-\lambda_{GT,ml}\right)\dot{W}_{p,max} \tag{4.22}$$

where $\lambda_{ME,ml}$ is the fraction of propulsion power $\dot{W}_{p,max}$ delivered by the gas turbines and is an independent variable of the optimization problem.

Relations (4.21) and (4.22) lead to inequality (4.23), which expresses the requirement for the sum of nominal power ratings of the gas turbines:

$$\sum_{i=1}^{n_{GT}} \dot{W}_{GTi,N} \geq \dot{W}_{p,max}\left(\lambda_{GT,ml} + 1/\mu_s - 1\right). \tag{4.23}$$

The rest of the procedure is similar to the one described in Section 4.2.

Chapter 5

The Optimization Problem and Solution Approach

In the present chapter, the mathematical statement of the optimization problems studied in the present work are defined. Two alternative objective functions based on techno−economic criteria are defined. The independent variables are also determined and the solution approach with the utilization of genetic algorithms is outlined.

5.1 Mathematical Statement of the Optimization Problem

The first of the alternative objective functions is the Present Worth Cost (*PWC*) of acquiring and operating the integrated energy system for a defined number of years to be minimized. The objective is expressed as

$$\begin{aligned}\min PWC = & \sum_{k=ME,DG,HRSG,ST,AB,EGB}\left[\sum_{x=1}^{n_k} C_{c,k,x}\right] \\ & + PWF\left(N_Y, f, i\right)\sum_{y=1}^{N_T}\left\{\sum_{k=ME,DG,AB}\left[\sum_{x=1}^{x=n_k}\dot{m}_{f,kxy}t_{kxy}c_{f,k}\right]\right\} + \\ & + PWF\left(N_Y, f, i\right)\sum_{y=1}^{N_T}\left\{\sum_{k=ME,DG,ST}\left[\sum_{x=1}^{n_k} c_{om,kxy}\dot{W}_{kxy}t_{kxy}\right] + \sum_{k=HRSG,AB,EGB}\left[\sum_{x=1}^{n_k} c_{om,kxy}\dot{Q}_{kxy}t_{kxy}\right]\right\}\end{aligned} \tag{5.1}$$

subject to equality and inequality constraints written in general form

$$\mathbf{h}(\mathbf{x}) = 0 \tag{5.2}$$

$$\mathbf{g}(\mathbf{x}) \le 0 \tag{5.3}$$

The following symbols are used in Eq. (5.1):

$C_{c,k,x}$	capital cost of component *x* of type *k*
$\dot{m}_{f,kxy}$	fuel mass flow rate of component *x* of type *k* during mode *y*
t_{kxy}	time span of operation of component *x* of type *k* during mode *y*
$c_{f,k}$	fuel unit cost
com,kxy	operation and maintenance unit cost of component *x* of type *k* during mode *y*
$\dot{W}_{kxy}, \dot{Q}_{kxy}$	useful power produced by component *x* of type *k* during mode *y*
N_Y	number of years of operation
f	inflation ratio
i	interest rate.

In Eq. (5.1) the first line is the capital costs of the components, the second line is the present worth cost of fuel and the third line is the present worth cost of operation and maintenance (O&M). The operating costs are expressed with the use of the Present Worth Factor (*PWF*), which depends on the market interest rate, the inflation rate and the number of years of the investment, and is expressed as

$$PWF\left(N_Y, f, i\right) = \sum_{n=1}^{N_Y} \frac{\left(1+f\right)^{n-1}}{\left(1+i\right)^{n}} = \begin{cases} \dfrac{1}{i-f}\left[1-\left(\dfrac{1+f}{1+i}\right)^{N_Y}\right], & f \neq i \\ \dfrac{N_Y}{1+f}, & f = i \end{cases} \tag{5.4}$$

which is valid under the assumption that all expenses are accumulated at the end of each year.

Concerning the equality and inequality constraints of the optimization problem, the related expressions are, in fact, all related to the simulation models of the individual components described in Chapter 3 and the single−level modeling approach of the integrated system as a whole described in Chapter 4. In Eqs. (5.2) and (5.3), **x** is the set of independent variables.

One alternative objective function used in the present work is the Net Present Value (*NPV*) of the investment of acquiring and operating the ship's energy system for a specified number of years to be maximized. The *NPV* may be used, for example, when the velocity of the ship is to be determined by optimization. The choice of the maximization of *NPV* as objective in such a case is rather rational, as the higher the velocities of sailing, the more round trips may be made and the income per year is increased. On the other hand, higher velocities impose a higher propulsion load and fuel consumption, which generally is the predominant operating cost. So, sailing speeds cannot be readily decided, and the application of optimization procedures may be quite helpful. The *NPV* is expressed as

$$NPV = \left(Annual\ Income\right) \times PWF - PWC \tag{5.5}$$

The annual income is generally dependent on the sailing speeds as above mentioned, but its determination is also based on the specifics of each problem and a general expression cannot be formulated. In a numerical example presented in Chapter 6, an example of an appropriate expression of the annual income is presented.

The capital cost of the individual components is estimated with appropriate cost functions that are presented in Appendix C, where also economic parameters related to the maintenance costs are given.

5.2 Independent Variables of the Optimization Problem

The number and the technical significance of the independent variables of the optimization problem is dependent on the type of prime movers used and on the choice of one of the two alternative objective functions for the optimization problem. The most general set of independent variables that can be used is presented in Table 5.1.

Table 5.1: Independent variables of the optimization problem.

$n_{ME,y}, \quad y=1,2,...,N_T-1$	$n_{DG,y}, \quad y=1,2,...,N_T$
$g_{x,y}, \quad x=1,2,...n_{HRSG,max}, \quad y=1,2,...,N_T-1$	$\lambda_{ME,y}, \quad \lambda_{Q,y}, \quad y=1,2,...,N_T-1$
$W_{N,x,mult}, \quad x=1,2,...,n_{ME,max}$	$W_{DGN,x,mult}, \quad x=1,2,...,n_{DG,max}$
$\tilde{W}_{ME,x,y}, \quad x=1,2,...,n_{ME,max}-1, \quad y=1,2,...,N_T-1$	$\tilde{W}_{DG,x,y}, \quad x=1,2,...,n_{DG,max}-1, \quad y=1,2,...,N_T$
$m_{gz,mult}, \quad T_{gz,mult}, \quad z=1,2,...,n_{HRSG,max}$	$P_{HP}, \quad P_{LP}$
$\dot{m}_{k,z}, \quad T_{k,z}, \quad z=1,2,...,n_{HRSG,max}, \quad k=HP,LP$	
$\tilde{Q}_{hlz,y}, \quad z=1,2,...,n_{HRSG,max}-1, \quad y=1,2,...,N_T-1$	
$n_{ST,y}, \quad y=1,2,...,N_T-1$	
$\tilde{m}_{STkv,y}, \quad v=1,2,...,n_{ST,max}-1, \quad y=1,2,...,N_T-1, \quad k=HP,LP$	
$m_{kv,mult}, \quad T_{kv,mult}, \quad v=1,2,...,n_{ST,max}, \quad k=HP,LP$	
$n_{AB,y}, \quad y=1,2,...,N_T$	
$\dot{m}_{a,z,mult}, \quad T_{a1,z}, \quad \rho_{m,z}, \quad P_{a,z}, \quad z=1,2,...,n_{HRSG,\max}$	
$V_{ship}, \quad y=1,2,...,N_T-1$	

At this point, some explanations regarding the independent variables and their mathematical notation are required. Firstly, the last line in Table 5.1 presenting the ship speed as an independent variable is meaningful only when the maximization of the *NPV* is chosen as the optimization objective. In cases where *PWC* is used, the ship speed is considered as predetermined along with the propulsion loads during each operating mode. Secondly, the line containing variables $\dot{m}_{a,z,mult}, T_{a1,z}, \rho_{m,z}, P_{a,z}$ is related to problems where the prime movers are Diesel engines and additional variables are required for the design of the charge air cooling part of the HRSG.

Without restricting the generality of the method, in the applications that follow it will be considered that there are N_T operating modes of the system, with $N_T - 1$ modes sailing and the last mode, N_T, at harbor, where the combined cycle does not operate. Consequently, variables related to this cycle do not appear in the harbor mode, while the rest of variables appear in every mode.

The number of components of type *k* existing in an optimal solution is symbolized with n_k. For the initiation of the optimization procedure, a maximum allowed number of components of type *k* is specified, which is symbolized with $n_{k,max}$ in Table 5.1. In an optimal solution, it may be $n_k < n_{k,max}$, but until n_k is determined by the optimization procedure, the number of independent variables should be such that all the possibly existing components can be simulated. The values of $n_{k,max}$ can be thought of as boundary (inequality) constraints of the synthesis part of the optimization problem.

By using the set of variables presented in Table 5.1, the objective function is evaluated in a single step, making the single−level approach for the SDO optimization problem applicable.

5.3 Description of the Simulation Procedure of the Integrated Energy System

For the purposes of the present work, a dedicated simulation algorithm incorporating all of the simulation procedures concerning the integrated system as a whole and the individual components design and operation performance was developed. The purpose of this algorithm is the calculation of the objective function in a single computational step, while at the same time the effects of the three distinct parts of the optimization problem, namely the synthesis, design and operation, are all taken into account.

It is reminded that the operation of the ship is approximated with a known number of operating modes N_T. Each mode *y* is characterized by its duration $t_{D,y}$ and three different types of loads, that is the propulsion power $\dot{W}_{p,y}$, electric power $\dot{W}_{e,y}$ and thermal power $\dot{Q}_{hl,y}$. The only requirement for these operating modes is that the power loads are constant during each mode. For the simulation of the energy system as a whole, the required inputs are the independent variables of the optimization problem, which are described in Section 5.2. These inputs are adequate for the simulation of the energy system with respect to the three levels of synthesis, design and operation. The simulation procedure roughly follows the series of calculations described in Section 4.2 (or 4.3 for the case of gas turbines as prime movers) and the simulation algorithms of the individual components described throughout Chapter 3 are employed.

There are certain parameters that remain constant during the optimization procedure, such as the following:

- Fuel costs for the prime movers, the gen-sets and the auxiliary boiler

- Fuel LHV for the prime movers, the gen-sets and the auxiliary boiler
- Maintenance costs in monetary units per useful energy produced, for the prime movers HRSGs, steam turbines, Diesel gen-sets and the auxiliary boiler
- Number of years of the ship's life span
- Inflation ratio
- Market interest rate.

HRSGs parameters

- Deaerator pressure
- Feed water temperature
- Efficiency (due to radiation losses)
- Minimum exhaust gas temperature permitted
- Minimum temperature difference required for heat transfer
- Two-phase steam quality at evaporator outlet at design point
- Geometric characteristics of the heat surface area elements, like the tubes diameters, fins diameter, fin thickness and spacing and tubes relative dimensions
- Reynolds number of the exhaust gas flow at design point
- Thermal conductivity of tubes and fins.

Steam turbine parameters

- Condenser pressure
- Pressure ratio of the Curtis wheel nozzle
- Mean diameter of the Curtis wheel
- Rotor clearance of the Curtis wheel
- Reaction section stages' loading factor
- Reaction sections' reaction degree
- Internal diameters initial values
- Blading heights (first stage of section)
- Minimum permitted steam quality at turbine outlet.

The technical parameters are set according to the expected magnitude of mass flow rates and temperatures for the different prime mover types. For example, the external diameters of the HRGS tube are set equal to 25 mm for the case of Diesel engines but for the case of gas turbines, where the expected mass flow rates of steam will be much higher, the value of 45 mm is used, which, as also seen in a commercially available HRSG for marine gas turbines, is a realistic value. Accordingly, the higher mass flow rates of steam in the case of gas turbines, dictates that the radii of the steam turbine will be generally higher. In order to test their significance, the optimization problem has been solved with certain of the aforementioned parameters treated as independent variables. It was noticed that there may be an effect of these variables on the objective function value, however it was much less significant in comparison with the effect of the variables finally chosen as independent variables of the problem.

5.4 Optimization Software and Solution Procedure

The optimization software used was the genetic algorithm integrated in the Global Optimization Toolbox of the Matlab® computational environment. This is a basic implementation of a standard genetic algorithm. The values of internal parameters of the Genetic Algorithm are presented in Table 5.2.

Table 5.2: Parameters of the genetic algorithm.

Population size	36
Elite members	1
Number of subpopulations	1
Crossover probability	75%
Mutation probability	25%
Stall generations limit	50
Objective function tolerance	100 $

The stopping criterion for the optimization algorithm was nearly always the criterion defined by the combination of the parameters "Stall generations limit" and "Objective function tolerance" presented in Table 5.2. These two parameters dictate that the solution has converged if the average relative change in the best objective function value over 50 generations is less than or equal to 100 $.

The set of values presented in Table 5.2 was chosen after several "trial and error" procedures, by comparing the convergence characteristics of the algorithm and other significant aspects, like the convergence time and the diversity of solutions in the final populations.

The population size of 36 individuals may seem to be small. However, the use of a larger population size did not give any significantly better results. In all cases, regardless of the population size, there was a tendency of the algorithm to converge to regions where small perturbations of the independent variables led to infeasibility of the solution. The use of a larger population size did not seem to be any beneficial towards this direction. Even more, the mutation function did not seem to be able to help the algorithm to escape the suboptimal solutions in an effective way. This may be attributed mainly to the fact that small perturbations of the input vector may modify a quite good solution (close to the optimum) to an infeasible one, so large modifications of the input variables due to mutations are unlikely to result in a better optimum or in a region of the search space with better values of the objective function. However, the use of smaller mutation fraction over the population than the value of 25% used to give a quite flat curve of the current optimal value found over the number of generations. The division of the population into several subpopulations did not seem to have any effect on the optimization efficiency either.

Chapter 6

Numerical examples

In the present chapter, the results of the application of the single−level approach for the synthesis, design and operation optimization of integrated marine energy systems are presented for three numerical examples. These examples include systems with different types of prime movers, different objectives of the overall optimization problem and additionally sensitivity analyses with respect to important parameters.

6.1 Integrated Marine Energy System with Four−stroke Diesel Engines as Prime Movers

In the first example, four−stroke Diesel engines are considered as main engines. The energy profile of the ship is approximated with three distinct sailing operating modes and one harbor residence mode, with defined magnitudes of the required energy loads and time duration during a typical year of operation. The problem is initially solved for a reference case.

6.1.1 Reference case solution

The energy profile is presented in Table 6.1 and is considered as a reference profile (that is because a sensitivity analysis will be performed for investigating the effect of the energy profile on the optimal solution).

Table 6.1: Annual energy profile of a ship (reference profile).

Mode y		$\dot{W}_{p,y}$ (kW)	$\dot{W}_{e,y}$ (kW)	$\dot{Q}_{hl,y}$ (kW)	t_y (hours)
Profile 1	1	26000	1500	400	2690
	2	22000	1500	300	1575
	3	14000	700	200	1620
	4	0	1200	150	1000

The objective of the optimization is the minimization of the Present Worth Cost (*PWC*) of the investment. The main economic parameters are presented in Table 6.2.

Heavy fuel oil (HFO) with LHV_{HFO}=39570 kJ/kg is used. Due to the potentially high sulfur content of HFO, the minimum allowable temperature for the exhaust gas in order for sulfuric acid condensation to be avoided at the HRSG outlet, is set at 160^{o}C.

The solution of the problem in technical and economic terms is presented in Table 6.3.

Table 6.2: Values of economic parameters.

Parameter	Value
c_f	300 $/ton
N_Y	20
f	3%
i	8%
$c_{om,D}$	0.006 $/kWh
$c_{om,DE}$	0.007 $/kWh
$c_{om,HRSG}$, $c_{om,AB}$	0.005 $/kWh
$c_{om,ST}$	0.004 $/kWh

Table 6.3: Optimal synthesis, design and operational characteristics of the energy system for the reference case.

Synthesis of the system	
Number of Diesel engines	2
Number of HRSGs	2
Number of STs	1
Number of auxiliary boilers	1
Number of Diesel Gen-sets	1
Design (nominal) characteristics of the components	
Engine 1 MCR	14537.82 kW
Engine 2 MCR	16077.74 kW
HRSG 1 thermal power	5374.91 kW
HRSG 1 exhaust gas mass flow rate	21.45 kg/s
HRSG 1 HP mass flow rate	1.421 kg/s
HRSG 1 LP mass flow rate	0.351 kg/s
HRSG 1 HP pressure	10.600 bar
HRSG 1 l LP pressure	5.159 bar
HRSG 1 inlet/outlet exhaust gas temperature	358.93 / 171.65°C
HRSG 1 HP superheated steam temperature	324.58°C
HRSG 1 LP superheated steam temperature	170.83°C
HRSG 2 thermal power	5002.68 kW
HRSG 2 exhaust gas mass flow rate	26.99 kg/s
HRSG 2 HP mass flow rate	1.405 kg/s
HRSG 2 LP mass flow rate	0.289 kg/s
HRSG 2 HP pressure	10.600 bar
HRSG 2 LP pressure	5.159 bar
HRSG 2 inlet/outlet exhaust gas temperature	321.89 / 183.65°C
HRSG 2 HP superheated steam temperature	293.62°C
HRSG 2 LP superheated steam temperature	165.75°C
Steam turbine 1 power	2256.80 kW
Steam turbine 1 HP mass flow rate	2.513 kg/s
Steam turbine 1 LP mass flow rate	0.658 kg/s
Steam turbine 1 HP steam temperature	307.77°C

Steam turbine 1 LP steam temperature		176.89°C
Steam turbine 1 rotational speed		3000 RPM
Gen-set MCR		1269.57 kW
Operational characteristics of the components (voyage)		
Operating mode 1	**Operating mode 2**	**Operating mode 3**
Engine 1 brake power kW		
11851.58	6402.93	13570.34
Engine 1 load factor		
0.8152	0.4404	0.9335
Engine 1 SFOC gr/kWh		
196.7819	209.3568	193.1587
Engine 1 exhaust gas temperature °C		
295.56	348.63	299.92
Engine 1 exhaust gas mass flow rate kg/s		
26.77	16.12	29.08
Engine 2 brake power kW		
13498.1	15000.05	0
Engine 2 load factor		
0.8396	0.933	0
Engine 2 SFOC gr/kWh		
194.9317	192.6099	0
Engine 2 exhaust gas temperature °C		
295.49	300.31	0
Engine 2 exhaust gas mass flow rate kg/s		
30.68	32.62	0
HRSG 1 thermal power kW (exhaust gas)		
4535.46	3634.59	5125.86
HRSG 1 inlet/outlet exhaust gas temperature °C		
295.56 / 171.19	348.63 / 168.42	299.92 / 172.20
HRSG 1 HP superheated steam mass flow rate kg/s		
1.137	0.941	1.31
HRSG 1 HP superheated steam temperature ^{o}C		
278.142	324.176	280.175
HRSG 1 LP superheated steam mass flow rate kg/s		
0.386	0.238	0.43
HRSG 1 LP superheated steam temperature ^{o}C		
169.021	170.952	169.05
HRSG 1 mass flow rate for thermal loads kg/s		
0.0895	0.0756	0.0778
HRSG 2 thermal power kW (exhaust gas)		
4723.68	5234.74	0
HRSG 2 inlet/outlet exhaust gas temperature °C		
295.49 / 182.86	300.31 / 184.02	0.00 / 0.00
HRSG 2 HP superheated steam mass flow rate kg/s		
1.3	1.475	0

HRSG 2 HP superheated steam temperature ºC		
274.612	276.687	0
HRSG 2 LP superheated steam mass flow rate kg/s		
0.308	0.334	0
HRSG 2 LP superheated steam temperature ºC		
165.104	165.153	0
HRSG 2 mass flow rate for thermal loads kg/s		
0.0662	0.0411	0
Steam turbine 1 power kW		
2152.07	2099.36	1131.32
Gen-set Brake power kW		
0	0	0
Harbor mode		
Gen-set brake power kW	1200	
Gen-set SFOC gr/kWh	213.549	
Auxiliary Boiler thermal power kW	150	
Economic analysis		
Capital costs		
Engine 1 capital cost	5,634,455 $	
Engine 2 capital cost	6,019,436 $	
HRSG 1 capital cost	865,786 $	
HRSG 2 capital cost	833,370 $	
Steam turbine 1 capital cost	728,135 $	
Gen-set capital cost	880,141 $	
Auxiliary boiler capital cost	102,777 $	
Operational costs		
Operating mode 1	**Operating mode 2**	**Operating mode 3**
Engine 1 annual fuel cost $		
1,882,066.59	633,385.19	1,273,917.49
Engine 2 annual fuel cost $		
2,123,384.84	1,365,126.81	0
Total annual fuel cost	7,277,880.92 $	
Engine 1 annual maintenance cost $		
191,284.57	60,507.73	131,903.69
Engine 2 annual maintenance cost $		
217,859.36	141,750.45	0
HRSG 1 annual maintenance cost $		
49,925.53	25,506.45	33,537.6
HRSG 2 annual maintenance cost $		
51,804.26	33,300.25	0
Steam turbine 1 annual maintenance cost $		
23,156.22	13,225.99	7,330.96
Harbor mode		
Gen-set annual fuel cost $	76,877.74	
Gen-set annual maintenance cost $	8400	

Auxiliary Boiler annual fuel cost $	3,820.03
Objective function	
PWC	117,337,514 $
Present worth factor	12.25004

The optimal system includes two prime movers which is the minimum possible number for covering the loads. However, the optimization procedure dictates that only prime mover 1 should be operating in the third mode. In the second operating mode, the brake power is distributed quite unevenly to the two prime movers. Executions of the optimization procedure with the load deliberately distributed equally to the two prime movers in modes 1 and 2 showed that the PWC could not reach the value of the present example and this could be attributed to the higher fuel cost per year of operation and to the generally lower power production from the bottoming cycle, especially in mode 2. In the optimal solution, the bottoming cycle is able of covering the whole of the electric and thermal loads during the voyage. The bottoming cycle also has a considerable contribution to the propulsion load, that is approximately 2.5%, 2.7% and 3.1% for modes 1,2 and 3 respectively.

The present worth cost of the investment of building and operating the energy system is 117,337,514 $. Optimization with the bottoming cycle deliberately excluded from the system resulted in PWC = 121,556,350 $, indicating a benefit of 4,218,836 $ if a bottoming cycle is installed.

In the subsections to follow, the effects that the fuel price, the capital cost and the energy profile have on the optimal solution are studied.

6.1.2 Effect of the fuel price on the optimal solution

Initially, the effect the fuel price has on the synthesis, design and operation of the energy system is investigated. The energy profile remains profile 1. In addition to the fuel price of 300 $/ton, the optimization was performed for prices of 100, 200, 400, 500 and 600 $/ton.

The synthesis of the system in the optimal solutions does not change for fuel price of 200 $/ton and higher. The energy system consists of two prime movers, two HRSGs (each attached to one of the prime movers), one steam turbine, one gen-set and one auxiliary boiler. It is also found that in the optimal solutions, the bottoming cycle covers the whole of both the electric and thermal loads during the voyage operating modes. At the fuel price of 100 $/ton no bottoming cycle is present in the system, but an EGB is only utilized for covering the thermal loads during voyage. Still, the optimization determines the appropriate loading factors of the two prime movers, and their MCRs. In Figure 6.1 the PWC with and without combined cycle and the difference between these as a function of fuel price are depicted. The difference between the two values of PWC is nearly linear. By fitting the curve of the difference and extrapolating it to the value where the difference is zero, the marginal fuel price found for which the inclusion of a bottoming cycle becomes profitable is approximately 148.27 $/ton.

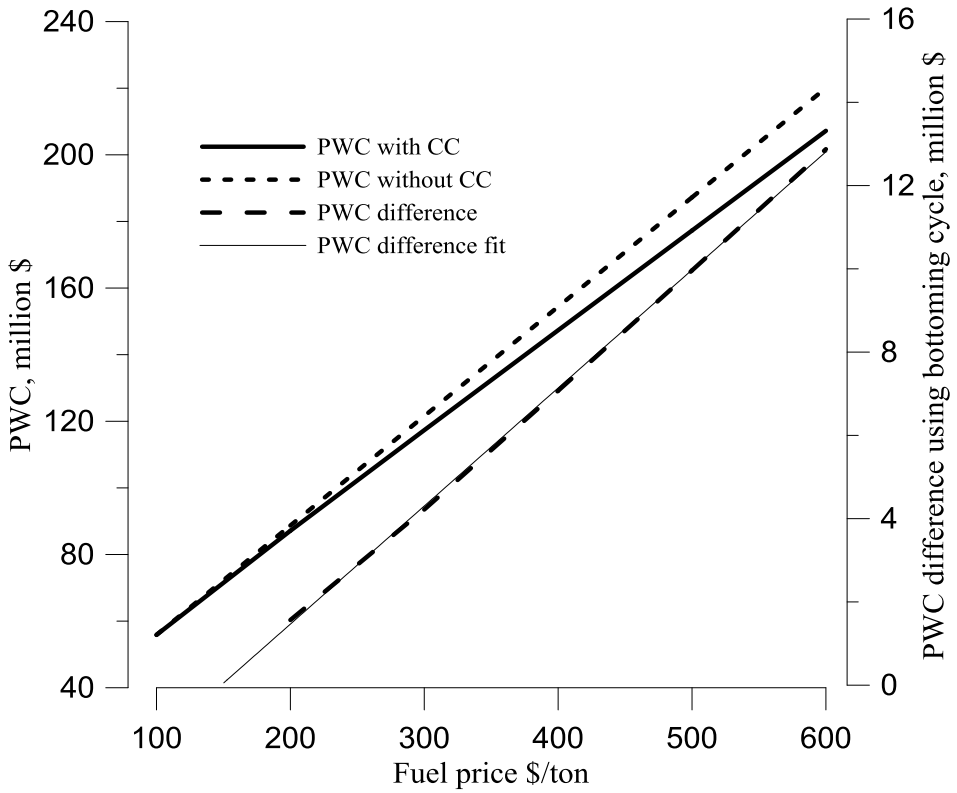

Figure 6.1: Present worth cost with and without bottoming cycle and their difference as a function of fuel price.

In the optimal solutions, the system consists of two prime movers with nearly the same MCRs between the fuel prices of 200 and 600 $/ton, with a slightly larger difference for the fuel price of 100 $/ton, as seen in Table. 6.4. The brake powers and the load factors f_D for these two engines are also presented in Table 6.4. It is observed that at the optimal solutions, the engines are not equally loaded, especially in mode 2. As will be seen later, the unequal loading of the engines has a beneficial effect on the power producing capability of the bottoming cycle. The fact that the unequal loading still exists for the case of fuel price 100 $/ton, where no bottoming cycle is present, means that this unequal loading is also beneficial for the fuel consumption of the prime movers (as the main contributor in the PWC is the fuel cost).

In all three voyage modes for fuel prices of 200 $/ton and higher, the steam turbine contributes to the propulsion load. The propulsion power part of the steam turbine $\dot{W}_{STp,1,y}$ per mode *y* is presented in Table 6.5.

In Figure 6.2 the values of the independent variables λ_D per mode of operation are presented as functions of fuel price (λ_D is the variable mentioned to as λ_{ME} in Chapter 4, but as the main engine is specified to be of the Diesel type, the subscript is changed to *D*). It is observed that as the fuel price rises, more contribution to the propulsion load by the steam turbine is required. This trend is clearly evident in modes 1 and 2, while in mode 3 this is a less important attribute, as the total power for propulsion is quite small compared to the other modes.

Table 6.4: Brake power and load factors of the two engines.

Fuel price	$\dot{W}_{D1,N}$	$\dot{W}_{D1,1}$	$\dot{W}_{D1,2}$	$\dot{W}_{D1,3}$	$f_{D1,1}$	$f_{D1,2}$	$f_{D1,3}$
100	15009.87	12773.51	7469.75	0	0.851	0.4977	0
200	14664.3	12388.41	6738.16	13675.11	0.8448	0.4595	0.9325
300	14537.82	11851.58	6402.93	13570.34	0.8152	0.4404	0.9335
400	14511.25	11974.67	6319.51	13572.42	0.8252	0.4355	0.9353
500	14516.17	11906.47	6318.22	13548.83	0.8202	0.4353	0.9334
600	14579.55	11992.38	6402.2	13572.59	0.8225	0.4391	0.9309
Fuel price	$\dot{W}_{D2,N}$	$\dot{W}_{D2,1}$	$\dot{W}_{D2,2}$	$\dot{W}_{D2,3}$	$f_{D2,1}$	$f_{D2,2}$	$f_{D2,3}$
100	15578.36	13226.49	14530.25	14000	0.849	0.9327	0.8987
200	15956.88	13210.49	14894.61	0	0.8279	0.9334	0
300	16077.74	13498.1	15000.05	0	0.8396	0.933	0
400	16101.32	13339.63	15039.06	0	0.8285	0.934	0
500	16080.36	13364.23	15005.62	0	0.8311	0.9332	0
600	16011.82	13273.11	14907.79	0	0.829	0.931	0

Table 6.5: Propulsion power delivered by the steam turbine as the fuel price is varying, values in kW.

Fuel price	$\dot{W}_{STp,1,1}$	$\dot{W}_{STp,1,2}$	$\dot{W}_{STp,1,3}$
200	401.1	367.23	324.89
300	650.32	597.02	429.66
400	685.7	641.43	427.58
500	729.3	676.16	451.17
600	734.51	690.01	427.41

In Fig. 6.3 the present worth cost of the bottoming cycle, which consists of the capital cost of the related components and the maintenance cost, is presented. The pertaining capital cost is also presented, along with the ratio of the bottoming cycle PWC to the total PWC. A large gradient is observed between the values of fuel prices 200 to 300 $/ton for the capital and total cost curves, but the curves tend to acquire smaller gradients as the fuel price increases. However, the ratio of the bottoming cycle cost to the total PWC is continuously decreasing with increasing fuel price. This form of the curves indicates that the beneficial inclusion of a bottoming cycle in the energy system is, generally, more apparent as the fuel price rises.

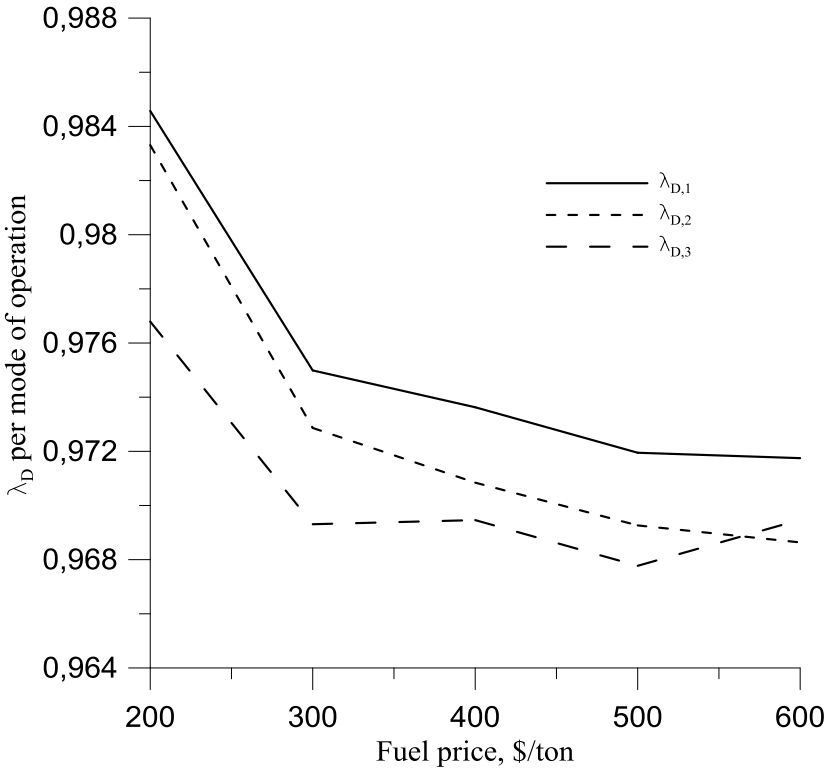

Figure 6.2: Effect of the fuel price on the variables λ_D, that is, on the percentage of propulsion power covered by the prime movers.

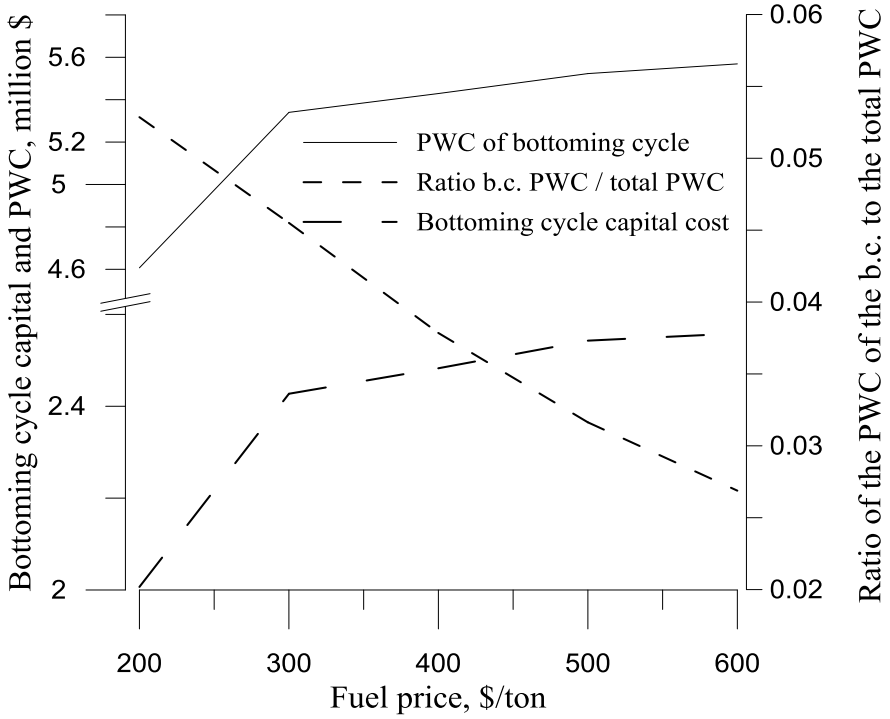

Figure 6.3: Capital cost and PWC of the bottoming cycle, as well as ratio of the PWC of the b.c. to the PWC of the system.

The thermal power extracted from the exhaust gas by the operating HRSGs and the total power produced by the steam turbine are presented in Fig. 6.4 for the three voyage

modes. In the same figure the ratio of the steam turbine power to the power produced by the prime movers is presented. The aforementioned ratio is higher in mode 2, and this is attributed to the fact that one of the prime movers is operating at a quite low load factor, producing exhaust gas of higher temperatures and thus higher potential for power production by the bottoming cycle.

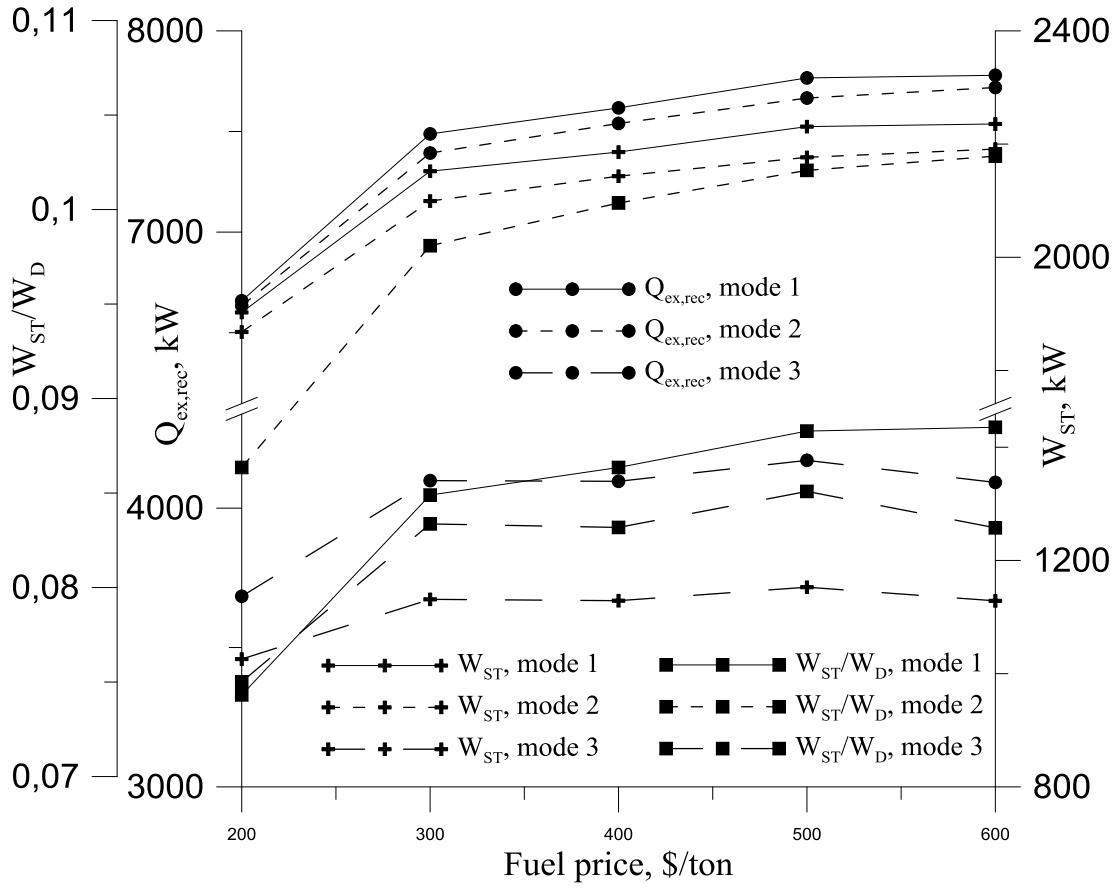

Figure 6.4: Effect of the fuel rice on of exhaust gas heat recovered, steam turbine power and steam turbine to prime movers power ratio, for the three voyage modes.

6.1.3 Effect of the capital cost on the optimal solution

For fuel price of 300 $/ton, the optimization procedure was also executed for two additional cases, in which the capital cost was multiplied with the factors of 0,5 and 2, for all the components possibly present. No change in the synthesis of the system was found at the optimal solutions, as also no significant changes were observed in the nominal and operational characteristics of the prime movers except of a slight reduction of the sum of the brake powers in all operating modes in the case of capital cost factor of 0,5. Moreover, the capital cost of the prime movers varies linearly with the capital cost factor, with the same attribute also valid for the gen-set and the auxiliary boiler (as their nominal characteristics are the same in the three problems presented in this section, because they are determined by the harbor mode). The results for the total PWC as also the capital, maintenance and present

worth cost of the bottoming cycle components are presented in Table 6.6. Decreasing capital cost in general, and of the bottoming cycle in particular (from capital cost factor 1 to 0.5), gives the opportunity of a bottoming cycle with higher power output. As a consequence the mechanical and/or the electric energy produced by the bottoming cycle is higher, and the maintenance cost is also increased.

Table 6.6: PWC and bottoming cycle costs for different capital cost factors.

Capital cost factor	Total PWC	Total PWC of b.c.	Capital cost of b.c. components	Maintenance cost of b.c. operation
0.5	109,805,601 $	4,320,838 $	1,328,830 $	3,001,908 $
1	117,337,514 $	5,340,194 $	2,427,291 $	2,912,903 $
2	132,319,531 $	7,655,300 $	4,762,733 $	2,892,567 $

Figure 6.5 depicts the variation of the heat recovered along with the power produced by the steam turbine for changing capital cost factors. The heat recovered and the power produced by the bottoming cycle is slightly increased for capital cost factor 0,5, and for this reason the maintenance cost is also increased accordingly. The fact that the cost factor is half of the nominal one, leaves room for a higher power output of the bottoming cycle. When the capital cost factor is double in comparison with the reference case, the effect on the power production of the bottoming cycle is less prominent. This explains why the bottoming cycle capital cost is closer to linear variation with the capital cost factor and the maintenance cost is close the reference case, as the operational characteristics of the bottoming cycle are also quite close for these two cases.

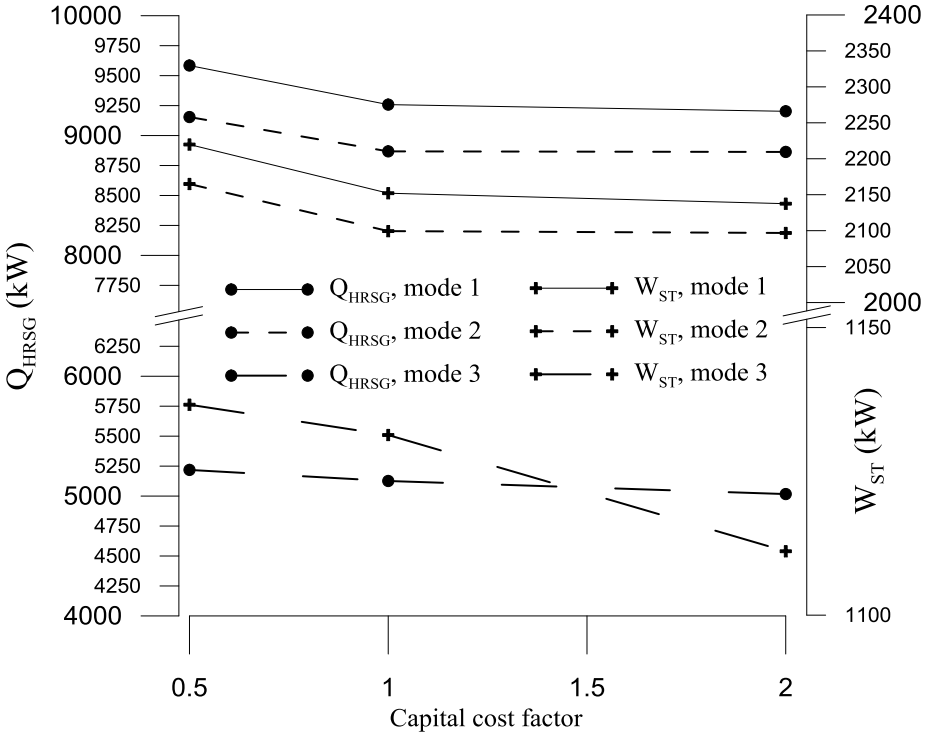

Figure 6.5: Effect of the capital cost factor on the exhaust gas heat recovered and steam turbine power, for the three voyage modes.

6.1.4 Effect of the energy profile on the optimal solution

In all the results presented up to this point, in the optimal system the electric and thermal loads are fully covered by the bottoming cycle for the fuel price of 200 $/ton and higher. The inclusion of a Diesel gen-set and an auxiliary boiler are required for covering the pertaining loads during the harbor residence mode. An execution of the optimization algorithm for the fuel price of 300 $/ton and excluding mode 4 (harbor) from energy profile 1 resulted in a system without these two components. From a technical point of view, the optimal solution for the three voyage modes was virtually the same between these two problems of including and excluding the harbor mode. Moreover, the difference in the PWC (117,337,514$ with harbor residence and 115,308,202$ without) is roughly equal to the added capital, fuel and maintenance cost related to the two added components.

For further studying the effect that the energy profile has on the synthesis, design and operation of the energy system, optimization was performed also with the two energy profiles presented in Table 6.7 (denoted as profiles 2 ad 3) for the fuel price of 300 $/ton. In profile 2, the propulsion load is roughly half of the basic energy profile 1 of Table 6.1, in all voyage modes. In profile 3, the electric loads are doubled compared to the profile 1.

Table 6.7: Alternative energy profiles of a ship.

Mode y		$\dot{W}_{p,y}$ (kW)	$\dot{W}_{e,y}$ (kW)	$\dot{Q}_{hl,y}$ (kW)	t_y (hours)
Profile 2	1	14000	1500	400	2690
	2	11000	1500	300	1575
	3	7000	700	200	1620
	4	0	1200	150	1000
Profile 3	1	26000	3000	400	2690
	2	22000	3000	300	1575
	3	14000	1400	200	1620
	4	0	2400	150	1000

For the energy profile 2, the optimization results in a system with one prime mover and one HRSG and a steam turbine, while there are also a gen-set and an auxiliary boiler. Operational characteristics of the system are given in Table 6.8. One main difference compared to the case of profile 1 is that in modes 1 and 2 the propulsion power is provided solely by the prime mover, that is, it is preferred that the power produced by the steam turbine is directed to the electric loads. However, this power does not suffice for fully covering the electric loads, and the rest of the demand is covered by the gen-set. The direction of the steam turbine power towards the electric loads rather than propulsion may be attributed to the need of an optimal solution to minimize the use of the gen-sets as they generally have lower efficiency than the prime movers. Only in mode 3, where the load factor of the prime mover is quite low, the power of the steam turbine is high enough for fully covering the electric load (which is lower though) and also contributing to the propulsion load.

Comparing the solutions for the energy profiles 1 and 3, the difference in the synthesis between the two problems was the inclusion of a second gen-set in the system for the profile

3. It is noted that the technically permitted lowest load factor for the gen-sets was set to 20%. With only one gen-set present, it was found that the last should be operating on very low load factor in mode 3 (approximately 7%). This attribute was revealed by an execution of the optimization procedure where it was deliberately permitted that only one gen-set would be possibly present in the system and the constraint for a lower limit of its load factor was temporarily removed. In the optimal solution for profile 3, the resulting two gen-sets have quite different power ratings, the smaller being of 729,91 kW nominal mechanical power and the larger of 1762,18 kW. During the voyage, only the smaller of the gen-sets operates, and the larger one is only used in the harbor mode in cooperation with the smaller. One more difference to be observed in comparison with the profile 2, is that even in mode 3 the steam turbine does not contribute to the propulsion power, as also holds in modes 1 and 2. Operational characteristics for the profile 3 are given in Table 6.9.

Table 6.8: Basic operational characteristics for the energy profile 2.

Mode y	$\dot{W}_{D1,y}$ (kW)	$f_{l,D}$	$\dot{Q}_{ex,rec,y}$ (kW)	$\dot{W}_{ST,y}$ (kW)	$\dot{W}_{DE1,y}$ (kW)	$f_{l,DE1}$
1	14000	0,8495	4562,65	1221,04	278,9568	0,2315
2	11000	0,6675	4223,95	1108,19	391,8048	0.3251
3	6766,44	0,4106	3771,45	936,26	0	0
4	-	-	-	-	1200	0.956175

Table 6.9: Basic operational characteristics for the energy profile 3.

Mode y	$\dot{W}_{D1,y}$ (kW)	$f_{l,D1}$	$\dot{W}_{D2,y}$ (kW)	$f_{l,D2}$	$\dot{W}_{ST,y}$ (kW)
1	12633,61	0,8492	13366,39	0,8499	2351,54
2	7196,98	0,4838	14803,02	0,9412	2305,55
3	0	0	14000	0,8902	1217,1
4	-	-	-	-	-
Mode y	$\dot{W}_{DE1,y}$ (kW)	$f_{l,DE1}$	$\dot{W}_{DE2,y}$ (kW)	$f_{l,DE2}$	
1	675,48	0,9254	0	0	
2	723,4	0,9911	0	0	
3	190,52	0,261	0	0	
4	723,39	0,9253	1676,60	0,9514	

6.2 Integrated Marine Energy System with Gas Turbines as Prime Movers

In the present numerical example, gas turbines are considered as prime movers. Three different types of gas turbines are examined, namely types 3, 4 and 5 presented in Chapter 3. Also, two appropriate different types of fuels are used, marine diesel oil (MDO) and natural gas (NG). The common characteristic of these types of gas turbines is that they have a separate power turbine mechanically coupled to the propeller, which is a practical necessity for delivering power in changing rotational speed, as it is assumed that the power and rotational speed relation follows the cubic law. The single shaft gas turbines do not operate satisfactorily in changing rotational speeds and may be more appropriate for other applications generally not considered in the present work, like the case of an "all-electric" ship, where the prime movers produce electricity for covering both the propulsion and electric loads and may be operating at constant speed.

6.2.1 Solution with alternative types of gas turbines and reference case solution

In the present section, the solution with the aforementioned types of gas turbines is presented. It is noted that the objective is again the minimization of the PWC and the annual energy profile considered is the one presented in Table 6.1. The economic parameters are also not changed compared to the values presented in Table 6.2, except of the fuel prices that are set to 400 \$/ton for the MDO and 150 \$/ton for the natural gas. Other specifications of the two fuels include their lower heating values: LHV_{MDO} = 42500 kJ/kg and LHV_{NG} = 47100 kJ/kg. The equivalent chemical formula of the MDO is $C_{12.8}H_{23.7}S_{0.05}$ and the composition of natural gas is presented in Table 6.10. For the case of MDO, due to the relatively low sulfur content the minimum allowable temperature of the exhaust gas can be set at 130^{o}C, while for the case of natural gas, the corresponding limit can be set even lower; it is set at 100^{o}C.

Table 6.10: Natural gas composition.

Component	Synthesis % volume
CH_4	88.5
C_2H_6	4.7
C_3H_8	1.6
C_4H_{10}	0.2
N_2	5.0

The solution of the SDO optimization problem results in the same optimal synthesis of the system for all six combinations of gas turbine units and fuels: it consists of one component of each type. It is noted that, as an optimization constraint, the maximum number for each type of components was set equal to two. It is also noted that the optimal configuration comprises one Diesel−generator set and one auxiliary boiler, because they are

needed for port operation (mode 4), while during the three voyage modes, the electric and thermal loads are covered by the steam bottoming cycle.

The main design characteristics of the components and their capital cost for the six cases are presented in Table 6.11.

Table 6.11: Design characteristics and capital cost of components with different gas turbine configurations and fuel.

Configuration / Fuel	A / MDO	B / MDO	C / MDO	A / NG	B / NG	C / NG
$\dot{W}_{GT}$ (kW)	23828	26941	28656	24662	27373	29379
$\dot{Q}_{HRSG}$ (kW)	23663	19708	13765	20623	15799	9605
$\dot{m}_{g,HRSG}$ (kg/s)	47.36	77.57	62.27	54.42	67.48	54.47
$\dot{m}_{HP,HRSG}$ (kg/s)	5.561	4.532	3.091	5.565	3.904	2.663
$\dot{m}_{LP,HRSG}$ (kg/s)	1.631	2.136	1.604	0.608	1.263	0.442
P_{HP} (bar)	63.58	17.65	19.23	63.67	21.66	23.29
P_{LP} (bar)	6.12	4.71	4.27	9.00	7.71	7.25
$T_{g,in,HRSG}$ (^{o}C)	584.90	377.12	348.63	554.08	420.34	387.15
$T_{g,out,HRSG}$ (^{o}C)	153.57	157.77	157.8	226.91	218.22	234.92
$T_{HP,HRSG}$ (^{o}C)	552.46	347.26	316.43	522.89	387.34	354.53
$T_{LP,HRSG}$ (^{o}C)	182.85	170.55	174.51	199.51	187.29	188.97
$\dot{W}_{ST}$ (kW)	8624	5009	3376	7589	4925	2706
$\dot{m}_{HP,ST}$ (kg/s)	6.431	4.696	3.139	6.276	4.505	2.944
$\dot{m}_{LP,ST}$ (kg/s)	1.608	2.111	1.590	0.549	1.320	0.458
$T_{HP,ST}$ (^{o}C)	543.53	327.49	307.88	513.43	386.07	324.17
$T_{LP,ST}$ (^{o}C)	179.87	162.31	171.1	187.96	207.95	193.76
$\dot{W}_{DG}$ (kW)	1206	1210	1203	1207	1209	1207
$C_{c,GT}$ ($)	10718229	13107957	15083626	10878489	13197730	15245075
$C_{c,HRSG}$ ($)	2684082	2344735	1905809	2332648	1621354	1110526
$C_{c,ST}$ ($)	1498472	1202482	993061	1425071	1151211	887139
$C_{c,DG}$ ($)	874689	875808	873849	874958	875529	874969

Figure 6.6 presents simulation results for the specific fuel consumption and exhaust gas mass flow rate and temperature as functions of the load factor derived from the gas turbines simulation program for the case of MDO. The curves for operation with natural gas have similar forms. Configuration 3 with the simple gas turbine has the highest specific fuel consumption, which also exhibits a higher increase as the load factor decreases.

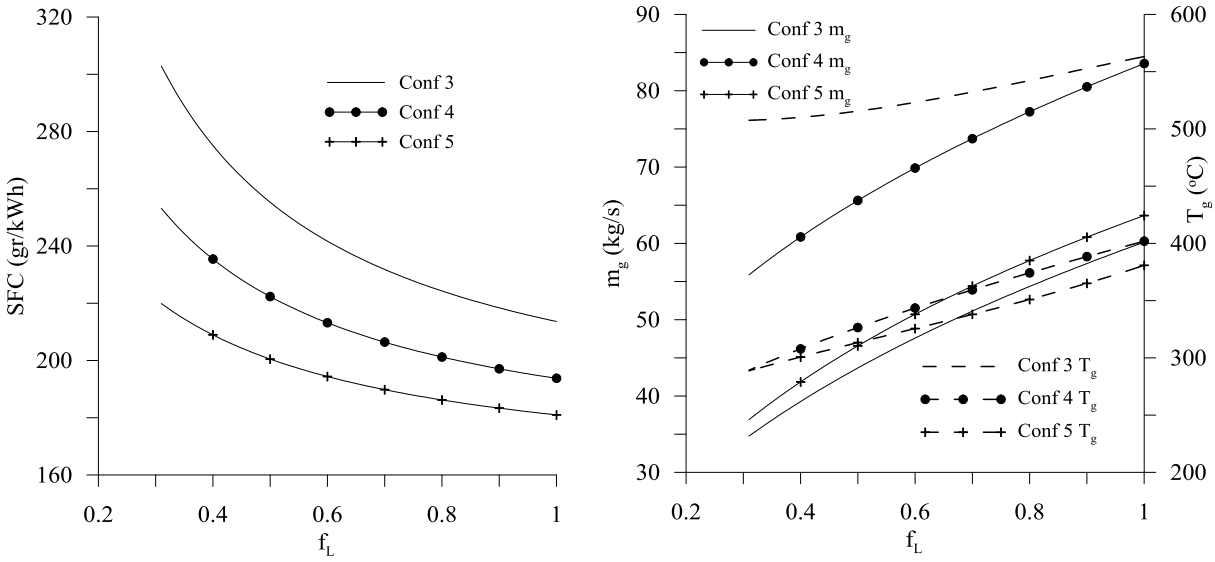

Figure 6.6: Variation of SFC and exhaust gas properties in partial load operation (fuel MDO).

The results in Table 6.11 show that, in the optimal design, the power capacity of the steam bottoming cycle (thermal power of HRSG and mechanical power of the steam turbine) decreases as the complexity of the gas turbine configuration increases from 3 to 5. This tendency can be attributed to the fact that the thermal efficiency of the gas turbine unit increases as its thermodynamic cycle becomes more advanced (Figure 6.6), with consequence the production of exhaust gases with decreasing energy content, i.e. decreasing capacity for additional power production.

The operational technical and economic characteristics of the six combinations are presented in Tables 6.12 – 6.17, where SFC_{GT} and SFC_{CC} refer to the specific fuel consumption of the gas turbine unit and the combined cycle, respectively.

As seen from the design and operational characteristics of the systems, gas turbine configuration 3 gives the highest potential of power production with the utilization of a bottoming cycle for both fuels. Its higher specific fuel consumption is counterbalanced by the exploitation of the thermal energy content of the exhaust gases, which results in a higher contribution of the steam turbine to the propulsion load and to the lowest annual fuel cost among the configurations. Even more, the combined cycle specific fuel consumption is the lowest when configuration 3 is used.

Table 6.12: Operational technical and economic characteristics for the system with gas turbine configuration 3 and fuel MDO.

Mode 1	Mode 2	Mode 3
$\dot{W}_{GT}$ (kW)		
19240.01	16256.68	9491.33
SFC_{GT} (gr/kWh)		
223.808	233.3587	275.5277
$\dot{Q}_{HRSG}$ (kW)		
25774.74	22915.2	16841.91
$\dot{m}_{g,HRSG}$ (kg/s)		
54.59	50.52	39.2
$T_{g,in,HRSG}$ / $T_{g,out,HRSG}$ (^{o}C)		
543.07 / 135.48	530.50 / 138.90	510.07 / 139.16
$\dot{m}_{HP,HRSG}$ (kg/s)		
6.329	5.635	4.186
$\dot{m}_{LP,HRSG}$ (kg/s)		
1.632	1.515	1.129
$\dot{m}_{hl}$ (kg/s)		
0.1545	0.1159	0.0772
$\dot{W}_{ST}$ (kW)		
8265.38	7274.15	5226.8
SFC_{CC} (gr/kWh)		
156.5536	161.2199	177.6805
GT annual fuel cost ($)		
4633329.06	2389991.03	1694600.04
GT annual O&M cost ($)		
310533.75	153625.61	92255.71
HRSG O&M cost ($)		
350171.93	182279.96	137797.45
Steam turbine O&M cost $		
88935.51	46041.35	33999.27

Table 6.13: Operational technical and economic characteristics for the system with gas turbine configuration 4 and fuel MDO.

Mode 1	Mode 2	Mode 3
$\dot{W}_{GT}$ (kW)		
22324.94	18887.21	11776.75
SFC_{GT} (gr/kWh)		
199.9417	206.3503	229.9452
$\dot{Q}_{HRSG}$ (kW)		
21188.97	18445.27	12476.87
$\dot{m}_{g,HRSG}$ (kg/s)		
78.21	73.76	62.69
$T_{g,in,HRSG}$ / $T_{g,out,HRSG}$ (^{o}C)		
378.40 / 144.49	359.51 / 143.62	314.96 / 143.13
$\dot{m}_{HP,HRSG}$ (kg/s)		
5.05	4.381	2.972
$\dot{m}_{LP,HRSG}$ (kg/s)		
2.12	1.928	1.379
$\dot{m}_{hl}$ (kg/s)		
0.1552	0.1164	0.0776
$\dot{W}_{ST}$ (kW)		
5175.14	4643.9	2938.45
SFC_{CC} (gr/kWh)		
162.3154	165.6268	184.0279
GT annual fuel cost ($)		
4802925.31	2455350.95	1754787.9
GT annual O&M cost ($)		
360324.5	178484.18	114469.96
HRSG annual O&M cost ($)		
287870.41	146723.72	102083.46
Steam turbine annual O&M cost ($)		
55684.52	29256.6	19365.14

Table 6.14: Operational technical and economic characteristics for the system with gas turbine configuration 5 and fuel MDO.

Mode 1	Mode 2	Mode 3
$\dot{W}_{GT}$ (kW)		
24058.85	20517.82	12884.59
SFC_{GT} (gr/kWh)		
185.0074	189.1652	204.3804
$\dot{Q}_{HRSG}$ (kW)		
14274.47	12308.24	8190.35
$\dot{m}_{g,HRSG}$ (kg/s)		
58.99	54.96	44.28
$T_{g,in,HRSG}$ / $T_{g,out,HRSG}$ (^{o}C)		
356.47 / 147.56	340.05 / 146.72	307.06 / 147.37
$\dot{m}_{HP,HRSG}$ (kg/s)		
3.304	2.81	1.84
$\dot{m}_{LP,HRSG}$ (kg/s)		
1.557	1.427	1.017
$\dot{m}_{hl}$ (kg/s)		
0.1554	0.1166	0.0777
$\dot{W}_{ST}$ (kW)		
3444.36	2997.19	1833.82
SFC_{CC} (gr/kWh)		
161.8380	165.0545	178.9159
GT annual fuel cost ($)		
4789345.29	2445191.84	1706415.29
GT annual O&M cost ($)		
388309.76	193893.47	125238.22
HRSG annual O&M cost ($)		
193930.97	97906.42	67011.93
Steam turbine O&M cost ($)		
37061.28	18882.29	12207.16

Table 6.15: Operational technical and economic characteristics for the system with gas turbine configuration 3 and fuel NG.

Mode 1	Mode 2	Mode 3
$\dot{W}_{GT}$ (kW)		
20074.11	17020.17	10089.86
SFC_{GT} (gr/kWh)		
206.1992	213.9852	248.7073
$\dot{Q}_{HRSG}$ (kW)		
22434.93	19618.54	14238.04
$\dot{m}_{g,HRSG}$ (kg/s)		
55.03	51.31	40.34
$T_{g,in,HRSG}$ / $T_{g,out,HRSG}$ (^{o}C)		
541.77 / 189.81	525.31 / 195.20	500.82 / 196.08
$\dot{m}_{HP,HRSG}$ (kg/s)		
6.186	5.472	4.037
$\dot{m}_{LP,HRSG}$ (kg/s)		
0.592	0.521	0.374
$\dot{m}_{hl}$ (kg/s)		
0.1535	0.1151	0.0768
$\dot{W}_{ST}$ (kW)		
7427.69	6482.47	4615.36
SFC_{CC} (gr/kWh)		
150.5089	154.9641	170.6484
GT annual fuel cost ($)		
1670193.45	860437.60	609789.37
GT annual O&M cost ($)		
323996.13	160840.64	98073.42
HRSG annual O&M cost ($)		
304797.79	156056.61	116493.10
Steam turbine O&M cost ($)		
79921.97	40839.54	29907.51

Table 6.16: Operational technical and economic characteristics for the system with gas turbine configuration 4 and fuel NG.

Mode 1	Mode 2	Mode 3
$\dot{W}_{GT}$ (kW)		
22785.05	19424.37	12170.46
SFC_{GT} (gr/kWh)		
185.0029	190.456	211.1788
$\dot{Q}_{HRSG}$ (kW)		
17376.5	15159.49	9817.69
$\dot{m}_{g,HRSG}$ (kg/s)		
77.38	73.12	62.1
$T_{g,in,HRSG}$ / $T_{g,out,HRSG}$ (^{o}C)		
382.16 / 188.30	363.97 / 184.99	319.25 / 182.76
$\dot{m}_{HP,HRSG}$ (kg/s)		
4.449	3.921	2.56
$\dot{m}_{LP,HRSG}$ (kg/s)		
1.349	1.196	0.828
$\dot{m}_{hl}$ (kg/s)		
0.1539	0.1154	0.0769
$\dot{W}_{ST}$ (kW)		
4716.93	4092.76	2532.37
SFC_{CC} (gr/kWh)		
154.2726	157.3103	174.8060
GT annual fuel cost ($)		
1700873.65	874003.99	624544.51
GT annual O&M cost ($)		
367750.71	183560.28	118296.86
HRSG annual O&M cost ($)		
236074.62	120586.84	80326.59
Steam turbine annual O&M cost ($)		
50754.12	25784.36	16409.77

Table 6.17: Operational technical and economic characteristics for the system with gas turbine configuration 5 and fuel NG.

Mode 1	Mode 2	Mode 3
$\dot{W}_{GT}$ (kW)		
24790.93	21155.23	13236.94
SFC_{GT} (gr/kWh)		
171.9147	175.8823	190.2175
$\dot{Q}_{HRSG}$ (kW)		
10311.13	8965.8	5865.57
$\dot{m}_{g,HRSG}$ (kg/s)		
59.51	55.89	45.2
$T_{g,in,HRSG}$ / $T_{g,out,HRSG}$ (^{o}C)		
360.39 / 210.81	342.95 / 204.46	308.26 / 196.24
$\dot{m}_{HP,HRSG}$ (kg/s)		
2.934	2.584	1.706
$\dot{m}_{LP,HRSG}$ (kg/s)		
0.459	0.409	0.286
$\dot{m}_{hl}$ (kg/s)		
0.154	0.1155	0.077
$\dot{W}_{ST}$ (kW)		
2709.48	2348.92	1471.93
SFC_{CC} (gr/kWh)		
153.9768	158.3053	171.1823
GT annual fuel cost ($)		
1719687.12	879046.09	611849.37
GT annual O&M cost ($)		
400125.68	199916.93	128663.12
HRSG annual O&M cost ($)		
140085.56	71318.87	47991.06
Steam turbine annual O&M cost ($)		
29154.02	14798.17	9538.08

The PWC (objective function) for each one of the six combinations is presented in Table 6.18, and is lower when configuration 3 is used for both fuels. As seen, the simplest of the gas turbine configurations is the best choice in terms of PWC, even if the specific fuel consumption of the gas turbine itself is higher. Even more, the simplicity of construction of this type of gas turbine in comparison to the two other types studied, probably makes it more appealing for application in integrated ship energy systems. For these reasons, the effects that important parameters of the optimization problem have on the optimal solution are investigated for energy systems in which gas turbines of the configuration of type 3 are used.

Table 6.18: Optimal PWC for the six combinations of gas turbines and fuels.

Configuration	PWC ($)	
	MDO	NG
3	141,171,375	71,545,007
4	145,300,524	72,237,706
5	143,784,701	71,711,376

6.2.2 Effect of fuel price on the optimal solutions

For the system with gas turbine configuration 3, which has the best economic performance, the effect of the fuel price on the optimal solution has been investigated. For this purpose, the SDO optimization problem has been solved for price of MDO in the range 300 – 700 $/ton and natural gas price in the range 100 – 300 $/ton, while the rest of parameters remain at their nominal value. The synthesis of the system remains unaltered, i.e. the inclusion of steam bottoming cycle is economically justified in all cases. The design characteristics of the system components are given in Tables 6.19 and 6.20 for the various prices of MDO and natural gas, respectively.

Table 6.19: Variation of design characteristics of the system components with varying MDO price.

Fuel price ($/ton)	300	400	500	600	700
$\dot{W}_{GT}$ (kW)	23976	23828	23803	23739	23731
$\dot{Q}_{HRSG}$ (kW)	22688	23663	24293	25893	26579
$\dot{m}_{g,HRSG}$ (kg/s)	47.53	47.36	48.22	51.07	51.82
$\dot{m}_{HP,HRSG}$ (kg/s)	5.461	5.561	5.708	6.078	6.224
$\dot{m}_{LP,HRSG}$ (kg/s)	1.351	1.631	1.696	1.799	1.838
P_{HP} (bar)	65.34	63.58	66.25	66.62	65.62
P_{LP} (bar)	8.24	6.12	5.73	5.67	5.68
$T_{g,in,HRSG}$ (^{o}C)	592.00	584.90	585.18	585.72	590.07
$T_{g,out,HRSG}$ (^{o}C)	179.90	153.57	150.20	148.03	147.24
$T_{HP,HRSG}$ (^{o}C)	560.26	552.46	550.63	555.46	561.56

$T_{LP,HRSG}$ (^{o}C)	193.51	182.85	180.53	179.56	176.17
$\dot{W}_{ST}$ (kW)	8677	8624	8613	8731	8636
$\dot{m}_{HP,ST}$ (kg/s)	6.380	6.431	6.412	6.396	6.384
$\dot{m}_{LP,ST}$ (kg/s)	1.320	1.608	1.658	1.670	1.730
$T_{HP,ST}$ (^{o}C)	567.72	543.53	542.84	553.76	541.26
$T_{LP,ST}$ (^{o}C)	188.78	179.87	178.17	182.69	176.23
$\dot{W}_{DG}$ (kW)	1205	1206	1204	1210	1205
$C_{c,GT}$ ($)	10746899	10718229	10713354	10700901	10699234
$C_{c,HRSG}$ ($)	2495601	2684082	2777585	2982490	3043967
$C_{c,ST}$ ($)	1485766	1498472	1500705	1506214	1507158
$C_{c,DG}$ ($)	874410	874689	874130	875808	874410

Table 6.20: Variation of design characteristics of the system components with varying price of natural gas.

Fuel price ($/ton)	100	150	200	250	300
$\dot{W}_{GT}$ (kW)	25167	24662	24380	24170	23831
$\dot{Q}_{HRSG}$ (kW)	19119	20623	22119	23320	23551
$\dot{m}_{g,HRSG}$ (kg/s)	57.50	54.42	50.92	50.17	47.30
$\dot{m}_{HP,HRSG}$ (kg/s)	5.396	5.565	5.464	5.582	5.498
$\dot{m}_{LP,HRSG}$ (kg/s)	0.325	0.608	1.196	1.503	1.634
P_{HP} (bar)	62.85	63.67	65.69	65.60	67.69
P_{LP} (bar)	7.54	9.00	9.45	7.15	6.44
$T_{g,in,HRSG}$ (^{o}C)	538.97	554.08	575.65	575.85	591.51
$T_{g,out,HRSG}$ (^{o}C)	251.91	226.91	200.61	174.60	161.73
$T_{HP,HRSG}$ (^{o}C)	507.53	522.89	544.63	544.11	559.62
$T_{LP,HRSG}$ (^{o}C)	191.47	199.51	199.82	189.16	185.16
$\dot{W}_{ST}$ (kW)	6983	7589	7943	8174	8491
$\dot{m}_{HP,ST}$ (kg/s)	6.254	6.276	6.152	6.231	6.329
$\dot{m}_{LP,ST}$ (kg/s)	0.290	0.549	1.096	1.386	1.531
$T_{HP,ST}$ (^{o}C)	476.26	513.43	529.52	530.73	544.12
$T_{LP,ST}$ (^{o}C)	180.24	187.96	185.65	167.34	162.92
$\dot{W}_{DG}$ (kW)	1205	1207	1208	1209	1207
$C_{c,GT}$ ($)	10973925	10878489	10824556	10784367	10718674
$C_{c,HRSG}$ ($)	2149778	2332648	2454784	2643177	2663628
$C_{c,ST}$ ($)	1378655	1425071	1452170	1469284	1469208
$C_{c,DG}$ ($)	874410	874958	875249	875529	874969

With increasing fuel price, the power capacity of the steam bottoming cycle generally also increases. For a better visualization of the operating performance of the bottoming cycle, the variation of $\dot{Q}_{HRSG}$, $\dot{W}_{ST}$ and the fraction $\dot{W}_{ST}/\dot{W}_{GT}$ is diagrammatically presented in Figures 6.7 and 6.8 for three voyage modes as functions of the fuel price. It is noticed that, generally, as the fuel price increases, the bottoming cycle recovers more thermal energy from the exhaust gas and produces more mechanical power during all operating modes. This trend is more evident in the case of natural gas, which has a relatively lower price compared to MDO, and the added capital and maintenance costs related to the bottoming cycle become more significant for the determination of the optimal solution as the fuel price decreases. In other words, the lower the fuel price, the less exploitation of the waste heat is posed in an optimal solution. On the other hand, the price of the MDO is quite high at 500 \$/ton, so that for this and even higher values of this parameter, the exploitation of the bottoming cycle in the optimal solutions does not exhibit large variations.

With both fuels and in the whole range of fuel prices examined, the fraction $\dot{W}_{ST}/\dot{W}_{GT}$ has a significantly high value, indicating the importance of the steam bottoming cycle in energy systems where gas turbines are used as main engines. One more important attribute observed in Figures 6.7 and 6.8 is that the value of the fraction $\dot{W}_{ST}/\dot{W}_{GT}$ increases significantly in operating mode 3, and in mode 2 is again higher than in mode 1, in which the gas turbine operates closer to the nominal power rating and has higher thermal efficiency. This means that the design of the bottoming cycle is carried out in a way that the need for increasing the thermal efficiency of the overall energy system in modes where the main engine does not operate quite efficiently is taken into account in the optimization procedure.

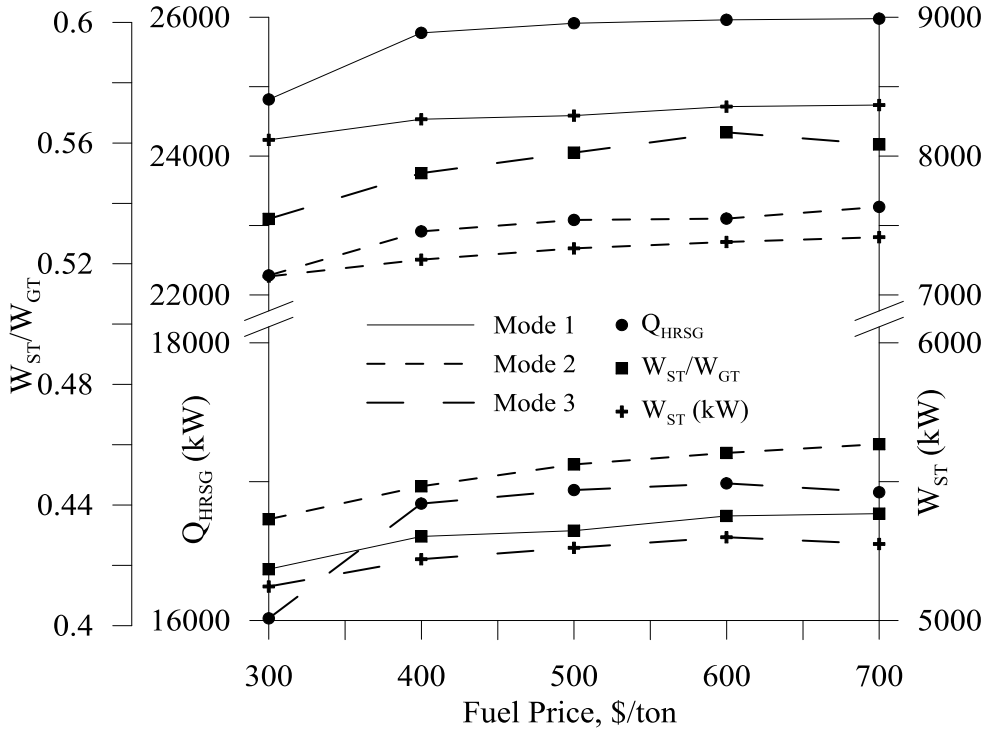

Figure 6.7: Effect of MDO price on the optimal values of $\dot{Q}_{HRSG}$, $\dot{W}_{ST}$ and $\dot{W}_{ST}/\dot{W}_{GT}$.

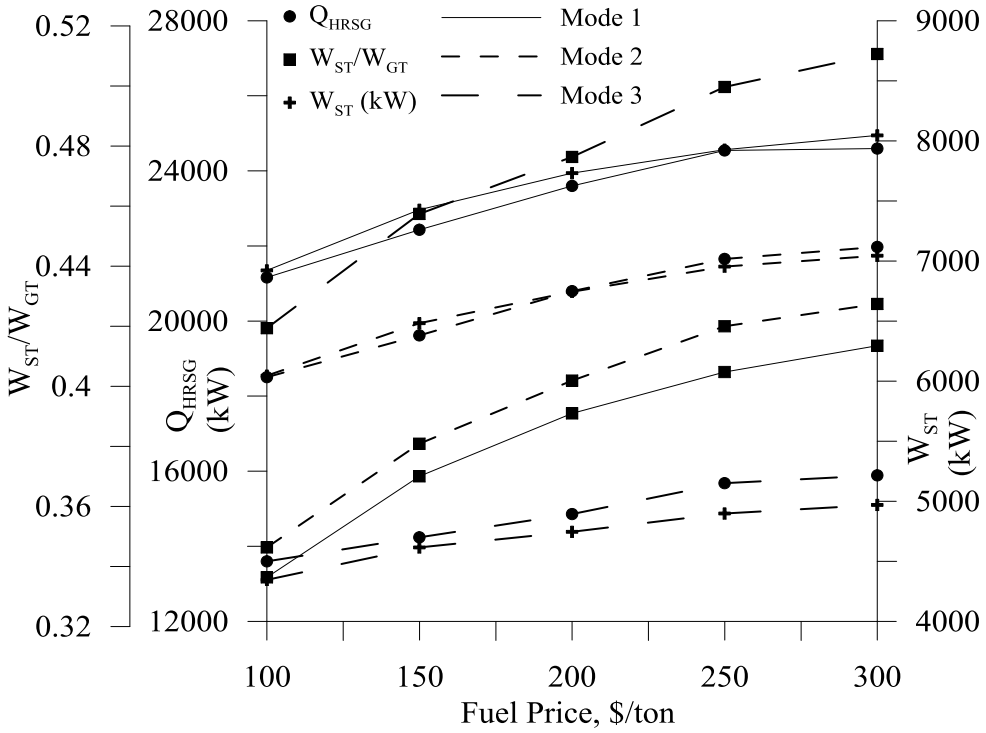

Figure 6.8: Effect of natural gas price on the optimal values of $\dot{Q}_{HRSG}$, $\dot{W}_{ST}$ and $\dot{W}_{ST}/\dot{W}_{GT}$.

The PWC of the investment for varying fuel price is presented in Table 6.21. The variation of the PWC with the fuel price is nearly linear for both fuels, indicating the major contribution that the cost of fuel has on the objective function.

Table 6.21: PWC for varying fuel price.

MDO		Natural gas	
Fuel price ($/ton)	PWC ($)	Fuel price ($/ton)	PWC ($)
300	114,302,675	100	58,889,296
400	141,171,375	150	71,545,007
500	167,995,232	200	84,112,723
600	194,661,060	250	96,522,638
700	221,544,251	300	110,365,050

6.2.3 Effect of capital cost on the optimal solutions

For the system with gas turbine configuration 3, the effect of the capital cost on the optimal solution has also been investigated. For this purpose, the capital costs of all the components were multiplied with a capital cost factor, which was given the values 0.5 and 2, and the optimization problems were solved for both fuels. The synthesis of the system again remains unaltered in the optimal solutions. The variation of the design characteristics of the components is reported in Table 6.22.

Table 6.22: Nominal characteristics of components with varying capital cost.

Fuel	MDO			Natural gas		
Capital cost factor	0.5	1	2	0.5	1	2
$\dot{W}_{GT}$ (kW)	23811	23828	24014	24420	24662	24793
$\dot{Q}_{HRSG}$ (kW)	24659	23663	23489	22124	20623	20427
$\dot{m}_{g,HRSG}$ (kg/s)	47.05	47.36	50.84	49.36	54.42	54.84
$\dot{m}_{HP,HRSG}$ (kg/s)	5.720	5.561	5.437	5.652	5.565	5.560
$\dot{m}_{LP,HRSG}$ (kg/s)	1.716	1.631	1.762	0.890	0.608	0.506
P_{HP} (bar)	65.52	63.58	57.47	64.09	63.67	52.50
P_{LP} (bar)	6.72	6.12	5.06	9.12	9.00	7.44
$T_{g,in,HRSG}$ (^{o}C)	602.23	584.90	571.27	586.45	554.08	554.76
$T_{g,out,HRSG}$ (^{o}C)	149.76	153.57	172.40	199.45	226.91	233.17
$T_{HP,HRSG}$ (^{o}C)	571.52	552.46	538.83	557.20	522.89	522.39
$T_{LP,HRSG}$ (^{o}C)	180.02	182.85	177.36	201.83	199.51	193.40
$\dot{W}_{ST}$ (kW)	9085	8624	8323	8471	7589	7491
$\dot{m}_{HP,ST}$ (kg/s)	6.264	6.431	6.386	6.281	6.276	6.296
$\dot{m}_{LP,ST}$ (kg/s)	1.701	1.608	1.625	0.879	0.549	0.494
$T_{HP,ST}$ (^{o}C)	607.69°C	543.53	575.96	590.38	513.43	535.96
$T_{LP,ST}$ (^{o}C)	191.89	179.87	175.92	204.76	187.96	200.54
$\dot{W}_{DG}$ (kW)	1206	1206	1209	1204	1207	1209
$C_{c,GT}$ ($)	5357419	10718229	21508254	5416119	10878489	21806551
$C_{c,HRSG}$ ($)	1398610	2684082	4927116	1251530	2332648	4315563
$C_{c,ST}$ ($)	767846	1498472	2947318	750324	1425071	2832784
$C_{c,DG}$ ($)	437345	874689	1751058	437065	874958	1751058

Figures 6.9 and 6.10 depict the variation of $\dot{Q}_{HRSG}$, $\dot{W}_{ST}$ and fraction $\dot{W}_{ST}/\dot{W}_{GT}$ with the capital cost factor in the three voyage modes. The variation of $\dot{Q}_{HRSG}$ and $\dot{W}_{ST}$ with the capital cost is not significant in the case of MDO, with a slight reduction of the mechanical power production being observed as the capital cost increases. More noticeable is the effect of capital cost in case of natural gas, with a significant increase of the contribution of the bottoming cycle when the capital costs are decreased to half the nominal prices.

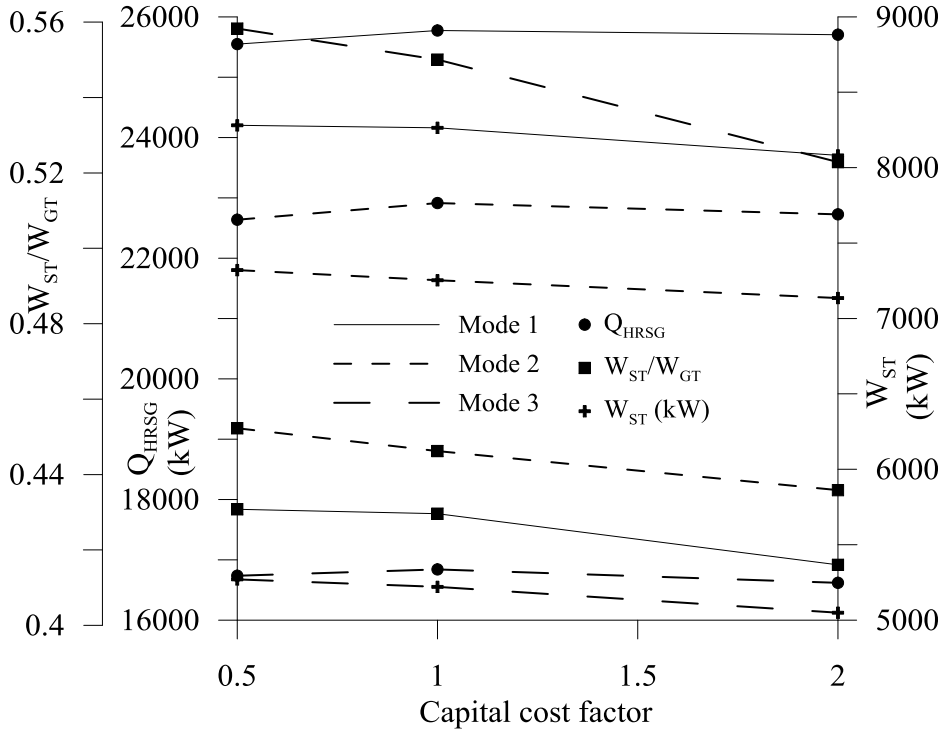

Figure 6.9: Effect of capital cost on the optimal values of $\dot{Q}_{HRSG}$, $\dot{W}_{ST}$ and fraction $\dot{W}_{ST}/\dot{W}_{GT}$ in case of MDO.

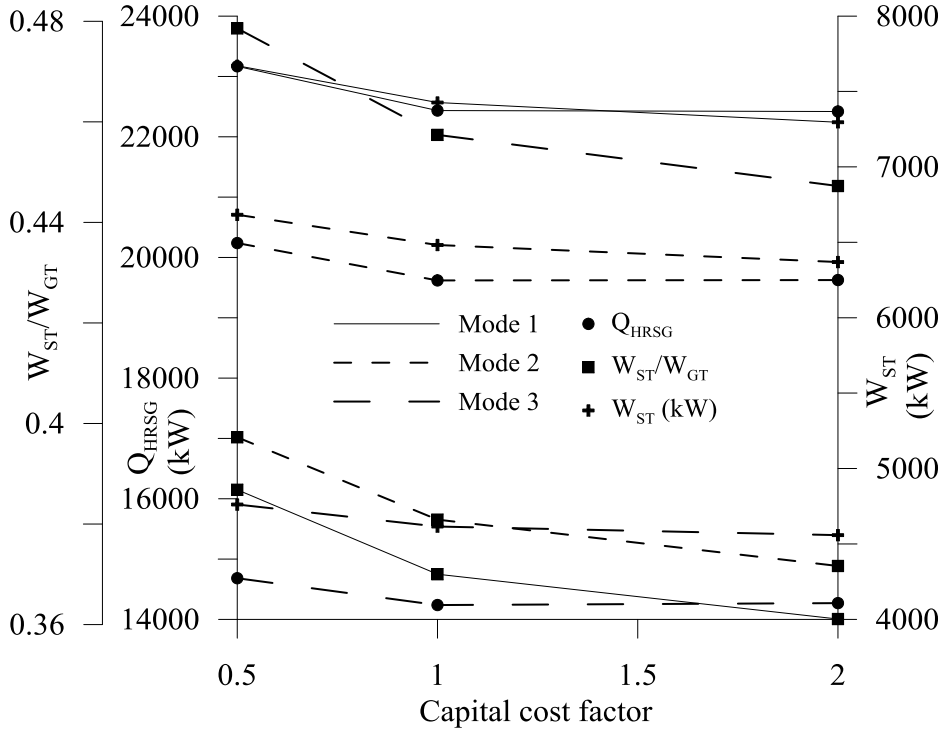

Figure 6.10: Effect of capital cost on the optimal values of $\dot{Q}_{HRSG}$, $\dot{W}_{ST}$ and fraction $\dot{W}_{ST}/\dot{W}_{GT}$ in case of natural gas.

The capital cost of the bottoming cycle components is given in Table 6.23, along with the O&M PWC of the of the bottoming cycle. The increased power production in the case of natural gas for capital cost factor 0.5 is reflected in the increased related O&M cost.

Table 6.23: PWC and bottoming cycle costs for varying capital cost factors.

Fuel	Capital cost factor	Total PWC ($)	Capital cost of B.C. ($)	PWC of O&M of B.C. ($)
MDO	0.5	132,975,803	2,148,514	10,310,416
	1	141,171,375	4,182,555	10,280,546
	2	157,641,585	7,892,692	10,269,102
NG	0.5	63,561,140	1,974,960	9,204,124
	1	71,545,007	3,757,720	8,918,232
	2	87,119,816	7,141,844	8,915,494

6.3 Application on a very large crude carrier (VLCC) Tanker

In the present case, the application of intertemporal synthesis, design and operation optimization is carried out for the energy system of a VLCC tanker.

6.3.1 Problem specific data and definitions

Apart from the design and operational characteristics of the energy system, the sailing speed of the ship during each mode of operation is also treated as an independent variable to be determined by optimization. The sailing speed has a prominent effect on the resistance of the ship's motion and the required propulsion load. The most important dimensions and hull coefficients related to the propulsion resistance are reported in Table 6.24.

Table 6.24: Ship dimensions and resistance related coefficients.

Length	L	333 m
Breadth	B	60 m
Draught (loaded)	T_L	21.06 m
Draught (ballast)	T_B	14.4 m
Block coefficient	C_b	0.8315
Midship coefficient	C_m	0.995
Wetted volume	∇	349971.7 m^3

The propulsion resistance of the ship is considered as a function of sailing speed, the loading condition which affects the draught and the wind speed. The ship resistance theory used is based on [1−5]. Representative curves of the required propulsion power used are depicted in Figures 6.11 and 6.12.

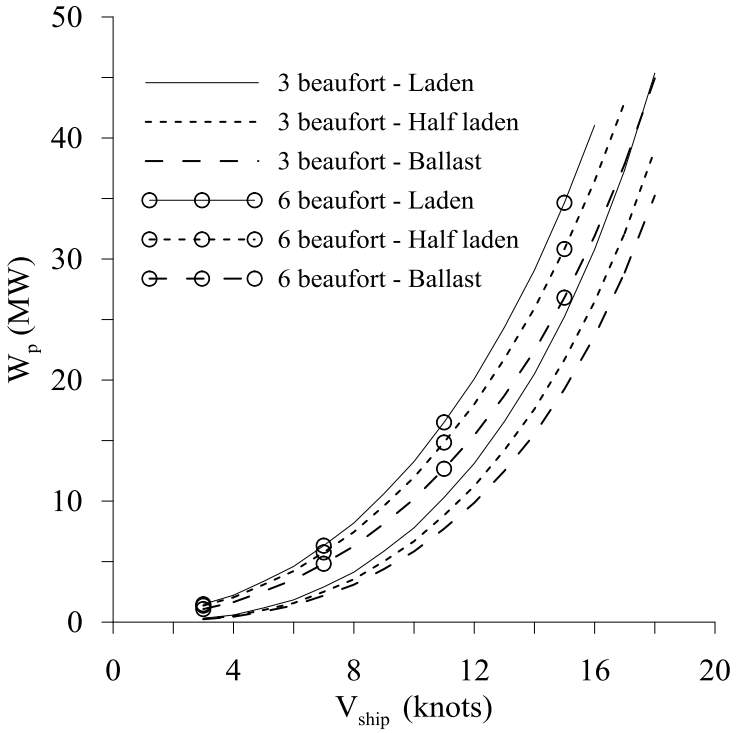

Figure 6.11: Propulsion power requirements as function of ship speed, loading conditions and wind of 3 and 6 Beaufort.

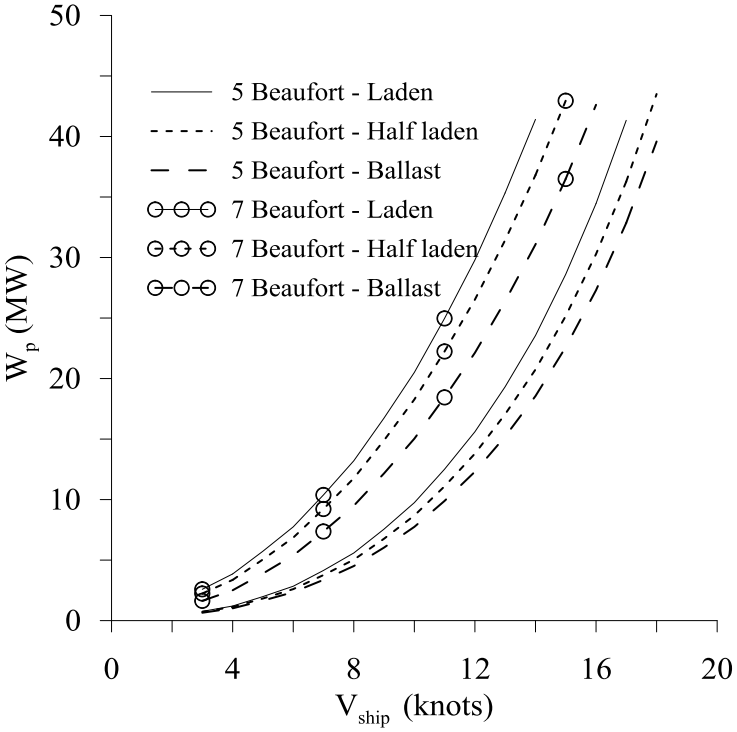

Figure 6.12: Propulsion power requirements as function of ship speed, loading conditions and wind of 5 and 7 Beaufort.

The type of prime movers in the present application example is considered to be two−stroke Diesel engines with operation modified appropriately for combined cycle

applications, as mentioned in Chapter 3. The engines operate on HFO with LHV_{HFO}=39570 kJ/kg. For load factors higher than 50%, a combination of exhaust gas turbocharger bypass (and the subsequent decrease of fresh scavenge air mass flow rate) and modifications of the engine's control system leads to increased temperature of the exhaust gases. The fuel consumption is increased, with respect to a non−modified Diesel engine. In Figure 6.13, the exhaust gas mass flow rate and temperature, as also the specific fuel oil consumption of an engine with MCR of 25 MW is presented as an example. The alteration of the curves form at load factors 35% and 30% is due to the operation of engine's blower in such low brake power output.

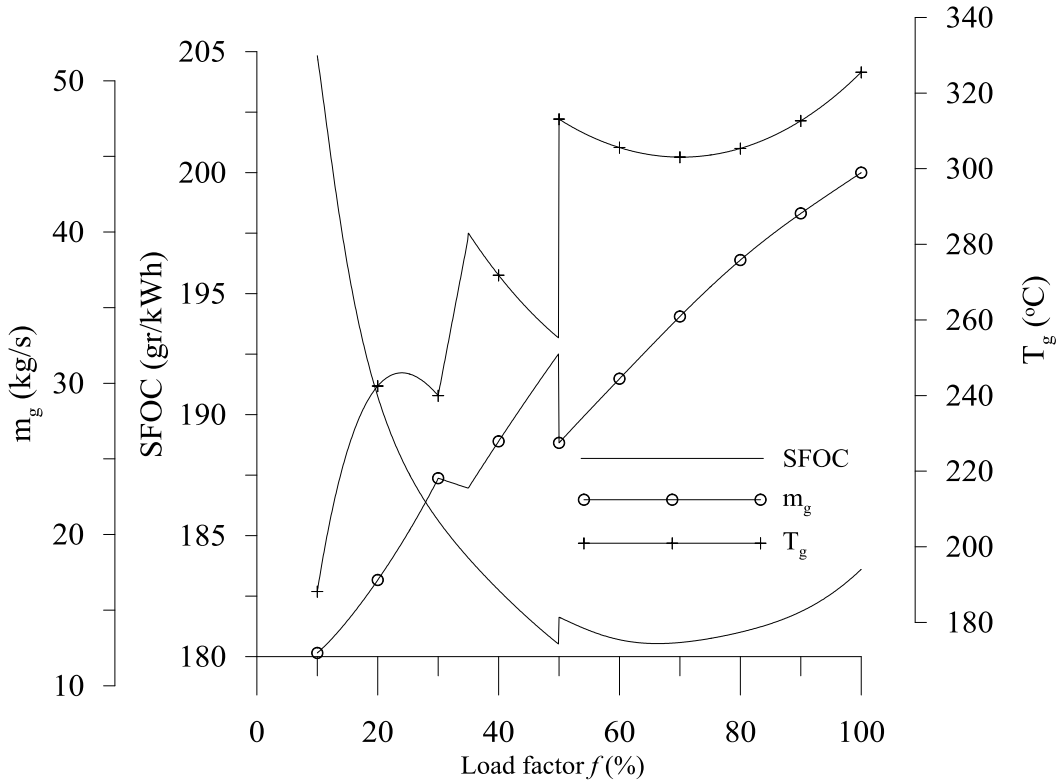

Figure 6.13: Exhaust gas mass flow rate and temperature and specific fuel consumption of a two stroke engine.

The ship is considered sailing on a route that contains three harbors, with harbor A being the loading station. At harbor B half of the cargo is offloaded and the remaining is offloaded at harbor C. Afterwards the ship returns at harbor A in ballast condition, closing a round trip. The distance between the stations is presented in Table 6.25. The operation for a whole year of service in terms of expected wind is approximated by assuming a mean value for the wind for each of the four seasons, which is also presented in Table 6.25. Thus, twelve different travelling operating modes are considered for the optimization problem. In the same table, the total hours of operation per season (h_s) and the freight rate (*fr,* in $ per metric ton and nautical mile) are also presented. For each season, the average number of round trips is to be determined by the optimization, as the sailing speeds are not predetermined.

Table 6.25: Characteristics of the round trip legs in terms of distance, cargo loading, freight rate and mean wind per season.

Mode	Departure harbor	Destination harbor	Distance (nm)	Wind (Bft)	Cargo (metric tons)	Freight rate ($/tnm)	Season	Season total hours
1	A	B	3950	7	285300	5.925	Winter	1488
2	B	C	1280	7	142650	6.5893		
3	C	A	5030	7	0	0		
4	A	B	3950	5	285300	5.925	Spring	2040
5	B	C	1280	5	142650	6.5893		
6	C	A	5030	5	0	0		
7	A	B	3950	3	285300	5.925	Summer	2040
8	B	C	1280	3	142650	6.5893		
9	C	A	5030	3	0	0		
10	A	B	3950	4	285300	5.925	Autumn	2040
11	B	C	1280	4	142650	6.5893		
12	C	A	5030	4	0	0		

The propulsion load in each mode is, as mentioned, a function of the ships' speed, which is treated as an independent variable of the optimization problem. The electric and thermal loads are considered constant on each trip leg and season, but they vary from one leg and season to the other. The related values are presented in Table 6.26. In the same table, the harbor loads are presented, which are considered as independent of season. The harbor is treated as an additional thirteenth operating mode, in which energy is used for loading or unloading and its duration (denoted as $\underline{h}_{hrt}$) is 33.5 hours per round trip.

Table 6.26: Electric and thermal power loads per leg and season and harbor loads.

Mode	Initial harbor	Destination harbor	$\dot{W}_e$ (kW)	$\dot{Q}_{th}$ (kW)	Season
1	A	B	950	1300	Winter
2	B	C	950	1300	
3	C	A	950	1300	
4	A	B	870	970	Spring
5	B	C	870	970	
6	C	A	750	970	
7	A	B	870	630	Summer
8	B	C	870	630	
9	C	A	750	630	
10	A	B	870	970	Autumn
11	B	C	870	970	
12	C	A	750	970	
Harbor			1900	400	

In the present application case, the maximization of the Net Present Value (NPV) of the investment of acquiring and operating the ship's energy system for a specified number of years

is selected as the objective. The NPV is preferred for a problem in which the ship speed is to be determined. This is because the higher the speed, the more round trips may be made and the income per year is increased. On the other hand, higher speeds impose a higher propulsion load and required fuel consumption, which generally is the predominant operating cost. So, sailing speeds cannot be readily decided, and the application of optimization may be quite helpful. The NPV is expressed as in Eq. (6.1)

$$NPV = \left(Annual\ Income \right) \times PWF - PWC \tag{6.1}$$

where *PWF* is the Present Worth Factor and *PWC* is the Present Worth Cost. The annual income is the sum of the incomes per season (*IPS*) which is expressed as:

$$IPS = \left[\left(fr \right)_{AB} \left(cargo \right)_{AB} + \left(fr \right)_{BC} \left(cargo \right)_{BC} \right] \times \frac{\frac{Dist_{AB}}{V_{AB}} + \frac{Dist_{BC}}{V_{BC}} + \frac{Dist_{CA}}{V_{CA}} + h_{hrt}}{h_s} \tag{6.2}$$

The bracketed term in Eq. (6.2) is the sum of incomes per leg of the round trip. The second multiplier is the mean number of round trips per season, which may have a non−integer value.

6.3.2 Solution for a nominal case

In the present section, the results of the optimization are reported. The problem is initially solved for a "nominal" case, in which the fuel price c_f is 300 \$/ton. Other economic parameters of the problem are given in Table 6.27.

Table 6.27: Values of economic parameters.

Parameter	Value
c_f	300 \$/ton
N_Y	20
f	3%
i	8%
PWF	12.250041
$c_{om,D}$	0.006 \$/kWh
$c_{om,DE}$	0.007 \$/kWh
$c_{om,HRSG}$, $c_{om,AB}$	0.005 \$/kWh
$c_{om,ST}$	0.004 \$/kWh

The optimal synthesis, design and operation are presented in Tables 6.28, 6.29 and 6.30, respectively. The analysis of PWC in its constituents as well as the present worth of the income (which is calculated as the first−year income multiplied by the PWF) are presented in Table 6.31.

Table 6.28: Optimal synthesis of the system.

$n_D = 1$	$n_{HRSG} = 1$	$n_{ST} = 1$
$n_{DE} = 2$	$n_{AB} = 1$	

Table 6.29: Optimal design (nominal) specifications of components.

$\dot{W}_D$ (kW)	15271	$\dot{W}_{ST}$ (kW)	875
$\dot{Q}_{HRSG}$ (kW)	4879	$\dot{m}_{HP,ST}$ (kg/s)	0.966
$\dot{m}_{g,HRSG}$ (kg/s)	20.99	$T_{HP,ST}$ (°C)	299.20
$T_{g,HRSG,in}$ (°C)	350.78	$\dot{m}_{LP,HRSG}$ (kg/s)	0.364
$T_{g,HRSG,out}$ (°C)	163.80	$T_{LP,ST}$ (°C)	155.13
P_{HP} (bar)	9.54	$\dot{W}_{DG1}$ (kW)	594
P_{LP} (bar)	4.41	$\dot{W}_{DG2}$ (kW)	1532
$\dot{m}_{HP,HRSG}$ (kg/s)	1.132	$\dot{Q}_{AB}$ (kW)	400
$T_{HP,HRSG}$ (°C)	321.27		
$\dot{m}_{LP,HRSG}$ (kg/s)	0.319		
$T_{LP,HRSG}$ (°C)	160.01		

Table 6.30: Optimal operating properties.

Season	Winter			Spring			Summer			Autumn			
Mode	1	2	3	4	5	6	7	8	9	10	11	12	Harbor
V (knots)	7.440	7.857	8.888	11.109	11.579	11.828	11.659	11.903	12.859	11.688	11.750	12.390	0.000
$\dot{W}_p$ (kW)	11544.1	11306.2	11866.2	12807.3	12501.4	11796.6	12163.1	11191.2	12388.5	12831.6	11336.1	11827.6	0.0
t (hours/year)	610.8	187.4	651.2	784.3	243.8	938.0	793.5	251.9	916.2	777.8	250.7	934.4	268.0
$\dot{W}_D$ (kW)	11544.1	11127.7	11866.2	12807.3	12031.3	11796.6	11843.8	10780.4	12263.7	12831.6	11336.1	11827.6	0.0
$\dot{Q}_{HRSG}$ (kW)	3940.4	3783.7	4068.4	4475.9	4126.4	4029.9	4038.5	3638.3	4215.4	4487.8	3850.7	4042.5	0.0
$\dot{m}_{g,HRSG}$ (kg/s)	21.94	21.4	22.33	23.41	22.53	22.25	22.31	20.92	22.8	23.43	21.67	22.29	0
$T_{g,HRSG,in}$ (°C)	308.20	306.25	310.05	317.17	311.11	309.62	309.91	304.99	312.73	317.39	307.17	309.81	0
$T_{g,HRSG,out}$ (°C)	163.01	162.74	163.22	163.81	163.29	163.13	163.12	162.44	163.4	163.83	162.84	163.15	0
$\dot{m}_{HP,HRSG}$ (kg/s)	0.692	0.644	0.732	0.981	0.872	0.842	0.971	0.849	1.026	0.984	0.787	0.846	0.000
$T_{HP,HRSG}$ (°C)	294.69	293.75	295.67	296.92	293.46	292.65	289.95	287.55	291.51	297.05	291.38	292.75	0
$\dot{m}_{LP,HRSG}$ (kg/s)	0.307	0.297	0.315	0.337	0.318	0.313	0.314	0.288	0.324	0.338	0.302	0.314	0.000
$T_{LP,HRSG}$ (°C)	159.46	159.47	159.46	159.48	159.44	159.43	159.40	159.42	159.41	159.48	159.43	159.43	0.00
$\dot{m}_{th,HRSG}$ (kg/s)	0.5066	0.5066	0.5066	0.3780	0.3780	0.3780	0.2455	0.2455	0.2455	0.3780	0.3780	0.3780	
$\dot{W}_{ST}$ (kW)	638.0	595.8	672.5	870.4	777.8	752.0	845.5	739.9	880.8	873.5	704.2	755.4	0.0
$\dot{W}_{DG1}$ (kW)	324.98	554.98	289.05	0	585.71	0	358.08	563.43	0	0	172.66	0	449.73
$\dot{W}_{DG2}$ (kW)	0	0	0	0	0	0	0	0	0	0	0	0	1450.2
$\dot{W}_{ST,p}$ (kW)	0.0	178.5	0.0	0.0	470.1	0.0	319.2	410.8	124.8	0.0	0.0	0.0	0.0
$\dot{W}_{ST,e}$ (kW)	625.0	395.0	661.0	870.0	284.3	750.0	511.9	306.6	750.0	870.0	697.3	750.0	0.0
$\dot{Q}_{AB}$ (kW)	0	0	0	0	0	0	0	0	0	0	0	0	400

Table 6.31: Economic parameters of the optimal solution.

Capital cost	8,924,940 $
PWC of fuel	60,194,506 $
PWC of O&M	8,526,088 $
Total PWC	77,645,534 $
Present worth of income	174,946,572 $
NPV (objective function)	97,301,037$
Annual mean number of round trips	7.99

In the optimal solution, the energy system contains one prime mover and a bottoming cycle with one HRSG and one steam turbine. For all of these components, the maximum possible number was set equal to 2 for the optimization. Two Diesel gen-sets are present, with the larger one being used only when the ship is in harbor operation. An auxiliary boiler is also used in harbor operation, as the heat load during the sailing modes is fully covered by the HRSG. The steam turbine serves a part or whole of the electric load in the 12 sailing modes, with the remaining part being covered by the smaller of the Diesel gen-sets, when required. A part of the steam turbine power is also used for the propulsion load in certain of the sailing modes. It is reminded that for the determination of the nominal power rating of the prime mover, a sea margin of 15% is posed in the simulation of the energy system.

For investigating the gain of the bottoming cycle utilization and making comparisons with the common practice in energy systems of VLCCs, three additional optimization problems were formulated, in which certain restrictions are posed to the possible values of the MCR and the inclusion of a bottoming cycle. These three problems are defined as follows:

- Problem A: the bottoming cycle is deliberately excluded and the MCR of the prime mover is set at 25 MW.
- Problem B: the bottoming cycle is also excluded, but the MCR is determined by the optimization procedure.
- Problem C: the inclusion or not of a bottoming cycle is left as a result of optimization, but the MCR is deliberately set at 25 MW.

In all three problems, only one prime mover was allowed in the system. For making comparisons of the optimal solutions for the design and operational characteristics of the three problems to the “nominal” case, the related quantities are presented in Tables 6.32 − 6.35.

Table 6.32: Design characteristics of the components for problems A, B, C.

	Problem A	Problem B	Problem C
$\dot{W}_D$ (kW)	25000	15181	25000
$\dot{Q}_{HRSG}$ (kW)	-	-	4996
$\dot{m}_{g,HRSG}$ (kg/s)	-	-	24.26
$T_{g,HRSG,in}$ (°C)	-	-	339.78
$T_{g,HRSG,out}$ (°C)	-	-	170.63
P_{HP} (bar)	-	-	9.43
P_{LP} (bar)	-	-	4.53
$\dot{m}_{HP,HRSG}$ (kg/s)	-	-	1.152
$T_{HP,HRSG}$ (°C)	-	-	305.57
$\dot{m}_{LP,HRSG}$ (kg/s)	-	-	0.36
$T_{LP,HRSG}$ (°C)	-	-	161.50
$\dot{W}_{ST}$	-	-	999
$\dot{m}_{HP,ST}$ (kg/s)	-	-	1.077
$T_{HP,ST}$ (°C)	-	-	325.30
$\dot{m}_{LP,HRSG}$ (kg/s)	-	-	0.395
$T_{LP,ST}$ (°C)	-	-	159.07
$\dot{W}_{DG1}$	969	970	492
$\dot{W}_{DG2}$	932	931	1410
$\dot{Q}_{AB}$	400	400	400
$\dot{Q}_{EGB}$	1300	1300	-

Table 6.33: Operational characteristics for problems A and B.

	Mode	1	2	3	4	5	6	7	8	9	10	11	12	Harbor
Problem A	V (knots)	7.792	7.896	9.719	11.642	11.713	11.675	11.661	11.895	13.605	11.654	11.757	13.571	0.000
	$\dot{W}_p$ (kW)	12481.3	11427.4	14082.3	14281.1	12868.5	11351.3	12169.8	11166.4	14370.9	12716.2	11355.9	15062.4	0.0
	t (hours/year)	618.2	197.7	631.2	758.2	244.2	962.8	813.4	258.4	887.8	811.6	260.7	887.5	0.0
	$\dot{W}_D$ (kW)	12481.25	11427.4	14082.33	14281.08	12868.5	11351.29	12169.79	11166.4	14370.87	12716.16	11355.92	15062.44	0.0
	$\dot{m}_g$ (kg/s)	31.95	29.55	35.44	35.86	32.81	29.37	31.25	28.94	36.05	32.48	29.38	37.49	0.00
	T_g (°C)	255.24	261.46	247.95	247.22	253.24	261.95	256.95	263.18	246.90	254.01	261.92	244.70	0.00
	$\dot{W}_{DG1}$ (kW)	950.0	950.0	950.0	870.0	870.0	750.0	870.0	870.0	750.0	870.0	870.0	750.0	968.4
	$\dot{W}_{DG2}$ (kW)	0.0	0.0	0.0	0.0	0.0	0.0	0.0	0.0	0.0	0.0	0.0	0.0	931.6
	$\dot{Q}_{AB}$ (kW)	0	0	0	0	0	0	0	0	0	0	0	0	400
	$\dot{Q}_{EGB}$ (kW)	1300	1300	1300	970	970	970	630	630	630	970	970	970	-
Problem B	V (knots)	7.670	7.724	8.341	10.944	11.675	11.669	11.638	11.752	12.470	11.668	11.702	11.860	0.000
	$\dot{W}_p$ (kW)	12149.6	10932.1	10408.1	12349.2	12746.3	11334.2	12109.3	10742.2	11356.1	12760.3	11187.7	10377.0	0.0
	t (hours/year)	581.7	187.2	681.2	787.4	239.2	940.3	782.2	251.0	929.6	762.7	246.4	955.5	0.0
	$\dot{W}_D$ (kW)	12149.6	10932.1	10408.1	12349.2	12746.3	11334.2	12109.3	10742.2	11356.1	12760.3	11187.7	10377.0	0.0
	$\dot{m}_g$ (kg/s)	28.31	26.22	25.27	28.64	29.27	26.93	28.24	25.88	26.97	29.29	26.67	25.21	0.00
	T_g (°C)	243.76	240.34	240.08	244.70	246.91	241.03	243.58	240.16	241.08	247.00	240.73	240.09	0.00
	$\dot{W}_{DG1}$ (kW)	950.0	950.0	950.0	870.0	870.0	750.0	870.0	870.0	750.0	870.0	870.0	750.0	969.6
	$\dot{W}_{DG2}$ (kW)	0.0	0.0	0.0	0.0	0.0	0.0	0.0	0.0	0.0	0.0	0.0	0.0	930.4
	$\dot{Q}_{AB}$ (kW)	0	0	0	0	0	0	0	0	0	0	0	0	400
	$\dot{Q}_{EGB}$ (kW)	1300	1300	1300	970	970	970	630	630	630	970	970	970	-

Table 6.34: Operational characteristics for problem C.

	1	2	3	4	5	6	7	8	9	10	11	12	Harbor
V (knots)	7.823	8.991	9.708	11.650	11.693	12.077	11.760	12.427	13.604	12.607	12.144	13.510	0.000
$\dot{W}_p$ (kW)	12590.1	14866.5	14054.4	14301.1	12801.8	12521.6	12511.9	12756.8	14369.2	16084.7	12537.6	14893.8	0.0
t (hours/year)	626.7	176.7	643.0	769.8	248.5	945.6	813.7	249.5	895.7	775.2	260.8	921.2	281.7
$\dot{W}_e$ (kW)	950	950	950	870	870	750	870	870	750	870	870	750	1900
$\dot{Q}_{th}$	1300	1300	1300	970	970	970	630	630	630	970	970	970	400
$\dot{W}_D$ (kW)	12590.1	14866.5	14054.4	14301.1	12801.8	12521.6	12511.9	12756.8	14038.0	16084.7	12537.6	14732.2	0.0
$\dot{Q}_{HRSG}$ (kW)	4266.4	4685.5	4529.6	4569.6	4297.5	4247.9	4239.5	4282.9	4513.6	4934.3	4250.7	4652.7	0.0
$\dot{m}_{g,HRSG}$ (kg/s)	26.22	30.08	28.72	29.13	26.59	26.1	26.08	26.51	28.69	32.11	26.13	29.85	0
$T_{g,HRSG,in}$ (°C)	312.75	305.87	307.83	307.18	311.92	313.02	313.06	312.09	307.88	303.90	312.96	306.16	0
$T_{g,HRSG,out}$ (°C)	170.16	171.26	170.87	170.93	170.21	170.06	170	170.13	170.75	171.82	170.07	171.14	0
$\dot{m}_{HP,HRSG}$ (kg/s)	0.779	0.893	0.850	0.985	0.910	0.897	1.022	1.034	1.097	1.087	0.898	1.008	0.000
$T_{HP,HRSG}$ (°C)	293.583	285.918	288.229	284.632	289.556	290.656	287.491	286.582	282.503	280.671	290.592	283.495	0
$\dot{m}_{LP,HRSG}$ (kg/s)	0.344	0.394	0.376	0.381	0.348	0.342	0.341	0.347	0.375	0.421	0.342	0.390	0.000
$T_{LP,HRSG}$ (°C)	161.42	161.14	161.23	161.17	161.36	161.39	161.36	161.33	161.17	161.01	161.39	161.13	0.00
$\dot{m}_{th,HRSG}$ (kg/s)	0.5067	0.5067	0.5067	0.3781	0.3781	0.3781	0.2456	0.2456	0.2456	0.3781	0.3781	0.3781	
$\dot{W}_{ST}$ (kW)	721.4	829.7	789.4	889.1	779.7	774.0	896.6	883.5	965.2	892.3	776.5	914.5	0.0
$\dot{W}_{DG1}$ (kW)	238.09	125.32	167.33	0	102.43	0	0	0	120.86	0	98.85	0	491.96
$\dot{W}_{DG2}$ (kW)	0	0	0	0	0	0	0	0	0	0	0	0	1408.04
$\dot{W}_{ST,p}$ (kW)	0.0	0.0	0.0	0.0	0.0	0.0	0.0	0.0	331.2	0.0	0.0	161.7	0.0
$\dot{W}_{ST,e}$ (kW)	711.9	824.7	782.7	870.0	767.6	750.0	870.0	870.0	629.1	870.0	771.2	750.0	0.0
$\dot{Q}_{AB}$ (kW)	0	0	0	0	0	0	0	0	0	0	0	0	400

Table 6.35: Economic parameters of the optimal solution for problems A, B, C.

	Problem A	Problem B	Problem C
Capital cost	10,159,887 $	7,717,209 $	11,190,153 $
PWC of fuel	68,990,184 $	61,191,257 $	67,878,974 $
PWC of O&M	8,079,213 $	7,229,062 $	9,764,473 $
Total PWC	87,229,284 $	76,137,528 $	88,833,600 $
Annual mean number of round trips	8.26	7.86	8.41
Present worth of income	180,412,515 $	172,072,484 $	183,868,293 $
NPV (objective function)	93,183,231 $	95,934,956 $	95,034,693 $

It is seen that the NPV in these three problems is slightly lower than the nominal case, which justifies the utilization of a bottoming cycle and the determination of the nominal power rating of the prime mover by optimization.

6.3.3 Effect of fuel price on the optimal solution

In the present section, the optimization problem is solved with fuel prices of 200, 400, 500 and 600 $/ton. The synthesis and design characteristics are presented in Tables 6.36 and 6.37, respectively, and certain operational characteristics are given in Table 6.38. It is noted that a minimum permissible value of 6 knots is imposed on the speed of the vessel. The economic parameters are presented in Table 6.39.

Table 6.36: Synthesis of the system as a function of fuel price.

Fuel price $/ton	200	400	500	600
n_D	1	1	1	1
n_{HRSG}	1	1	1	0
n_{ST}	1	1	1	0
n_{DE}	2	2	2	2
n_{AB}	1	1	1	1
n_{EGB}	0	0	0	1

The most prominent effect of the increasing fuel price is the decreasing of sailing speed, in order for the fuel operational costs to be kept to a minimum. The brake power of the prime mover is naturally reduced as the sailing speed is decreasing and, subsequently, the exhaust gas has lower thermal content to be utilized in a bottoming cycle. Thus, as fuel price increases, the available power production in the steam turbine becomes lower and lower. At the fuel price of c_f = 500 $/ton, a bottoming cycle is still included in the system, but the HRSG is not producing steam for the thermal loads, as it is preferred that the thermal content of the exhaust gas is better utilized for producing mechanical power in the steam turbine. Ultimately, for fuel price c_f = 600 $/ton, the optimization procedure results in an energy system without a bottoming cycle. This is because the generally lower heat content of the exhaust gas, which would result in an

even lower mechanical power production by the steam turbine, does not justify the expenses related to the capital and maintenance costs of a bottoming cycle.

Table 6.37: Design characteristics as functions of fuel price.

Fuel price \$/ton	200	400	500	600
$\dot{W}_D$ (kW)	22958	11344	9307	9118
$\dot{Q}_{HRSG}$ (kW)	5575	4308	3245	-
$\dot{m}_{g,HRSG}$ (kg/s)	28.70	17.76	14.69	-
$T_{g,HRSG,in}$ (°C)	301.98	355.36	341.84	-
$T_{g,HRSG,out}$ (°C)	174.62	163.14	164.73	-
P_{HP} (bar)	10.01	9.86	10.16	-
P_{LP} (bar)	5.67	4.18	4.63	-
$\dot{m}_{HP,HRSG}$ (kg/s)	1.325	0.948	0.936	-
$T_{HP,HRSG}$ (°C)	277.88	324.71	310.96	-
$\dot{m}_{LP,HRSG}$ (kg/s)	0.3622	0.293	0.268	-
$T_{LP,HRSG}$ (°C)	171.67	158.53	164.84	-
$\dot{W}_{ST}$	1434	620	611	-
$\dot{m}_{HP,ST}$ (kg/s)	1.669	0.659	0.713	-
$T_{HP,ST}$ (°C)	296.22	307.40	279.59	-
$\dot{m}_{LP,HRSG}$ (kg/s)	0.4	0.291	0.222	-
$T_{LP,ST}$ (°C)	176.56	157.95	148.86	-
$\dot{W}_{DG1}$	501	623	509	992
$\dot{W}_{DG2}$	1504	1531	1547	1012
$\dot{Q}_{AB}$	400	400	1300	400
$\dot{Q}_{EGB}$	-	-	-	1300

Table 6.38: Operational characteristics as function of fuel price.

Fuel price $/ton	Mode	1	2	3	4	5	6	7	8	9	10	11	12	13
200	V_{ship} (knots)	8.875	10.073	11.354	13.098	13.542	13.675	13.599	13.670	14.393	13.605	13.590	13.822	0.000
	$\dot{W}_p$ (kW)	16288.2	18558.1	19645.7	19684.0	18810.4	17254.2	18893.3	16534.8	17320.1	19615.9	16958.8	15982.7	-
	$\dot{W}_D$ (kW)	16288.2	18087.3	19184.5	19044.3	18010.0	16727.8	18189.4	15898.5	16820.9	19087.3	16359.9	15627.9	-
	$\dot{Q}_{HRSG}$ (kW)	5087.1	5827.0	6383.4	6297.1	5781.1	5241.9	5854.4	4926.1	5267.3	6320.2	5103.1	4843.3	-
	$\dot{W}_{ST}$ (kW)	951.4	1093.3	1306.6	1372.4	1232.5	1085.6	1344.5	1093.1	1143.1	1402.3	1047.6	976.4	-
	$\dot{W}_{DG1}$ (kW)	0	347.61	108.89	143.07	456.11	198.76	239.04	430.47	108.72	0	438.87	133.78	480.57
	$\dot{W}_{DG2}$ (kW)	0	0	0	0	0	0	0	0	0	0	0	0	1419.43
	$\dot{Q}_{AB}$ (kW)	0	0	0	0	0	0	0	0	0	0	0	0	400
400	V_{ship} (knots)	6.138	6.740	7.616	9.722	9.787	10.522	9.802	10.932	11.508	9.747	10.962	11.553	0.000
	$\dot{W}_p$ (kW)	8106.7	8602.3	8586.5	8971.3	8168.4	8863.6	7468.1	8887.6	8912.1	7775.4	9497.7	9617.8	0.0
	$\dot{W}_D$ (kW)	8106.7	8602.3	8586.5	8971.3	8168.4	8863.6	7468.1	8887.6	8912.1	7775.4	9497.7	9617.8	0.0
	$\dot{Q}_{HRSG}$ (kW)	2841.6	3040.0	3033.4	3191.4	2854.0	3142.4	2588.1	3141.8	3152.9	2707.6	3452.3	3517.5	0.0
	$\dot{W}_{ST}$ (kW)	354.5	408.4	406.6	540.0	449.6	526.9	471.9	618.0	619.9	410.3	609.6	622.6	0.0
	$\dot{W}_{DG1}$ (kW)	620.32	564.12	566.01	343.79	437.97	232.43	414.67	262.5	138.83	478.86	271.3	132.74	462.55
	$\dot{W}_{DG2}$ (kW)	0	0	0	0	0	0	0	0	0	0	0	0	1437.45
	$\dot{Q}_{AB}$ (kW)	0	0	0	0	0	0	0	0	0	0	0	0	400
500	V_{ship} (knots)	6.011	6.209	6.024	8.763	9.501	9.718	9.747	9.677	9.718	9.483	9.717	9.706	0.000
	$\dot{W}_p$ (kW)	7770.4	7346.1	5426.1	7084.8	7628.6	7137.2	7329.2	6193.9	5496.3	7278.0	6715.7	5967.4	0.0
	$\dot{W}_D$ (kW)	7770.4	7346.1	5426.1	7084.8	7628.6	7137.2	7329.2	6193.9	5496.3	7278.0	6715.7	5967.4	0.0

	$\dot{Q}_{HRSG}$ (kW)	2629.9	2473.9	1906.2	2383.7	2576.3	2401.4	2467.9	2106.9	1923.1	2449.9	2263.3	2044.1	0.0
	$\dot{W}_{ST}$ (kW)	622.9	614.6	468.4	591.5	619.9	596.1	613.4	519.9	472.7	608.7	560.3	503.8	0.0
	$\dot{W}_{DG1}$ (kW)	340.77	349.41	501.67	290.08	260.48	160.29	267.35	364.66	288.82	272.19	322.56	256.51	441.96
	$\dot{W}_{DG2}$ (kW)	0	0	0	0	0	0	0	0	0	0	0	0	1458.04
	$\dot{Q}_{AB}$ (kW)	1300	1300	1300	970	970	970	630	630	630	970	970	970	400
600	V_{ship} (knots)	6.000	6.030	6.010	7.774	7.880	7.790	7.813	9.686	9.714	7.777	8.921	9.664	0.000
	$\dot{W}_{p}$ (kW)	7743.8	6924.2	5398.0	5146.7	4828.4	4181.3	3932.0	6206.5	5490.7	4201.8	5472.8	5909.5	0.0
	$\dot{W}_{D}$ (kW)	7743.8	6924.2	5398.0	5146.7	4828.4	4181.3	3932.0	6206.5	5490.7	4201.8	5472.8	5909.5	0.0
	$\dot{W}_{DG1}$ (kW)	950.0	950.0	950.0	870.0	870.0	750.0	870.0	870.0	750.0	870.0	870.0	750.0	958.9
	$\dot{W}_{DG2}$ (kW)	0.0	0.0	0.0	0.0	0.0	0.0	0.0	0.0	0.0	0.0	0.0	0.0	941.1
	$\dot{Q}_{AB}$ (kW)	0	0	0	0	0	0	0	0	0	0	0	0	400
	$\dot{Q}_{EGB}$ (kW)	1300	1300	1300	970	970	970	630	630	630	970	970	970	0

Table 6.39: Economic parameters as functions of fuel price.

	200	400	500	600
Capital cost ($)	11,001,371	7,790,729	7,155,593	6,225,445
PWC of fuel ($)	57,296,212	59,993,868	60,836,513	62,322,037
PWC of O&M ($)	11,948,225	6,302,563	5,428,059	3,854,517
Total PWC ($)	80,245,808	74,087,160	73,420,165	72,401,999
Annual mean number of round trips	9.25	7.04	6.38	5.77
Present worth of income ($)	202,184,750	153,899,659	139,574,637	126,273,042
NPV (objective function) ($)	121,938,941	79,812,499	66,154,471 $	53,871,043

6.3.4 Fuel price effect with double freight rate

In the present section, the sensitivity analysis of the fuel price is executed again for the same prices, but with the freight rate being doubled in comparison with the values reported in Table 6.25. The synthesis, design and operation characteristics of the optimal solutions are reported in Tables 6.40 to 6.43.

Table 6.40: Synthesis characteristics as functions of fuel price with double freight rate.

Fuel price $/ton	200	400	300	500	600
n_D	1	1	1	1	1
n_{HRSG}	0	1	1	1	1
n_{ST}	0	1	1	1	1
n_{DE}	2	2	2	2	2
n_{AB}	1	1	1	1	1
n_{EGB}	1	0	0	0	0

Table 6.41: Design characteristics as function of fuel price with double freight rate.

Fuel price $/ton	200	400	300	500	600
$\dot{W}_D$ (kW)	54604	37913	27077	22172	16965
$\dot{Q}_{HRSG}$ (kW)	-	8321	6696	5903	5634
$\dot{m}_{g,HRSG}$ (kg/s)	-	42.74	34.36	27.31	24.41
$T_{g,HRSG,in}$ (°C)	-	306.32	321.12	336.38	348.71
$T_{g,HRSG,out}$ (°C)	-	175.16	167.16	162.22	164.52
P_{HP} (bar)	-	9.71	9.55	9.37	10.02
P_{LP} (bar)	-	5.45	4.96	4.38	4.65
$\dot{m}_{HP,HRSG}$ (kg/s)	-	2.219	1.719	1.448	1.355
$T_{HP,HRSG}$ (°C)	-	275.61	295.06	306.36	318.34
$\dot{m}_{LP,HRSG}$ (kg/s)	-	0.486	0.432	0.397	0.378
$T_{LP,HRSG}$ (°C)	-	170.44	165.72	161.23	161.25
$\dot{W}_{ST}$	-	2151	1701	1340	1079

$\dot{m}_{HP,ST}$ (kg/s)	-	2.575	1.93	1.525	1.161
$T_{HP,ST}$ (°C)	-	284.29	312.52	300.11	331.89
$\dot{m}_{LP,HRSG}$ (kg/s)	-	0.528	0.516	0.47	0.403
$T_{LP,ST}$ (°C)	-	172.85	159.12	153.41	156.79
$\dot{W}_{DG1}$	989	544	496	523	700
$\dot{W}_{DG2}$	1134	1504	1524	1520	1476
$\dot{Q}_{AB}$	400	400	400	400	400
$\dot{Q}_{EGB}$	1300	-	-	-	-

In the case of double freight rate, the sailing speeds are generally much higher compared to the nominal freight rate. This leads to increased number of round trips per year and present worth of the income. One notable difference compared to the nominal freight rate is that the exclusion of a bottoming cycle now appears at the c_f = 200 $/ton. This can be explained by considering the economic data presented in Table 6.43. For c_f = 300 − 600 $/ton, the PWC of fuel is relatively unaltered. The NPV is maximized (among other reasons also) by decreasing the capital and maintenance costs as the fuel price decreases. In the case of c_f = 200 $/ton the fuel PWC is substantially lower than in the other cases, even if there is no bottoming cycle in the system. Even more, the relatively increased capital and maintenance costs should not be further increased by the inclusion of a bottoming cycle.

Table 6.42: Operational characteristics as function of fuel price with double freight rate.

Fuel price $/ton	Mode	1	2	3	4	5	6	7	8	9	10	11	12	13
200	V_{ship} (knots)	13.755	15.560	16.067	17.491	17.510	17.533	17.501	17.520	18.366	17.497	17.521	17.986	0.000
	$\dot{W}_p$ (kW)	39708.8	46405.6	43082.3	44705.0	39354.3	35906.5	41028.6	35546.2	38470.3	41999.6	36604.6	36774.8	0.0
	$\dot{W}_D$ (kW)	13.8	15.6	16.1	17.5	17.5	17.5	17.5	17.5	18.4	17.5	17.5	18.0	0.0
	$\dot{W}_{DG1}$ (kW)	950.0	950.0	950.0	870.0	870.0	750.0	870.0	870.0	750.0	870.0	870.0	750.0	825.9
	$\dot{W}_{DG2}$ (kW)	0.0	0.0	0.0	0.0	0.0	0.0	0.0	0.0	0.0	0.0	0.0	0.0	1074.1
	$\dot{Q}_{AB}$ (kW)	0	0	0	0	0	0	0	0	0	0	0	0	400
	$\dot{Q}_{EGB}$ (kW)	1300	1300	1300	970	970	970	630	630	630	970	970	970	-
300	V_{ship} (knots)	11.722	13.489	13.826	15.553	15.648	16.186	15.594	16.403	17.348	15.549	15.966	17.009	0.000
	$\dot{W}_p$ (kW)	28264.7	33823.5	30138.8	31398.1	28173.2	28341.7	28477.6	29134.4	31122.7	29030.8	27572.2	30424.2	0.0
	$\dot{W}_D$ (kW)	27331.9	32220.3	29010.2	30096.6	26930.8	27231.5	27143.7	27681.3	29660.4	27867.8	26369.2	29073.6	0.0
	$\dot{Q}_{HRSG}$ (kW)	8146.5	10044.6	8722.5	9123.2	8008.1	8104.6	8066.6	8242.7	8945.3	8314.6	7832.1	8736.4	0.0
	$\dot{W}_{ST}$ (kW)	1759.3	2161.5	1916.1	2076.1	1765.0	1863.1	1920.8	1968.3	2134.1	1895.4	1764.4	1994.1	0.0
	$\dot{W}_{DG1}$ (kW)	128.62	407.94	169.27	112.59	367.69	0	294.94	369.58	90.12	143.33	321.55	118.58	452.55
	$\dot{W}_{DG2}$ (kW)	0	0	0	0	0	0	0	0	0	0	0	0	1447.45
	$\dot{Q}_{AB}$ (kW)	0	0	0	0	0	0	0	0	0	0	0	0	400
400	V_{ship} (knots)	9.926	11.367	11.649	13.703	13.785	14.972	13.749	15.177	15.538	13.679	15.212	15.513	0.000
	$\dot{W}_p$ (kW)	20176.0	23697.3	20648.1	22059.4	19802.2	22475.5	19596.8	22745.9	21614.8	19970.5	23752.5	22467.3	0.0
	$\dot{W}_D$ (kW)	19619.7	22732.2	20128.7	21383.9	19016.0	21517.6	18969.9	21942.7	20680.9	19148.3	22660.3	21620.1	0.0
	$\dot{Q}_{HRSG}$ (kW)	6361.3	7626.1	6544.2	7020.3	6142.8	7075.6	6116.4	7246.2	6730.5	6187.6	7582.0	7118.5	0.0

	$\dot{W}_{ST}$ (kW)	1274.9	1618.0	1324.7	1545.9	1306.7	1558.8	1392.9	1437.4	1558.0	1318.9	1674.9	1604.5	0.0
	$\dot{W}_{DG1}$ (kW)	241.04	309.49	150.69	0	364.12	165.25	108.34	253.98	142.82	388.86	299.22	0	452.55
	$\dot{W}_{DG2}$ (kW)	0	0	0	0	0	0	0	0	0	0	0	0	1447.45
	$\dot{Q}_{AB}$ (kW)	0	0	0	0	0	0	0	0	0	0	0	0	400
500	V_{ship} (knots)	9.033	9.905	10.198	12.864	13.536	13.614	13.525	13.601	13.622	13.470	13.657	13.615	0.000
	$\dot{W}_{p}$ (kW)	16841.3	17890.4	15711.4	18813.5	18792.3	17008.0	18636.9	16257.8	14428.9	19139.4	17217.1	15187.2	0.0
	$\dot{W}_{D}$ (kW)	16460.1	17370.9	15711.4	18239.3	18050.5	16546.5	17942.7	15703.4	14095.9	18614.3	16722.6	14676.2	0.0
	$\dot{Q}_{HRSG}$ (kW)	5484.0	5817.2	5229.2	6155.3	6076.9	5505.0	6023.3	5207.1	4709.5	6316.6	5567.8	4891.4	0.0
	$\dot{W}_{ST}$ (kW)	1030.4	1120.0	961.9	1299.5	1278.6	1101.8	1332.4	1108.4	974.6	1283.2	1143.0	962.2	0.0
	$\dot{W}_{DG1}$ (kW)	313.34	364.13	0	150.7	347.13	113.23	241.39	339.45	112.14	114.54	230.75	311.2	461.88
	$\dot{W}_{DG2}$ (kW)	0	0	0	0	0	0	0	0	0	0	0	0	1438.12
	$\dot{Q}_{AB}$ (kW)	0	0	0	0	0	0	0	0	0	0	0	0	400
600	V_{ship} (knots)	7.934	8.430	9.729	11.636	11.725	12.392	11.717	12.590	13.579	11.686	12.471	13.392	0.000
	$\dot{W}_{p}$ (kW)	12981.4	13105.2	14116.9	14264.3	12908.7	13442.3	12362.7	13242.1	14301.4	12823.5	13538.2	14571.2	0.0
	$\dot{W}_{D}$ (kW)	12981.4	13105.2	14116.9	14094.9	12346.3	13239.5	12362.7	12904.5	13930.7	12823.5	13538.2	14307.6	0.0
	$\dot{Q}_{HRSG}$ (kW)	4381.4	4427.7	4835.6	4815.6	4143.3	4468.1	4138.1	4331.5	4734.9	4312.7	4584.8	4891.3	0.0
	$\dot{W}_{ST}$ (kW)	734.6	737.8	803.2	886.2	782.1	808.1	874.2	905.4	975.8	878.6	889.6	1021.0	0.0
	$\dot{W}_{DG1}$ (kW)	236.94	237.59	149.78	157.45	677.48	152.5	0	322.29	149.52	0	0	0	516.58
	$\dot{W}_{DG2}$ (kW)	0	0	0	0	0	0	0	0	0	0	0	0	1383.42
	$\dot{Q}_{AB}$ (kW)	0	0	0	0	0	0	0	0	0	0	0	0	400

Table 6.43: Economic parameters as functions of fuel price with double freight rate.

	200	300	400	500	600
Capital cost ($)	17,631,061	15,217,461	12,366,807	10,910,850	9,550,452
PWC of fuel ($)	128,574,967	137,184,059	134,676,230	136,166,264	133,823,657
PWC of O&M ($)	21,755,155 $	19,211,727	14,323,286 $	11,656,733	9,504,421
Total PWC ($)	167,961,183	171,613,247	161,366,323	158,733,847	152,878,530
Annual mean number of round trips	12.07	10.98	9.83	9.06	8.00
Present worth of income ($)	527,959,395	480,443,362	430,090,763	396,464,209	365,571,310
NPV (objective function) ($)	359,998,212	308,830,116	268,724,441	237,730,362	212,692,780

References

1. Holtrop J. A Statistical Re-Analysis of Resistance and Propulsion Data. International Shipbuilding Progress; 31:272−274.
2. Fujiwara T, Ueno M, Ikeda Y. A New Estimation Method of Wind Forces and Moments acting on Ships on the basis of Physical Component Models. Journal of the Japan Society of Naval Architects and Ocean Engineers 2005; 2:243−255.
3. Tsujimoto M, Shibata K, Kuroda M, Takagi K. A Practical Correction Method for Added Resistance in Waves. Journal of the Japan Society of Naval Architects and Ocean Engineers 2008; 8:177−184.
4. ITTC (2012) Recommended Procedures and Guidelines, Speed and Power Trials, Part 2, 7.5-04-01-01.2, pp. 1–25.
5. Politis GK, Skamnelis FA, Ship Resistance, 2nd edition, National Technical University of Athens, Athens, 2007.

Chapter 7

Closure

7.1 Concluding Remarks

In the present work, a method for the synthesis, design and operation optimization of integrated energy systems of ships is developed. Such systems are proposed for covering the various types of the energy loads appearing during the operation of a ship, which may naturally exhibit large time variations during different time periods.

The three levels on which optimization is applied are tackled simultaneously with the use of a dedicated modeling procedure of the system as a whole, specially developed for this purpose. The effort has been directed towards the development of this method in a manner that permits for a unified approach for the modeling and optimization, while the effects of all the three aforementioned levels on the optimal solutions are all simultaneously taken into account. This leads to a method, which is characterized as a single−level approach of the synthesis, design and operation optimization problem, differing from the ones appearing in the literature of thermal energy systems optimization, which solve the problem on two or three levels. With the two or three level approaches, if the conditions for decomposition are not strictly applicable, global optimal solutions may be overlooked. Such an incidence is avoided with the single-level approach presented here.

The single−level approach for the SDO optimization of energy systems inherently takes into account the effects that all the various operating conditions have on the synthesis of the system and the design characteristics of its components simultaneously. It also conversely takes into account the fact that the synthesis of the system and the design characteristics of the components define the possibilities for the operating options at all of the instances of time during which the system is going to operate.

From a mathematical point of view, the development of the method was carried out with keeping in mind that the complete problem of synthesis, design and operation optimization should be adequately expressed with a formulation suitable for the employment of proven mixed integer nonlinear optimization algorithms. The objective function formulated is highly discontinuous and multimodal but the application of a standard genetic algorithm implementation was proven to be adequate for the specific optimization problem.

Other formulations were tried out during early stages of the present work, in which attempts were made for expressing the complete SDO optimization problem with the use of exclusively continuous variables in order for gradient based algorithms to be applied. However, to the author's sense, the complete problem could not be adequately expressed for the application of the single−level approach.

In the applications presented in this thesis, it is shown that the single−level optimization approach can be successfully applied for aiding the engineering decisions considering the appropriate synthesis of the energy system, the suitable design characteristics of the components included and the most appropriate operation states of the energy system, taking into account techno−economic criteria. Interesting results include the finding that in the optimal solution the prime movers may not be equally loaded or having the same nominal power (in cases where more than one is present), or the fact that a simple cycle gas turbine may be more preferable economically instead of more advanced gas turbine configurations in cases where a steam bottoming cycle is to be included taking into account all the operating modes.

7.2 Future Work Recommendations

The application of the method in the present work has been carried out with the type of prime movers of the energy system being predetermined. In order for the method to be capable of handling several types of prime movers, the extension of the modeling approach of the system described in Chapter 4 would be required, in order for taking into consideration the possibility that the number of a specific type of prime movers present in the system could be equal to zero, while the number of prime movers of another type should be different from zero. The inclusion of the possibility of zero number of prime movers of a specific type would require an important modification of the mathematical expression of the objective function in a single computational step, as required by the a single−level approach, possibly with the inclusion of certain *if−then* rules. Such an alteration could probably also lead to the need for employing more sophisticated optimization algorithms, other than the standard implementation of a genetic algorithm, as was the case in the present work.

The inclusion of the possibility of zero number of prime movers of a specific type becomes even more difficult to handle, if one considers the fact that in the single−level approach developed, the synthesis of the system may be different among different operating modes, and that the final synthesis is determined by taking into account the *temporary* synthesis of each operating mode. That is, a candidate solution may be composed by a combination of a Diesel engine operating in one mode, a number of gas turbines operating in another mode and mixed type of prime movers in another mode. The final synthesis determined by such a sequence of temporary syntheses should be examined for being technically acceptable with criteria other than that of the value of the objective function of the optimization problem, which expresses the optimality of the solution in techno−economic terms.

One other consequence of the possibility of considering different types of prime movers among a population of candidate solutions is that the variables regarding the steam bottoming cycle components should be of different orders of magnitude, accordingly to the type of the prime movers (generally the use of gas turbines leads to quite larger nominal and operating power characteristics of the steam cycle). This would result in a very high diversity

of these variables among the population, and the repetitive modification of their bounds described in Chapter 5 would not be practical. This problem could be possibly solved with a definition of non-dimensional counterparts of these independent variables, but in which the different operational characteristics of the different types of HRSGs used should be considered.

In parallel with the use of the genetic algorithms software, an optimization software based on the Particle Swarm Optimization algorithm was developed. The utilization of PSO seemed to be outperforming the genetic algorithm software used, but this held true only in sub−problems in which the integer part of the problem was fixed. The PSO algorithm did not seemed to be able to perform in a steady manner when the integer part was to be optimized, even though several solutions for coping with the integers in PSO proposed in the literature were implemented. The development of a novel way for tackling the integer part within the utilization of a PSO based algorithm specifically for the SDO optimization could be an important improvement for the overall optimization procedure.

The HRSGs presented in this thesis have a pre-determined internal structure with respect to the succession of the individual heat exchangers in the direction of the exhaust gas flow. Especially for the case with Diesel main engines, the structure chosen is the one appearing in practical systems that have been constructed in recent years. Investigations were made during the execution of the present work, regarding the optimal internal structure of the HRSGs, based on a generic superconfiguration, including several possible positions for the individual heat exchangers, as also possibilities of heat exchangers being parallel to each other with respect to the exhaust gas flow. The intention was the development of a method used for applying optimization algorithms in order to determine the best internal layout of the HRSG. The HRSG superconfiguration was not incorporated in the modeling procedure of the system as a whole, due to the computational implications and the need for the definition of several additional independent variables of the general optimization problem, which would also formulate even a more complicated optimization objective function in terms of multimodality and discontinuity. An effort to formulate the general SDO optimization problem so that the internal structure of the HRSG is the result of optimization could possibly reveal more efficient ways for exploitation of the exhaust gas thermal energy.

Another enhancement of the HRSG modeling may include the alternative choices regarding the type of the extended or finned heat transfer area. In the present work, helical extruded fins are considered, but other types include H-type fins, serrated helical extruded or circular fins, serrated twisted fins, plain continuous fins or even pin fins. Each type exhibits different heat transfer and pressure drop characteristics, and the investigation of the HRSGs performance using these alternatives is needed in order to determine the most suitable type. Regarding the determination of the exhaust gas heat transfer coefficients, it is observed that the experimentally determined values are slightly dependent on the number of tubes passes, with the magnitude of this dependency being also related to the type of the fins, and formal investigation of the type of fins used would require taking into account such an implication.

With respect to the gas turbines modeling, recent applications in combined cycle configurations dictate the use of variable geometry compressors (or adjustable flow angles of the inlet guide vanes) in conjunction with the adjustment of the fuel feeding rate in order for the desired power output to be achieved. Besides the power output adjustment, these two off−design control techniques are jointly used for the adjustment of the exhaust gas temperature or the maximum temperature in the combustion chamber during off−design operation. The overall effect is the enhancement of the combined cycle thermal efficiency, and these possibilities for the gas turbines operation could be considered in future works.

The steam turbines modeling in the present work was chosen to be based on a one−dimensional analysis, due to the simplicity of the computations. Taking into account the purposes of the present work, such an approach may be considered quite sufficient for the high and intermediate pressure sections of the steam turbines, but for the low pressure stages, where large fin heights with respect to mean diameters are observed, a more sophisticated modeling procedure could be more suitable. As for the off−design simulations of the steam turbines performance, a stage by stage analysis for the determination of the flow capacity and the flow losses of each blade row could probably give better accuracy, but except from being overly computationally demanding it would also require the determination of all the geometrical details of each row of blades, which is beyond the purposes of the work presented within this thesis.

The simulation models of the bottoming cycle components were developed keeping in mind the need for a compromise between a comprehensive modeling based on the principles of thermodynamics, fluid mechanics and the internal structural details of the parts comprising the components, and the need for fast and efficient computations, which is dictated by the requirements of applying optimization algorithms. In the development of these models, the internal structural characteristics of the components play a key role to the operating capabilities and efficiency at varying conditions of operation. Other modeling approaches could be proposed, including possibly CFD calculations taking into account the internal geometric characteristics of the components and the simulation at various operating conditions. Of course, such a modeling approach would not be suitable for the application of optimization algorithms, but such more detailed modeling calculations could be used for the derivation of performance data of the components. Such an approach would require the employment of techniques such as artificial neural networks or other machine learning schemes utilizing the data obtained with models based on CFD, and could be an enhancement of the overall optimization procedure in terms of accuracy of the results and the efficient application of optimization algorithms, as such models would also probably be quite computationally fast and efficient, once the computationally heavy calculations of the CFD techniques have been executed beforehand.

Appendices

Appendix A
Derivation of exhaust gas mass flow rate calculation of two−stroke Diesel engines

In this appendix, the derivation of Eq. (3.7) for the calculation of the exhaust gas mass flow rate in two−stroke Diesel engines modified for combined cycle application is described. It is considered that the known quantities that are modified with respect to an engine with standard operation are the increase of the exhaust gas temperature $\Delta T_{g,TES}$ and the increase of fuel consumption $\Delta sfoc_{TES}$ and that they are functions of the load factor. The purpose of the analysis to follow is the derivation of the mass flow rate by these known modified quantities. In the following, the primed quantities represent the modified engine operation. By the application of an energy balance for an operating engine Eq. (A.1) is obtained

$$\dot{Q}_f = \dot{W}_D + \dot{Q}_{eg} + \dot{Q}_{other} \tag{A.1}$$

where

$\dot{Q}_f$ heat input with fuel
$\dot{W}_D$ engine brake power
$\dot{Q}_{eg}$ heat content of exhaust gas
$\dot{Q}_{other}$ other thermal losses.

By assuming two engines with a common brake power, the one being modified and the other one standard, Eq. (A.2) is obtained

$$\dot{W}_D = \dot{W}_D' \xrightarrow{\dot{Q}_{other}=\dot{Q}_{other}'} \dot{Q}_{eg}' = \dot{Q}_{eg} + \dot{Q}_f' - \dot{Q}_f \tag{A.2}$$

for which it was assumed that the thermal losses other than the thermal content of the exhaust gas are the same for the two engines. By assuming a constant mean value for exhaust gas specific heat capacity Eq. (A.3) is obtained

$$\dot{m}_g' c_{pg} \left(T_g' - T_{ref} \right) = \dot{m}_g c_{pg} \left(T_g - T_{ref} \right) + \dot{m}_f' LHV - \dot{m}_f LHV \tag{A.3}$$

where $\dot{m}_f$ if the fuel mass flow rate, which is given by the equation

$$\dot{m}_f = \frac{sfoc\dot{W}_D}{3600000} \tag{A.4}$$

where *sfoc* is in gr/kWh, $\dot{W}_D$ in kW and $\dot{m}_f$ in kg/s. By manipulation of the above equations, and for a specified value for $\dot{W}_D$, Equation (3.7) is readily derived.

Appendix B

Coefficients for gas turbine regression models

In this appendix, the coefficients for the regression equations of gas turbines operation are tabulated.

Table B1: Coefficients for Eq. (3.11) for the case of Marine Diesel Oil and variable rotational speed.

Coefficient	GT type 3	GT type 4	GT type 5
a	0.16747603366432	0.160194281455247	0.156316307021543
b	4.47322148958418E-02	3.40535166767963E-02	2.55724865179442E-02
c	1.18487577805961E-04	9.30721391042421E-05	8.57021055693055E-05
d	-1.40018054320153E-03	-2.02828827391553E-03	-2.19696261488125E-03
e	-4.94722194897516E-07	-2.07050882902318E-07	6.7023230452934E-08
f	6.57288912327401E-05	9.93958700940327E-07	-7.0430439569635E-06
g	3.86776395238505E-05	8.71419526359929E-05	8.78103193254754E-05
h	2.28641414165223E-08	2.97171717203612E-09	4.36111111198909E-09
i	7.38936572295412E-07	5.32726785897216E-07	6.3967139845393E-08
j	-7.11476981512448E-06	-3.16281020841368E-06	-3.02312290737275E-07

Table B2: Coefficients for Eq. (3.11) for the case of natural gas and variable rotational speed. For type 5 gas turbine Eq. (3.12) must be used.

Coefficient	GT type 3	GT type 4	GT type 5
a	0.15865038044987	0.149293611225946	0.167299800197653
b	3.60924489592989E-02	3.05876962373858E-02	-1.98067819723202E-02
c	2.09195092403407E-04	9.28503495602506E-05	6.29588847371636E-05
d	-1.85222631596449E-04	-1.82650567543538E-03	9.79410451796374E-03
e	1.53564399429493E-06	-1.46601479906072E-07	-3.3655703895271E-07
f	-9.017294201841E-06	1.41845675500335E-06	-3.33989121640666E-05
g	-3.1709295575164E-05	7.7146668907183E-05	3.90835622559957E-04
h	5.25031565656576E-08	3.24494949523476E-09	2.72146464903152E-09
i	2.28250372309038E-07	4.69551219011391E-07	-5.40113555199449E-07
j	-5.43421318063611E-07	-2.70980457283102E-06	-2.8890393340136E-05

Table B3: Coefficients for Eq. (3.11) for the case of Marine Diesel Oil and constant rotational speed.

Coef.	GT type 1	GT type 2	GT type 3	GT type 4	GT type 5
a	0.166920025273092	0.12231971511122	0.167113479934909	0.163802122140118	0.159542292960996
b	6.04047814762002E-02	7.78493041092278E-02	4.46633655241478E-02	2.93055340590884E-02	2.11414665537214E-02
c	1.90183854649082E-04	2.42329098761908E-04	1.33131881748179E-04	1.09479024535566E-04	9.08287724407912E-05
d	1.78855071877543E-03	2.08021450565568E-03	-1.37541649612284E-03	-9.6324409793186E-04	-1.04978735030314E-03
e	-2.96299581947156E-07	-8.04933621792511E-07	-4.76661116787075E-07	-7.77166803599985E-08	-1.13010337726987E-07
f	-3.04676055703027E-04	-4.7505177301188E-04	4.04779872551978E-05	-2.20540621166243E-05	-1.54979994097536E-05
g	-1.04157451337736E-04	-1.91630979130 64E-04	5.0330428333077E-05	4.61547634645985E-05	4.91130833875314E-05
h	5.71196969727718E-08	1.34000000055323E-08	2.71694444444551E-08	5.9217171739203E-09	6.31843434345119E-09
i	3.51244897106657E-06	2.72320589715057E-06	6.8089974452004E-07	4.42998809958016E-07	1.44354073256599E-07
j	1.21660142548954E-06	2.17930559725491E-05	-4.84656960456119E-06	-1.35643505738606E-06	6.24371417219321E-07

Table B4: Coefficients for Eq. (3.11) for the case of natural gas and constant rotational speed. For type 3 gas turbine Eq. (3.12) must be used.

Coef.	GT type 1	GT type 2	GT type 3	GT type 4	GT type 5
a	0.15425640184346	0.115225998915845	0.193393325427401	0.152570051814713	0.148170162038358
b	5.38950455913707E-02	7.00227382035553E-02	-0.040127853908163	2.62901597156861E-02	2.00795065772117E-02
c	1.73110284792721E-04	2.3197338258936E-04	1.89934543228722E-04	1.0604931326585E-04	6.83950296714464E-05
d	1.60015451593382E-03	2.05519394406206E-03	9.27236644452857E-03	-8.72757679883298E-04	-1.11174653621867E-03
e	-2.62111581088368E-07	-1.02360749472812E-06	2.30047022884743E-06	-5.44450440799245E-08	-4.07230486250137E-07
f	-2.71328052874466E-04	-4.37474848905329E-04	9.43421939392996E-05	-1.81253060734096E-05	-3.42604584052396E-06
g	-9.31548437540703E-05	-1.87362196066817E-04	-1.20334518020157E-02	4.14710913624081E-05	5.40197562456677E-05
h	5.01116161616174E-08	1.81214646464664E-08	8.12878787878846E-08	6.40277777780779E-09	4.60669191938159E-09
i	3.13107207729635E-06	2.56660928863866E-06	4.99653031234473E-07	3.94210338853679E-07	1.87132152316059E-07
j	1.01231875096344E-06	2.04676710107273E-05	2.03765295573366E-05	-1.27152592845414E-06	-3.75641804741861E-07

Table B5: Coefficients for Eqs. (3.13) for the case of Marine Diesel Oil and variable rotational speed, pertaining to exhaust gas mass flow rate.

Coefficient	GT type 3	GT type 4	GT type 5
Eq	3.13b	3.13b	3.13b
a	52.4221965742543	64.2853521107584	45.552770572884
b	23.4743192877585	22.6980818212493	19.9345595993456
c	-0.13243138774802	-0.154864130560964	-7.42653092377262E-02
d	4.22040396155979	4.23397711520542	2.86307201823613
e	2.9151045291044E-04	3.43091771406577E-04	-7.762284210587E-05
f	-5.29168932000773E-02	-5.43364233329207E-02	-6.18522704403755E-02
g	0.243267865733056	0.343345062094716	1.2506849783719E-04
h	-3.06764444444481E-06	-3.36918686878926E-06	-1.97034949495278E-06
i	5.15289421237948E-05	4.71537122461296E-05	-1.12221301734591E-05
j	-6.77988830307778E-03	-7.80731422253311E-03	-0.015566200600955

Table B6: Coefficients for Eqs. (3.13) for the case of natural gas and variable rotational speed, pertaining to exhaust gas mass flow rate.

Coefficient	GT type 3	GT type 4	GT type 5
Eq	3.13a	3.13b	3.13a
a	9.60101886683308	62.5519990270566	7.91799996306167
b	81.4275872310345	22.3968116627826	72.063268867552
c	-3.61158356170661E-02	-0.149859816309833	-1.64184325645609E-02
d	-63.5841842152902	4.25105421087342	-53.5851523799515
e	7.80455296708517E-04	3.34824489251578E-04	4.51216287510847E-04
f	-0.111280956173501	-5.29436635209969E-02	2.19273838467911E-02
g	23.7704464951176	0.365510483540444	18.3832818807361
h	-9.21229229808337E-06	-3.28770050512921E-06	-8.45696818195217E-06
i	-1.3187158026499E-03	4.57193577721419E-05	-1.00716515871166E-03
j	5.26400410330153E-03	-7.65381410214999E-03	-9.51877448591187E-02

Table B7: Coefficients for Eqs. (3.13) for the case of Marine Diesel Oil and constant rotational speed, pertaining to exhaust gas mass flow rate.

Coef.	GT type 1	GT type 2	GT type 3	GT type 4	GT type 5
Eq	3.13c	3.13d	3.13b	3.13b	3.13a
a	75.401143144955	70.3043953167306	52.4452704267704	64.3196246666549	12.2326655460967
b	0.559475519593813	0.355182532817556	24.9136994912414	24.8021985971138	50.7912327925024
c	0.218086610154931	0.213195949020993	-0.132601723924317	-0.154460634277619	-8.49124614472687E-03
d	-0.370315331930615	0.101951845693099	5.47665063999771	5.71172624911145	-22.3957357951559
e	0.360216771024485	3.43491292030689E-02	2.88219026724336E-04	3.51836414358083E-04	-4.10367262291487E-05
f	-0.14411702262616	5.36090016530106E-03	-4.79120222333321E-02	-4.53055810693076E-02	-4.93655126282455E-02
g	-0.258543918539378	-0.239340032827491	0.370842177299553	0.43224850065808	4.89440493815674
h	3.45087723457855E-04	3.70053443434539E-04	-2.78937828282877E-06	-2.98978182299811E-06	-1.77797222541351E-06
i	-2.61951692818909E-05	-2.33153262533818E-05	3.20587065970081E-05	5.96371163459548E-05	-3.10872941705529E-05
j	6.72036868601695E-08	7.98322128922762E-08	-5.86148496230001E-03	-4.77022252770333E-03	-1.99687513464982E-02
k	6.15357246921484E-09	4.90172145186009E-09	0	0	0

Table B8: Coefficients for Eqs. (3.13) for the case of natural gas and constant rotational speed, pertaining to exhaust gas mass flow rate.

Coef.	GT type 1	GT type 2	GT type 3	GT type 4	GT type 5
Eq	3.13c	3.13d	3.13a	3.13b	3.13a
a	72.6084911883906	68.4713309834232	12.7024894777511	62.586460633167	11.825649419108
b	0.497784977514605	0.326951745489461	64.3876387917157	24.46245397714	50.5951492431718
c	0.236767186575125	0.203344131160576	-3.50393513009092E-02	-0.149574687379355	-1.73174255535704E-02
d	-0.405951767020791	0.100757223550621	-38.2500723511524	5.66876540030689	-20.9165218921907
e	0.387093197473042	3.44743050452479E-02	9.1606140006452E-04	3.41293517703075E-04	4.84638860723352E-04
f	-0.150671756388146	5.38560290185739E-03	-0.130271274126394	-4.47884277031681E-02	2.11114548985403E-02
g	-0.248967531240026	-0.233161246237154	12.3737000527499	0.434539312602449	3.19188174994112
h	3.31127862326115E-04	3.59994496496126E-04	-1.32104588385084E-05	-2.8675055555561E-06	-8.29155580890742E-06
i	-2.52442307259618E-05	-2.27257169188866E-05	-1.49591781022662E-03	5.62791983925176E-05	-1.04809076109909E-03
j	6.48564600378616E-08	7.7825153634138E-08	2.88596667575673E-02	-5.05185492284597E-03	-9.33630627654096E-02
k	5.93237022552304E-09	4.78259012938284E-09	0	0	0

Table B9: Coefficients for Eqs. (3.13) for the case of Marine Diesel Oil and variable rotational speed, pertaining to exhaust gas temperature.

Coefficient	GT type 3	GT type 4	GT type 5
Eq	3.13c	3.13b	3.13a
a	479.328923996221	371.583096162224	231.443237350056
b	-109.333862595985	128.310142510197	195.794071607319
c	244.857716988544	2.04751318140772	0.409261059285603
d	-92.9550461665769	35.9527134348119	-140.34446537647
e	0	-1.5335057712115E-03	1.0561275612819E-03
f	0	0.214838700757304	0.17790997142692
g	2.75651372708477	5.24092509570646	77.8385999876857
h	-1.36999382122916E-04	-2.9241319962956E-05	-2.0579857071134E-05
i	-3.81829673509925E-07	-4.79757651810382E-04	-9.87849963827771E-04
j	-1.98281154903861E-08	2.14004303610979E-02	0.48625248287977
k	0	0	0

Table B10: Coefficients for Eqs. (3.13) for the case of natural gas and variable rotational speed, pertaining to exhaust gas temperature.

Coefficient	GT type 3	GT type 4	GT type 5
Eq	3.13a	3.13b	3.13a
a	494.888270611009	374.762216402611	236.524637887021
b	-211.128774766577	128.701885745584	175.689487534676
c	2.92515303053377	2.05730979125852	0.416636527208128
d	395.169122756215	35.7518710669323	-108.433456539305
e	-2.06325071437591E-02	-1.56598606048238E-03	-1.40990079284711E-03
f	-1.98473083983274	0.218488603565096	9.00846927336226E-02
g	-164.249802532019	5.16255538472513	64.8803124696544
h	2.26149452146458E-04	-2.91449831000598E-05	2.35183340800779E-05
i	4.54159215349932E-02	-4.94923493972602E-04	2.68139887899227E-03
j	2.15504339263288	2.27370772130127E-02	0.578719877896645

Table B11: Coefficients for Eqs. (3.13) for the case of Marine Diesel Oil and constant rotational speed, pertaining to exhaust gas temperature.

Coef.	GT type 1	GT type 2	GT type 3	GT type 4	GT type 5
Eq	3.13a	3.13b	3.13d	3.13b	3.13b
a	209.454068629412	371.147041016806	521.28537353062	371.247875300003	363.099638271585
b	191.424543343698	119.506462305121	98.9467812624197	127.657558051612	113.741359234465
c	0.783588272075115	1.44566537743054	62.3754878067682	2.04017497679283	1.00284428140563
d	12.2595685312927	60.8415484377472	14.4380500808241	36.8139847636961	52.1519648537406
e	6.8437892301617E-03	5.00543312524387E-03	0	-1.53255661924384E-03	3.12619726550735E-04
f	1.24872286753482	0.669994467440127	0	0.22249188659073	0.617594633270507
g	6.78909328616671	13.3416443429072	2.72441945742991	5.76461339312362	11.8134307494959
h	5.16399780127902E-05	1.5100214894731E-05	-6.24407077614825E-04	-2.76686429541802E-05	-1.96569134014158E-05
i	5.04958059613089E-03	1.96855776577553E-04	6.47425823062211E-06	-4.39117645126291E-04	-9.23566969626972E-06
j	-4.01876901680723E-02	0.236075906910825	3.21883530828661E-07	2.09404777411803E-02	0.153972476124211
k	0	0	-6.05271230995808E-09	0	0

Table B12: Coefficients for Eqs. (3.13) for the case of natural gas and constant rotational speed, pertaining to exhaust gas temperature.

Coef.	GT type 1	GT type 2	GT type 3	GT type 4	GT type 5
Eq	3.13a	3.13b	3.13a	3.13b	3.13b
a	208.070998934439	373.862632410423	457.832723416719	374.414856298265	367.460042374675
b	195.184310124564	123.810599366301	3.37183833422759	127.814501257167	121.921703499219
c	0.78110872021006	1.46659317468449	2.45356326018814	2.04939961984864	1.02205180418853
d	11.0898714058047	63.4174267501927	55.3423285462006	36.54082271647	58.9892099752067
e	6.91245354915521E-03	4.97790716898959E-03	-2.45769699160855E-02	-1.56829147709522E-03	8.12416027731017E-04
f	1.27833485068709	0.697285860204272	-0.432523152290442	0.222036378007707	0.693504993721288
g	6.14723448141996	13.9589777305297	-3.01001330001047	5.73674707196835	13.3965317503218
h	4.76196845854032E-05	1.72115462121189E-05	3.8074741174676E-04	-2.74168318316028E-05	2.61559694312403E-05
i	4.52361697420779E-03	1.58681997390718E-04	5.04306414523251E-02	-4.49374141150264E-04	1.22372286160447E-03
j	-0.077580152750784	0.24430884041486	0.837041321691016	2.02062285543887E-02	0.183903148891881

Appendix C
Capital and Maintenance Cost Functions

In the present appendix the capital cost models of the individual components of the system used in the objective function are described.

C.1 Diesel Engines

The capital cost function of two-stroke Diesel engines has been developed by regression analysis of confidential data. A simple linear function is adequate for relating the capital cost of the engine with the nominal power rating

$$C_{c,D} = 250 \times MCR + 2000000 \tag{C.1}$$

where

$C_{c,D}$ capital cost of the Diesel engine in \$.

MCR maximum continuous rating of the engine in kW, range 12 MW − 74 MW

C.2 Heat Recovery Steam Generators

The cost model of the HRSGs used was developed in [1], while the values of certain parameters have been modified. The cost of each HRSG is expressed with the equation

$$C_{c,HRSG} = C_{HX} + C_{piping} + C_{gaspath} + C_{pumps} \tag{C.2}$$

where:

C_{HX}	cost of heat exchangers
C_{piping}	cost of piping, dependent mainly on the water/steam mass flow rates
$C_{gaspath}$	cost of the heat exchange area on the gas side
C_{pumps}	cost of the various pumps present in the HRSG

For the cost of the heat exchangers Eq. (C.3) is used

$$C_{HX} = c_1 \sum_{i=1}^{n_{HX}} \left[F_{P\,ST} F_{T\,ST} F_{T\,g} \left(UA\right)^{0,8} \right]_i \tag{C.3}$$

where n_{HX} is the number of individual heat exchangers. The F factors are calculated with Eqs. (C.4) to (C.6)

$$F_{P\,ST,i} = 0.0971 \left(\frac{P_{ST,i}}{30\,\text{bar}} \right) + 0.9029 \tag{C.4}$$

where $P_{ST,i}$ is the pressure of the water/steam.,

$$F_{T\,ST,i} = 1 + \exp\left(\frac{T_{ST,i} - 830K}{500K} \right) \tag{C.5}$$

where $T_{ST,i}$ is the inlet temperature of the water/steam

$$F_{T\,g,i} = 1 + \exp\left(\frac{T_{g,i} - 990\text{K}}{500\text{K}} \right) \tag{C.6}$$

where $T_{g,i}$ is the inlet temperature of the exhaust gas.

The product UA is calculated according to the equation

$$\dot{Q}_{HX} = UA \frac{\left(T_{g,out} - T_{st,in}\right) - \left(T_{g,in} - T_{st,out}\right)}{\ln \dfrac{T_{g,out} - T_{st,in}}{T_{g,in} - T_{st,out}}} \tag{C.7}$$

The piping cost is calculated according to equation

$$C_{piping} = c_2 \sum_{j=HP,LP} F_{P\,j} \dot{m}_j \tag{C.8}$$

where $\dot{m}_j$ is the total mass flow rate of steam produced in high or low pressure level.

For the gas path cost it holds

$$C_{gaspath} = c_3 \dot{m}_g^{1.2} \tag{C.9}$$

where $\dot{m}_g$ is the total exhaust gas mass flow rate.

Finally, for the pumps it holds

$$C_{pumps} = c_4 \sum_{j=HP,LP} \left[\dot{W}_p^{0.71} \left(1 + \frac{1-0.8}{1-\eta_{p,is}} \right) \right]_j \tag{C.10}$$

where $\dot{W}_p$ and $\eta_{p,is}$ are the pump power rating in kW and isentropic efficiency, respectively

The values of the c coefficients appearing in Eqs. (C.3) – (C.10) are presented in Table C.1.

Table C1: Cost coefficients for the HRSGs.

Coefficient	Value
c_1	9650 \$/(kW/K)$^{0.8}$
c_2	11820 \$/(kg/s)
c_3	658 \$/(kg/s)$^{1.2}$
c_4	623 \$/(kW)$^{0.71}$

C.3 Steam Turbines

For the steam turbines, the capital cost is calculated as follows

$$C_{c,ST} = 300 \left(\frac{\dot{W}_{ST,n}}{15000 \text{ kW}} \right)^{-0.67} \dot{W}_{ST,n} \quad , \quad \dot{W}_{ST,n} > 5000 \text{ kW} \tag{C.11a}$$

$$C_{c,ST} = 260 \left(\frac{\dot{W}_{ST,n}}{4000 \text{ kW}} \right)^{-0.53} \dot{W}_{ST,n} \quad , \quad \dot{W}_{ST,n} \leq 5000 \text{ kW} \tag{C.11b}$$

where

$C_{c,ST}$ capital cost of the steam turbine in \$.

$\dot{W}_{ST,n}$ nominal power rating of the steam turbine in kW.

This cost equation is based on [1]. The need of having two distinct equations for the capital cost of steam turbines was due to the fact that the energy systems with gas turbines as prime movers have bottoming cycles which produce much more power than the ones that

have as prime movers Diesel engines. So, the capital cost of the steam turbines should be adjusted according to the order of magnitude of the steam turbine nominal power rating.

C.4 Diesel-Generator Sets

The cost of a Diesel-generator set is estimate with equation

$$C_{c,DE} = 800 \times \left(\frac{\dot{W}_{DE,n}}{1000\ \text{kW}} \right)^{-0.6} \dot{W}_{DE,n} \tag{C.12}$$

where

$C_{c,DE}$ capital cost of the Diesel-generator set in \$.

$\dot{W}_{DE,n}$ nominal power rating of the Diesel-generator set in kW, range 0.4–12 MW.

C.5 Gas turbines

The capital cost of the gas turbines is estimated with the related cost model presented in [2]. The unit cost parameters presented in [2] are modified for taking into account the current level of technology and to approximate capital cost data available from various sources. A common regression formula is developed for the gas turbine configurations with separate power turbine examined in the present work and has the general mathematical expression of Eq. (C.13). The values of the parameters for each gas turbine configuration are presented in Table C2.

$$C_{c,GT}\,(\$) = \left(\dot{W}_{GT,N}\,(kW)\right)^{a} \exp\left(b\text{-}c\dot{W}_{GT,N}\,(kW)\right) \tag{C.13}$$

Table C2: Coefficients for Eq. (C.13).

Coefficient	Configuration 3	Configuration 4	Configuration 5
a	0.451124718450259	0.451124718937363	0.45112471762403
b	11.6601660998132	11.8085861004949	11.9225303717006
c	$8.15305188415185 \times 10^{-7}$	$8.15305206333862 \times 10^{-7}$	$8.15305153736658 \times 10^{-7}$

C.6 Maintenance costs

The maintenance costs of the components are expressed as monetary units per unit of useful energy produced (mechanical or thermal) in kWh. The values used are derived from [1] with a modification due to inflation, and are presented in Table C3.

Table C3: Maintenance Costs of the components

Component	Maintenance cost ($/kWh)
Diesel engines	0.006
HRSGs	0.005
Steam turbines	0.004
Diesel-Gen sets	0.007
Gas Turbines	0.006

References

1. Dimopoulos GG. Synthesis, Design and Operation Optimization of Marine Energy Systems. Ph.D. Thesis, NTUA, 2009.
2. Frangopoulos CA. Application of the thermoeconomic functional approach to the CGAM problem. Energy 1994;19:323−342.

Publications

1. Sakalis GN, Frangopoulos CA. Towards synthesis and design optimization of steam bottoming Rankine cycles with different ship propulsion engines. 27th International Conference on Efficiency, Cost, Optimization, Simulation and Environmental Impact of Energy Systems, (ECOS 2014), 15−19 June, 2014, Turku, Finland.

2. Frangopoulos CA, Sakalis GN, Tzortzis GJ. Intertemporal and Dynamic Optimization of Synthesis, Design and Operation of Energy Systems. 4th International Conference on Contemporary Problems of Thermal Engineering, (CPOTE 2016), 14−16 October, 2016, Katowice, Poland.

3. Sakalis GN, Frangopoulos CA. Intertemporal optimization of synthesis, design and operation of integrated energy systems of ships: General method and application on a system with Diesel main engines. Applied Energy, 2018; 226: 991–1008.